Volume 7 • No 1 • June 2019 • ARO ISSN: 2410-9355 • DOI: 10.14500/2307-549X

ARO
The Scientific Journal of Koya University

KOYA UNIVERSITY

ISSN: 2410-9355 (printed version) ISSN: 2307-549X (electronic version)
ARO - DOI: 10.14500/2307-549X

ARO-The Scientific Journal of Koya University

The ARO ("Today" in Hewramí Kurdish), is an international scientific journal published by the Koya University with p-ISSN: 2410-9355, e-ISSN: 2307-549X and DOI: 10.14500/2307-549X. ARO is a journal of original research articles, review articles, and letters to editor. The ARO Scientific Journal is a peer-reviewed, open access journal that publishes original works in all areas of Science and Engineering.

ARO the Scientific Journal Office

Koya University, University Park
Danielle Mitterrand Boulevard, Koya KOY45
Kurdistan Region - F.R. Iraq

Tel.: +964 (0) 748 012 7423
Mobile: +964 (0) 750 187 5489
E-mail: aro.journal@koyauniversity.org
url: aro.koyauniversity.org

June 2019 | Pûşper– 2719

ARO

The Scientific Journal of Koya University

Vol VII, No 1(2019)

Contents

DOI: 10.14500/2307-549X ARO p-ISSN: 2410-9355, e-ISSN: 2307-549X

ARO Editorial Words

Dear readers,

Aro, the Scientific Journal of Koya University, is closing its twelfth issue (Vol VII, No 1, 2019). It has been a challenging, exciting and yet progressive season for our journal. Aro is publishing its 7th issue as an internationally listed Scientific Journal in Kurdistan Region of Iraq. Notably, Aro has been accepted for indexing in the Emerging Sources Citation Index (ESCI), a new edition of Web of Science™ as of Feb 2016. Content in this issue is under consideration by Clarivate to be accepted in the Science Citation Index Expanded™ (SCIE) during 2019. Aro's individual articles are currently listed by Clarivate using articles unique DOI numbers which is a historical achievement for our academic community. Aro is starting its seventh-year journey in leading the quality of regional scientific publications with global impact. The editorial team have been working tirelessly to keep the novel mission and sustain Aro's future publications with greater impacts and citations. It is exciting that Aro has been awarded to DOAJ Seal listing which is an indication of a trusted high standard open access scientific work that so far has allocated to 88 journals worldwide only. The upcoming new season will be an even more exciting period in Aro's life as Thomson Reuters will examine our journal for a full permanent listing.

Aro continues its mission to provide resources, support and advice for researchers in the process of publishing their scientific papers with a global standard quality for an internationally recognised scientific publication, while at the same time offering free public access to scientific research by open online access. This is a daunting task which we hope to advance in the years to come. Thus, in the sections to follow, we would like to share and elaborate on the core elements that constitute Aro. However, finding reliable and skilled reviewers remain a big challenge for us.

Aro was created with a long-term vision of becoming accessible to all researchers in Kurdistan and beyond, and covering a wide range of scholarly disciplines in the sciences. Aro is a peer-reviewed, open access journal that publishes original scientific research, global news, letters and commentary as well as review articles in areas of science and engineering. In this issue, you will have access to original research papers in a variety of areas, such as Physics, Chemistry, Biology, Material Science, Civil Engineering, Architectural Engineering, Software Engineering, Electrical and Electronics Engineering, Petroleum Engineering and Geology.

The great responses from researchers, academics and professionals in the last five years have made us create a wider Editorial Board which serves the wider submitted scientific manuscripts. However, it is clear that having a dedicated and well-organised editorial board for the journal is only one side of the coin. The other is the ability to attract submissions of quality research and scholarly work. We are thankful to all of those who put their trust in Aro and presented their original research work for publication in Vol VII, No 1 (2019) of the journal, as well as, our thanks are extended to the 23 peer-reviewers from the Universities worldwide for their efforts in reviewing and enabling this issue of Aro.

Your support and feedback are invited and appreciated.

Dilan M. Rostam
Editor-in-Chief

Wali M Hamad
Executive Publisher

Dilan M. Rostam, Salah I. Yahya, Basim M.Fadhil, Fahmi F. Muhammad, Mohammed H. S. Zangana, Jorge Correia, Fouad Mohammad, Jacek Binda, Nadhir Al-Ansari
Executive Editorial Board

DOI: 10.14500/2307-549X ARO p-ISSN: 2410-9355, e-ISSN: 2307-549X

Molecular Typing of Human *Brucella melitensis* Isolated from Patients in Erbil, Iraq

Bushra K. Amin[1], Khulod I. Hassan[2]

[1]Department of Biology, College of Science, Salahaddin University, Erbil, Kurdistan Region - F.R. Iraq

[2]Department Food Science and Human Nutrition, College of Agriculture, University of Sulaimani, Kurdistan Region - F.R. Iraq

***Abstract*– Brucellosis is a reemerging infectious zoonotic disease of worldwide importance. In the Kurdistan Region of Iraq, it is a widely spread disease and remains a challenging health problem. This disease is mainly caused by *Brucella melitensis*, in human. For confirmation of these isolates, a study was performed, by isolation and molecular typing of *Brucella* Spp. from human patients in Rizgari Hospital at Erbil city (Iraq), between March 2014 and November 2016. One hundred sixty seven samples of blood collected from patients suspected for brucellosis, one hundred twenty one samples from these were recorded as genus of *Brucella*, using biochemical test and confirmed by applying polymerase chain reaction (PCR), using genus specific primer for *omp*31 gene which was specific for *B. melitensis*. These results support using molecular method that based on PCR as diagnostic test for the control of brucellosis in Erbil. Further studies are needed from different geographical areas of the country with different level of endemicity to plan and execute control strategies against human brucellosis.**

***Index Terms*—Brucellosis, Biochemical test, *Brucella melitensis*, Polymerase chain reaction.**

I. Introduction

Brucellosis, also known as Malta fever, is one of the most infectious zoonotic disease, with >500,000 new cases reported each year and becomes a major public health challenge in many countries (Seleem et al., 2010), especially developing countries, due to various sanitary and socioeconomic factors (Pappas and Memish, 2007). In humans, this highly diverse illness initially presents as a fever and may later develop into a chronic illness affecting various organs and tissues (Probert et al., 2004). Brucellosis in humans occurs as an acute, sub-acute, or chronic illness, and it is usually transmitted from animal reservoirs such as cattle, buffalo, camels, sheep, and goats, through consumption of unpasteurized milk or dairy products and undercooked meat products, inhalation of contaminated dust, and contact with infected animal body fluids or tissues (Greenfield et al., 2002). Brucellosis caused by microorganisms belonged to the genus *Brucella*, Gram-negative facultative intracellular bacteria (Navarro et.al., 2004). To date, 12 *Brucella* species have been reported and each species has a preference to certain group (Scholz et al., 2016). Five of the known *Brucella* species can infect humans, but the most pathogenic species for human is *Brucella melitensis* (Acha and Szyfre, 2003; Valdezate et al., 2007). *B. melitensis* with *Brucella suis* and *Brucella abortus* are listed as potential bioweapons by the Centers for Disease Control and Prevention in the USA due to the highly infectious nature of these species, as they can be readily aerosolized (Hoover and Friedlander, 2010). The intracellular location of the bacteria protects it from some of the basic mechanisms of the host's immune system and from antibiotic therapy; moreover, an outbreak of brucellosis would be difficult to detect because the initial symptoms are easily confused with those of influenza (Chain et al., 2005). Identification of *Brucella* species in developing countries still depends on culture isolation and biochemical test as there is no reliable, reproducible, and validated molecular tests for confirmation (Affi et al., 2011); moreover, several serological tests such as Rose Bengal plate test and enzyme-linked immunosorbent assay are also used for the diagnosis of human brucellosis (Mantur et al., 2010), and the major disadvantages with these serological tests are that they cannot differentiate between an acute and a chronic infection, besides cross reaction can occur with other Gram-negative bacteria such as *Escherichia coli*, *Yersinia enterocolitica,* and some *Salmonella* species, which have antigenic similarities with *Brucella* and can lead to false positive reactions (Nielsen et al., 2004). Hence, more reliable tests are needed, especially those which depend on using DNA techniques to overcome the problems associated with the traditional detection methods in terms of specificity and accuracy; among those, polymerase chain reaction (PCR) was the easiest and fastest (Ying et al., 2014). Several PCR-based assays have been developed and evaluated for identification of the genus *Brucella* (genus-specific PCR assay) based on a single unique locus that is highly conserved in all *Brucella* species including 16 s rRNA, 16–23 s intergenic transcribed

ARO-The Scientific Journal of Koya University
Volume VII, No.1 (2019), Article ID: ARO.10306, 4 pages
DOI: 10.14500/aro.10306
Received 30 April 2018; Accepted 03 March 2019
Regular research paper: Published 01 May 2019
Corresponding author's e-mail: bushra.amin@su.edu.krd

spacers, outer membrane proteins (*omp 2b, omp2a* and *omp31*) (Bricker et al., 2000, Gee et al., 2004, Imaoka et al., 2007). PCR have been described for identification of Brucella at the species level including *B. melitensis* (Baddour and Alkhalifa, 2008; Rees et al., 2009). Recently a real-time PCR based assay was used to identify *Brucella* genus in human sera (Shalini et al., 2018). The aim of this study was an attempt to evaluate a rapid and accurate technique for the detection of brucellosis in suspected patients in Erbil city of Iraq by PCR-based techniques using two kinds of primers; one of them was genus-specific primers and the other was species-specific primer for detect *B. melitensis*, the pathogenic species for human.

II. Materials and Methods

A. Sampling and Isolation of Brucella Spp.

From March 2014 to November 2016, 167 samples of bloods were collected from patients' suspects of Brucellosis from Rizgari Hospital at Erbil (Iraq), and all samples were collected aseptically in sterile tubes containing anticoagulant and send under refrigeration to the laboratory of Microbiology Division of Salahaddin University for analysis. The samples were inoculated on sterile plates of *Brucella* selective agar media with hemin and Vitamin k1 media (Hi-Media) and incubated at 37°C for 48h. The plates were observed at every 24h for the development of growth. After the growth, the colonies suspected for *Brucella* on the basis of cultural characteristics were picked up and streaked to another *Brucella* selective agar with hemin and Vitamin k1 plates and incubated at 37°C for 2 days to obtain pure culture. The pure cultures of the isolates examined by morphological tests, and some biochemical tests including: catalase, oxidase and urease production, hydrogen sulfate production, growth on media containing thionin and basic fuchsine (20 µg/ml).

B. DNA Extraction

DNA was extracted from the cell following cetyl trimethylammonium bromide (CTAB) method described by Wilson (1990) with slight modifications. Three loops of growth from pure *Brucella* culture grown on selective *Brucella* medium were transferred to a microfuge tube containing 400 µl of ×1 TE buffer. The cells were killed at 80°C for 20 min in a water bath followed by cooling at room temperature. Bacterial cell membranes were then disrupted by adding 70 µl of 10% sodium dodecyl sulfate solution and 5 µl of 10 mg/ml proteinase-K followed by incubation at 65°C for 10 min after brief vortexing. Following incubation, 100 µl of each of 5M NaCl and pre-warmed CTAB-NaCl solution was added. The mixture was vortexed until the liquid became milky white and incubated at 65°C for 10 min. Subsequently, 750 µl of phenol:chloroform:isoamyl alcohol (25:24:1) was added, vortexed briefly, and then centrifuged for 8 min at 11,000× *g*. The aqueous phase containing DNA was carefully transferred to a fresh microfuge tube and the DNA was precipitated by addition of 0.6 volume of isopropanol. The tubes were then kept in –20ºC for 30 min followed by centrifugation for 15 min at ×11,000 g. The supernatant was discarded, leaving about 20 µl above the pellet, which was then washed with 1 ml of cold 70% ethanol and centrifuged for 5 min at ×11,000 g. After discarding the supernatant, the pellet was subjected to drying at room temperature for 15–30 min and finally dissolved in 20–30µl of ×1 TE buffer and was stored at –20ºC until further use.

C. Application of PCR Assay

Two sets of PCR primers were used in this study; the first set was used to screen the *Brucella* as a genus, by amplification of genus-specific primers targeting the gene coding for 16 s rRNA as described earlier by Unver et al. (2006) with the following sequence: Fwd (5'-TGACAGACTTTTTCGCCGAA-3') and Rev (5'-TATGGATTGCAGCACCG-3'), and the second set was used for the detection of *B. melitensis* by amplification of *omp*31 genes for the confirmatory identification of *B. melitensis* which was previously described by Bricker (2002) with the sequences: Fwd 5'-TGCCGATCACTTAAGGGCCTTCAT-3' and Rev: 5'-AAATCGCGT C CTTGCTGGTCTGA-3'. PCR reaction was performed in a total volume of 25 µl containing 2 µl of DNA sample, 0.5 mM MgCl2, 0.2 mM dNTP Mix,1 U/reaction of *Taq* DNA polymerase, 1µL forward primer (10pmol/µL), and 1µL reverse primer (10pmol/µL); and the final volume completed with nuclease-free water. The amplification of 16S rRNA gene was conducted with initial denaturation at 95°C for 5 min, denaturation at 95°C for 30 s, annealing at 54°C for 1.5min, extension at 72°C for 1.5 min, and finally, the final extension at 72°C for 10 min. The *omp*31 gene amplification was performed with initial denaturation at 95°C for 5min, denaturation at 95°C for 1 min, annealing at 58°C for 1 min, extension at 72°C for 1 min, and finally the final extension at 72°C for 10 min. The PCR amplified products were examined by electrophoresis in a 1.2% agarose gel, stained with ethidium bromide (10 mg/mL) which was prepared to a final concentration of 0.5µg/mL. The PCR product (8µL) was mixed with 2µL of loading dye in gel apparatus and run at 70–80 volt/cm for 40–50min until the dye reached the half of the gel. The gel was photographed under the UV transilluminator.

III. Results and Discussion

A. Identification of Brucella Species using Biochemical Tests

In this study, both cultural isolation and identification were employed, as well as molecular detection by PCR of the causative agent of brucellosis. Of the 167 samples subjected to cultural isolation, 121 samples were recorded as *Brucella* species which initially identified as *Brucella* species based on gram staining and colony morphology, which observed on blood and *Brucella* selective agar plates after 4–5 days incubation at 37°C, and this is in coinciding with that recorded by Tille (2017); the colonies were round, convex, with smooth margin, translucent, honey-colored, glistening, and Gram-negative coccobacilli. Similar observations were also recorded by Habtamu et al. (2013). According to

biochemical reactions, *Brucella* organisms were found to be positive for catalase, oxidase, urease, and nitrate reduction tests and negative for methyl red, indole production, citrate utilization, and H2S production, The isolates were also able to grow in the presence of dyes, namely thionin, basic fuchsin, and safranin. Similar findings were reported by Erdenlig and Sen (2000).

B. Application of PCR

A PCR product of about 1412 bp was obtained from all the *Brucella* species isolates (Fig. 1) using genus-specific primer set for 16S rRNA as a target gene. Moreover, with a specific primer to an outer membrane protein (*omp*31), an amplified product size of about 731 bp (Fig. 2) was obtained from 97 isolates which was specific for *B. melitensis* with an overall isolation rate of 58%, and these results were in accordance with other studies who obtained similar size of amplified products for the detection of *B. melitensis* using the same pair of primers (Imaoka et al., 2007 and Al-Sanjary et al., 2014).

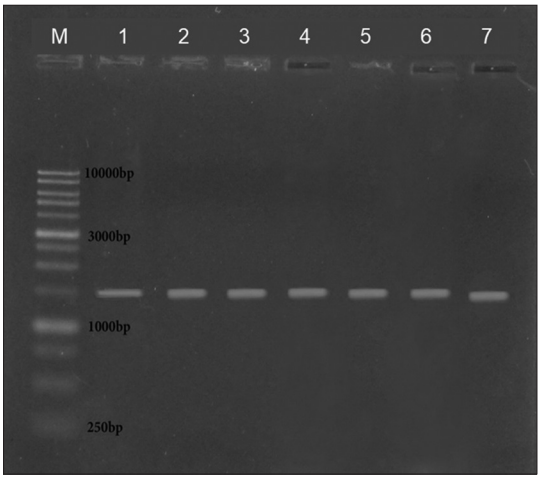

Fig. 1: DNA amplification of *Brucella* targeting 16 s gene using genus-specific primers, electrophorized on (1.2%) agarose gel, indicates positive sample that showed single band of 1412 bp.

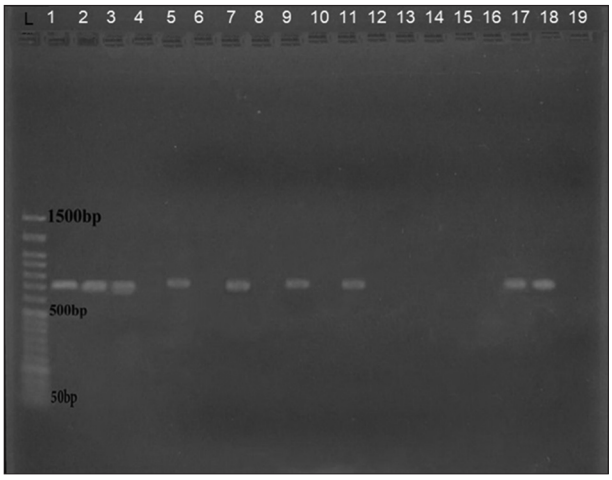

Fig. 2: DNA amplification of *B. melitensis* using species-specific primers targeting *omp*31 gene, electrophorized on 1.2 % agarose gel, indicates positive sample that showed single band of 731 bp.

The reason of selecting the gene *omp31*, that encode to the outer membrane proteins for detection of *B. melitensisis*, may due to that, *omp31* gene is highly diverse among *Brucella* species and strains therefore, it can be used to differentiate between them. Hence, molecular confirmation by PCR utilizing different gene targets has become the most common approach for confirmation of this pathogen (Shalini et al., 2018), due to that traditional methods are laborious, time consuming, and costly, and in addition, standard serological tests were used to detect *Brucella* lack sensitivity and specificity and are not able to distinguish between many species of *Brucella* (Elfaki et al., 2005). Obtaining high percentage of brucellosis in patients of Erbil city in Kurdistan region of Iraq agree with that reported by Gaff (2016) who mentioned to brucellosis as the most common bacterial zoonotic infections in Iraqi Kurdistan, which may due to insufficient preventive measures, the lack of adequate control programs, as well as, uncontrolled animal (as source of this bacteria) transportation through "open" borders, which increased the risk of spreading brucellosis in these regions, which remains a challenging health problem.

IV. Conclusion

The results of this study indicate that PCR technique efficiencies are higher than other methods used for species identification in terms of accuracy, specificity, sensitivity, and easy to perform, and hence, it has potential to be a promising tool for the diagnosis of acute disease; however, more studies from different geographical regions of the country on isolation of this important bacterial species are needed to understand the actual incidence of human brucellosis in the country, which will greatly help in the management of epidemiological studies.

References

Acha, N.P. and Zyfres, B.S., 2003. *Zoonoses and Communicable Diseases Common to Man and Animals*. 3rd ed., Vol. 1. Pan American Health Organization (PAHO), Washington, DC, pp.63-65.

Affi, M.M., Abdul-Raouf, U.M., El-Bayoumy, E.M., Montasser, A.M. and Mohamad, H.A., 2011. Isolation and biotyping of *Brucella melitensis* from upper Egypt. *Journal of American Science*, 7(3), pp.50-60.

Al-Sanjary, R.A., Mohammed, H.A. and Dahl, M.O., 2014. Using polymerase chain reaction technique (PCR) for detection *Brucella melitensis* in aborted ewes' milk in nineveh, Iraq. *Assiut Veterinary Medical Journal*, 60(140), pp.155-159.

Baddour, M.M. and Alkhalifa, D.H., 2008. Evaluation of three polymerase chain reaction techniques for detection of brucella DNA in peripheral human blood. *Canadian Journal of Microbiology*, 54, pp.352-357.

Bricker, B.J., 2002. PCR as a diagnostic tool for brucellosis. *Veterinary Microbiology*, 90, pp.435-446.

Bricker, B.J., Ewalt, D.R., MacMillan, A.P., Foster, G. and Brew, S., 2000. Molecular characterization of brucella strains isolated from marine mammals. *Journal of Clinical Microbiology*, 62, pp.38-48.

Chain, P.S., Comerci, D.J., Tolmasky,M.E., Larimer, F.W., Malfatti, S.A., Vergez, L.M., Aguero, F., Land, M.L., Ugalde, R.A. and Garcia, E., 2005. Whole-genome analyses of speciation events in pathogenic brucellae. Infection and Immunity, 73, pp.8353-8361.

Elfaki, M.G., Al-Hokail, A.A., Nakeeb, S.M. and Al-Rabiah, F.A., 2005. Evaluation of culture, tube agglutination, and PCR methods for the diagnosis of brucellosis in humans. *Medical Science Monitor*, 11(11), pp.69-74.

Erdenlig, S. and Sen, A., 2000. Isolation and biotyping of *Brucella* species in aborted sheep fetuses. *Pendik Veterinary Microbiology*, 31, pp.31-42.

Gaff, D., 2016. Brucellosis in Iraqi Kurdistan: An overview. *Journal of Entomology and Zoology Studies*, 4(4), pp.1113-1115.

Gee, J.E., De, B.K., Levett, P.N., Whitney, A.M., Novak, R.T. and Popovic, T., 2004. Use of 16 S rRNA genes sequencing for rapid confirmatory identification of brucella isolates. *Journal of Clinical Microbiology*, 42, pp.3649-3654.

Greenfield, R.A., Drevets, D.A., Machado, L.J., Voskuhl, G.W., Cornea, P. and Bronze, M.S., 2002. Bacterial pathogens as biological weapons and agents of bioterrorism. *American Journal of the Medical Sciences*, 323, pp.299-315.

Habtamu, T.T., Rathore, R., Dhama, K. and Karthik, K., 2013. Isolation and molecular detection of *Brucella melitensis* from disease outbreak in sheep and *B. abortus* from cattle farm by is711 and omp2a gene based PCR. *International Journal of Current Research*, 5(7), pp.1920-1925.

Hoover, D.L. and Friedlander, A., 2010. Brucellosis. In: Zajtchuk, R., editors. *Textbook of Military Medicine: Medical Aspects of Chemical and Biological Warfare*. US Department of the Army, Surgeon General, and the Borden Institute, Washington, DC, pp.513-521.

Imaoka, K., Kimura, M., Suzuki, M., Kamiyama, T. and Yamada, A., 2007. Simultaneous detection of the genus brucella by combinatorial PCR. *Japanese Journal of Infectious Diseases*, 60, pp.137-139.

Mantur, B., Parande, A., Amarnath, S., Patil, G., Walvekar, R., Desai, A., Parande, M., Shinde, R., Chandrashekar, M. and Patil, S. 2010. ELISA versus conventional methods of diagnosing endemic brucellosis. *American Journal of Tropical Medicine and Hygiene*, 83, pp.314-318.

Mugizi, D.R., Muradrasoli, S., Boqvist, S., Erume, J., Nasinyama, G.W., Waiswa, C., Mboowa, G., Klint, M. and Magnusson, U., 2015. Isolation and molecular characterization of brucella isolates in cattle milk in Uganda. *BioMed Research International*, 2015, pp.9-18.

Navarro, E., Casao, M.A. and Solera, J., 2004. Diagnosis of human brucellosis using PCR. *Expert Review of Molecular Diagnostics*, 4, pp.115-123.

Nielsen, K., Smith, P., Widdison, J., Gall, D., Kelly, L., Kelly, W. and Nicoletti, P., 2004. Serological relationship between cattle exposed to *Brucella abortus*, *Yersinia enterocolitica* O: 9 and *Escherichia coli* O157: H7. *Veterinary Microbiology*, 100, pp.25-30.

Pappas, G. and Memish, Z.A., 2007. Brucellosis in the Middle East: A persistent medical, socioeconomic and political issue. *Journal of chemotherapy*, 19, pp.243-248.

Probert, W.S., Schrader, K.N., Khuong, N.Y., Bystrom, S.L. and Graves, M.H., 2004. Real-time multiplex PCR assay for detection of *Brucella* Spp., *B. abortus*, and *B. melitensis*. *Journal of Clinical Microbiology*, 42, pp.1290-1293.

Rees, R.K., Graves, M., Caton, N., Ely, J.M. and Probert, W.S., 2009. Single tube identification and strain typing of *Brucella melitensis* by multiplex PCR. *Journal of Microbiological Methods*, 78, pp.66-70.

Scholz, H.C., Revilla-Fernández, S., Al Dahouk, S., Hammerl, J.A., Zygmunt, M.S., Cloeckaert, A., Koylass, M., Whatmore, A.M., Blom, J., Vergnaud, G. and Witte, A., 2016. *Brucellavulpis* Sp. Nov., Isolated from mandibular lymph nodes of red foxes (*Vulpes vulpes*). *International Journal of Systematic and Evolutionary Microbiology*, 66(5), pp.2090-2098.

Seleem, M.N., Boyle, S.M. and Sriranganathan, N., 2010. Brucellosis: A re-emerging zoonosis. *Veterinary Microbiology*, 140, pp.392-398.

Shalini, T., Jasbir, S.B., Randhir, S., Jatinder, P.S., Anil, K. and Arorac, N.K., 2018. Quantitative polymerase chain reaction based quantification of brucella DNA in serum of pre- and post-therapeutic occupationally exposed infected human population. *Journal of Infection and Public Health*, 11(4), pp.514-520.

Tille, P.M., 2017. *Bailey and Scott's Diagnostic Microbiology*. 14th ed. Mosby Elsevier, Philadelphia, PA, pp.470-474.

Unver, A., Erdogan, H.M., Atabay, H.I., Sahin, M. and Celebi, O., 2006. Isolation, identification, and molecular characterization of *Brucella melitensis* from aborted sheep fetuses in Kars, Turkey. *Revue de Medecine Veterinaire*, 157, pp.42-46.

Valdezate, S., Cervera, I., Hernández, P., Navarro, A. and Saéz-Nieto, J.A., 2007. Characterisation of outbreaks of human brucellosis and sporadic cases by the use of hyper-variable octameric oligonucleotide fingerprint (HOOF) variable number tandem repeats. *Clinical Microbiology and Infection*, 13, pp.887-892.

Wilson, K., 1990. Preparation of genomic DNA from bacteria, 241-245. In: Ausubel, F.M., Brent, R., Kimgston, R.E., Moore, D.D. and Struhl, K., editors. *Current Protocols in Molecular Biology*. Greene Publishing Associates, Inc., and John Wiley and Sons, Inc., New York.

Ying, W., Zhanli, W., Yaxian, Z., Liyun, B., Yue, Z., Chunfang, L. and Hui, Y., 2014. Polymerase chain reaction–based assays for the diagnosis of human brucellosis. *Annals of Clinical Microbiology and Antimicrobials*, 13, pp.31-43.

Study the Changes in (pH, Turbidity, Hardness, and Total Organic Carbon) Levels of Water using Plant Membrane (Palm Leaves Powder) and Aquatic Plant System (Vine Stems)

Ahmed A. Maaroof[1] and Fryad M. Sharif[2]

[1]Department of Chemical Engineering, Faculty of Engineering, Koya University, Koya KOY45, Kurdistan Region - F.R. Iraq

[2]Department of Manufacturing Engineering, Faculty of Engineering, Koya University, Koya KOY45, Kurdistan Region - F.R. Iraq

***Abstract*– Due to the increasing industrialization and urbanization, the requirement of clean water has been growing quite fast and it has the potential to keep increasing. There are many regions facing water crisis even some countries with a rich water source. In this study, three types of water (tap, ground, and light sewage) have been collected from different places in Ibrahim Ahmad site in Sulaymaniyah city/Kurdistan region – Iraq. The research studies the effects of plant membrane method, and aquatic plant system on the improvement of pH, turbidity, hardness, and total organic carbon (TOC) of water samples. In the plant membrane, palm leaves were crushed and used as a powder in filter bags; whereas in the aquatic plant system, vine stems were used by growing up the vines. The experimental results showed that the pH, hardness, turbidity, and TOC of water samples after using palm leaves powder and vine stems have been changed significantly with slight variation in some test results. The results of turbidity showed that using palm leaves powder as plant membrane was more effective than the vine stems in an aquatic plant system. On the other hand, the results of hardness and TOC tests of all water samples after using both methods proved that the vine stems method was more reliable than the palm leaves method. Finally, the pH results of all water samples after using both methods have been decreased to the normal range with a slight variation between the vine stems and palm leaves methods.**

***Index Terms*—Ground water, Light sewage water, Palm leaves, Tap water, Vine stems, Water improvement.**

ARO-The Scientific Journal of Koya University
Volume VII, No.1(2019), Article ID: ARO.10433, 8 pages
DOI: 10.14500/aro.10433
Received 02 July 2018; Accepted 14 March 2019
Regular research paper: Published 01 May 2019
Corresponding author's e-mail: fryad.mohammed@koyauniversity.org

I. Introduction

The global demand for clean water increases rapidly (Adewumi et al., 2010; Bixio et al., 2006), the major environmental concerns made and membrane filtration technology are chosen by the industry to reuse their wastewater and reduce their wastewater footprint on the environment. The membrane filtration will help increase plant efficiency by choosing the specific membrane system for the chosen wastewater, while reducing operating costs, and complying with increasingly stringent discharge regulations.

The term "wastewater" can be defined as the end-product or by-product liquids from municipal, industrial, and agricultural activities (Timothy, 2004: Tchobanoglous, 2003; Galan and Grossmann, 1998). In other words, liquid waste or wastewater is the water supply to the society after it has been used in several (Tchobanoglous, 2003). Fig. 1 demonstrates the general sources of wastewater in society.

II. Problems with Wastewater

There are several problems associated with discharging of wastewater into a water body (Kurniawan, et al., 2006). Foul gases are one of the main serious public concerns. Foul gases are generated as a result of decomposition of the organic matter of untreated wastewater when it is accumulated. Furthermore, untreated wastewater can affect human health through various kinds of harmful pathogenic microorganisms that can be found in the wastewater (Kalra, et al., 2011; Liberatore, et al., 2012; Wang et al., 2011). These microorganisms have the ability to live in the human intestinal tract. In addition, untreated wastewater is found to contain harmful compounds, such as toxic, mutagenic, or carcinogenic compounds; as well as a nutrient (Tchounwou, et al., 2012). The latter compounds can increase the growing rate of the aquatic plants. Therefore, to protect the environment and human from the diverse effects of

 http://dx.doi.org/10.14500/aro.10433

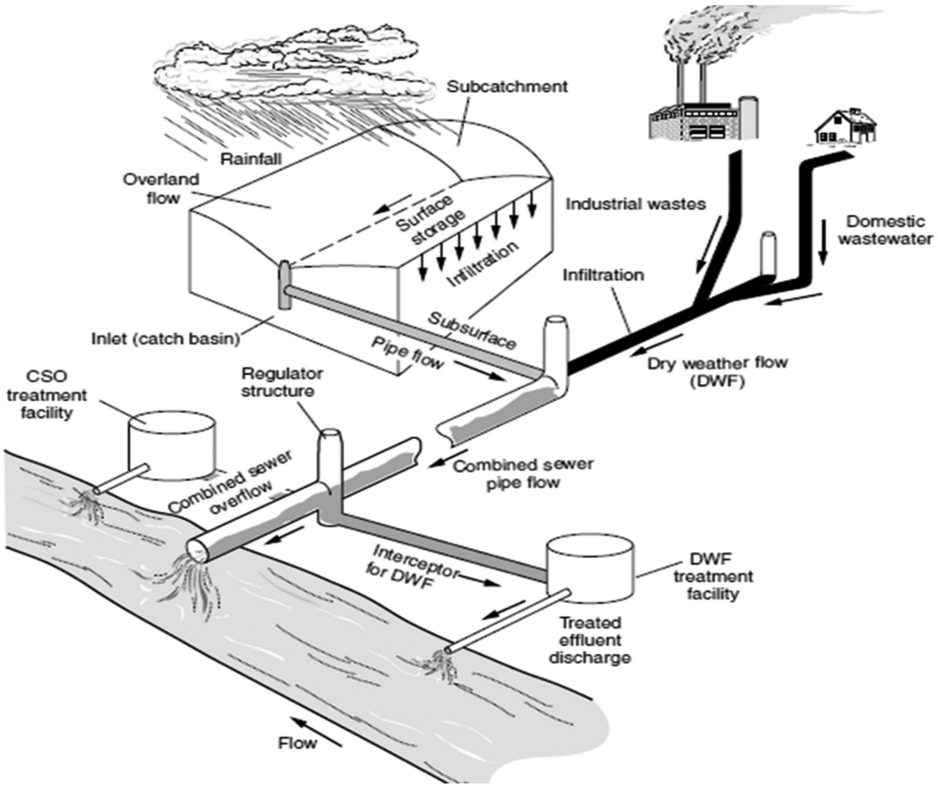

Fig. 1. A diagram of wastewater infrastructure (Timothy, 2004).

wastewater immediate and serious measures must be taken (Tchobanoglous et al., 2003; Salgot, et al., 2006).).

III. Wastewater Composition

Compositions of the most wastewater (both municipal and industrial) can be divided into three main categories according to its content: Physical, chemical, and biological characteristics. According to Muttamara (1996), actual quantities of chemical, physical, and biological characteristics present in wastewater refers to its compositions.

A. Physical Characteristics

The major physical characteristics of wastewater are solids (such as: Suspended and settled solids), color, odor, and temperature. Table I summarizes the main physical characteristics of wastewater and its sources.

B. Chemical Characteristics

The chemical compositions of wastewater can be divided into three groups: Organic compounds, inorganic compounds, and gases. Table II shows the sources of chemical composition found in wastewater and its sources.

C. Biological Characteristics

The biological constituents in the domestic and industrial wastewater (light and heavy wastewater) can be: Viruses, bacteria, plants, and animals (Dobson and Burgess, 2007). Table III summarizes all the biological constituents that can be found in the domestic and industrial wastewater with its possible sources.

TABLE I
Physical Characterizes of Wastewater (Metcalf and Eddy, 2003).

Physical properties	Source
Color	Domestic and industrial wastes, natural decay of organic materials
Odor	Decomposing wastewater, industrial wastes
Temperature	Domestic and industrial wastes
Solid	Domestic water supply, domestic and industrial wastes, soil erosion, inflow/infiltration

IV. Membrane Technology

Membrane technology can be defined as a physical treatment process in which the membrane is acting as a filter used for separating solid particles from water or wastewater (Pinnekamp and Friedrich, 2006: Pokhrel and Viraraghavan, 2004). This method cannot change the thermal, chemical, and biological properties of the separated materials (filtered liquid). The membrane technology can be used along with other purification and treatment methods such as biological treatment process. Globally, membrane technology application is becoming more and more broad. This technology was used for the first time in the field of water purification in the desalination of the brackish and sea in the arid zones, where its used for a long time in separating the valuable materials from small water volumes (e.g., in chemical and pharmaceutical industry, in biotechnology, and in food industry) (Pinnekamp and Friedrich, 2006).

TABLE II
Chemical Compositions of Wastewater (Metcalf and Eddy, 2003).

Chemical compounds	Source
Organic constituents	
Fats, oil, and grease	Domestic, commercial, and industrial wastes
Pesticides	Agriculture wastes
Carbohydrates	Domestic, commercial, and industrial wastes
Proteins	Domestic, commercial, and industrial wastes
Phenols	Industrial wastes
Priority pollutants	Domestic, commercial, and industrial wastes
Surfactants	Domestic, commercial, and industrial wastes
Others	Natural decay of organic materials
Inorganic constituents	
Chlorides	Domestic wastes, domestic water supply, and groundwater infiltration
Alkalinity	Domestic water supply, domestic wastes, and groundwater infiltration
Nitrogen	Domestic and agriculture
Heavy metals	Industrial wastes
pH	Commercial, domestic, and industrial wastes
Phosphorus	Natural runoff, domestic, commercial, and industrial wastes
Priority pollutants	Industrial, commercial, and domestic wastes
Sulfur	Domestic, commercial, and industrial wastes
Gases industrial waste	
Methane	Decomposition of domestic wastes
Hydrogen sulfide	Decomposition of domestic wastes
Oxygen	Surface water infiltration

TABLE III
Biological Compounds in Wastewater (Metcalf and Eddy, 2003).

Biological constituents	Sources
Plants and animals	Treatment plants and open watercourse
Viruses	Domestic wastes
Bacteria	Surface water infiltration, treatment plants, and domestic wastes

In fact, the operating principle of a membrane can be described in the wider sense like that of a filter. During the filtration, a substance mixture (feed of raw solution of water) is separated by the membrane. Permeate or filtrate is called on the part that passes through the membrane. The permeate represents the treated phase in the wastewater purification. The part of the wastewater that retained by the membrane is called brine or concentrate. Figure 2 illustrates the operational principles of membrane technology. The membrane technology is used in municipal and industrial wastewater treatment to satisfy the following; retention (e.g., solid matter including biomass and dissolved matter by reverse osmosis), purification (e.g., industrial water treatment and disinfection by retention of bacteria), concentration (e.g., recycling valuable substance), and finally fractionation (e.g., separation into two or more compounds) (Pinnekamp and Friedrich, 2006).

V. Aquatic Plant System

Aquatic plant system can be used for wastewater recovery and recycling by stabilizing the waste and removing the nutrient. The principal removal mechanisms of such a system are relaying on physical sedimentation and bacterial metabolic activity as in the conventional activated sludge and trickling filter (U.S. Environmental Protection Agency, 1991). In fact, plant assimilation of nutrients and its subsequent harvesting is another mechanisms for pollutant removal. The advantages of this system are low cost and easy maintenance compared to other treatment methods that, in turn, make it attractive to use. Recently, constructed ponds with aquatic plants are being applied widely as an effective way of treating municipal wastewater (Kanabkaew, and Puetpaiboon, 2004).

Pond with floating aquatic plants has been used for treating wastewater and/or improving water quality. For instance, the plant of the water chestnuts, water lettuce, heartleaf, hydrilla, duckweed and liverwort families, water hyacinths, and azollas have proven effective for water treatment. The duckweed family of plants provides for a biomass producing system wherein unwanted nutrients are harvested from aquatic systems by means of bioaccumulation to treat wastewater and/or improve water quality, and the plants are harvested as a cash crop (Ngo et al., 1993).

VI. Materials and Methods

The method used in this study was a simple direct way for water improvement by plant membrane and aquatic plant system. In this study, the samples were collected from three different places; homes (tap water), wells (groundwater), and drainages (light sewage water). The collected samples have been used to investigate the effects of two types of plants on improving the (pH, turbidity, hardness, and TOC) of water.

A. Experiments

In this study, all samples have been collected from Ibrahim Ahmad site in Sulaymaniyah city/Kurdistan region – Iraq. The following tests, turbidity, pH, hardness, and TOC, have been performed on the samples before and after applying the two methods. Usually, it takes up to 4 months to get good results, but generally, after 2 months of treatment process changes have been achieved.

Turbidity

Turbidity is the cloudiness or haziness of a fluid caused by large numbers of individual particles that are generally invisible to the naked eye, similar to smoke in the air (EPA, 2018). The measurement of turbidity is a key test of water quality. TN100 turbidimeter device was used in this study to measure the turbidity of the wastewater samples before and after treatment. This device uses an infrared light-emitting diode light source and delivers unprecedented laboratory repeatability and accuracy with a resolution of 0.01 nephelometric turbidity units (NTU) across an extended range of up to 20 NTU.

pH

pH is a measure of how acidic/basic water is. The range goes from 0 to 14, with seven being neutral. pH of <7 indicates acidity, whereas a pH of >7 indicates a base. pH is a measure of the relative amount of free hydrogen and hydroxyl ions in the water. The pH meter is a scientific instrument that measures the hydrogen ion concentration (or

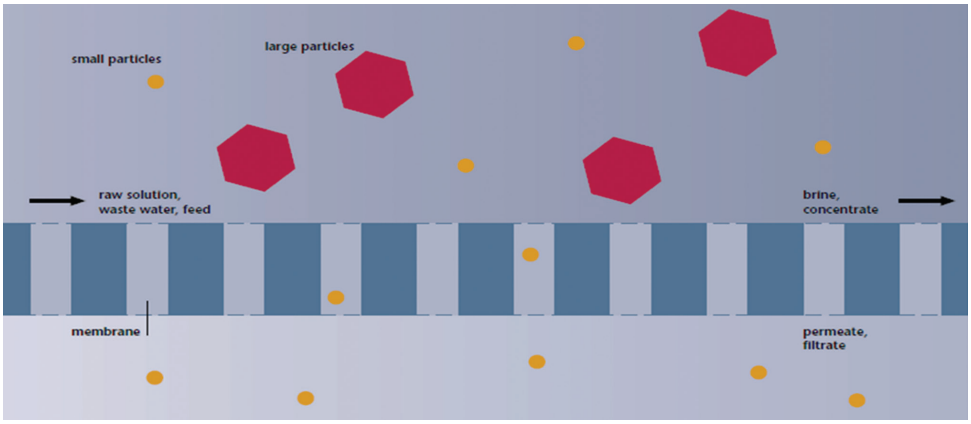

Fig. 2. Operation principle of the membrane (Pinnekamp and Friedrich, 2006).

pH) in a solution, indicating its acidity or alkalinity. The pH meter measures the difference in electrical potential between a pH electrode and a reference electrode. In this study, A Mettler Toledo pH meter was used to measure the pH of the wastewater samples before and after treatment.

Hardness

Hard water is water that has high mineral content (as opposed to "soft water"). Calcium is the most common mineral associated with water hardness. In general, hardness is not a health hazard; however, it can pose serious problems in industrial settings, where water hardness is monitored to avoid costly breakdowns in boilers, cooling towers, and other equipment. In domestic settings, hard water is often indicated by a lack of suds formation when soap is agitated in water, and by the formation of limescale in kettles and water heaters. In this study, ethylenediaminetetraacetic acid titration method was used to measure the permanent hardness of water samples before and after using membrane and aquatic plant system methods.

Total organic carbon (TOC)

An organic compound is any member of a large class of gaseous, liquid, or solid chemical compounds whose molecules contain carbon atoms. In this study, the TOC in the wastewater samples was measured by TOC analyzer (TOC fusion) Teledyne – Tekmar: Fusion – TOC analyzer. The fusion TOC analyzer utilizes powerful ultraviolet per-sulfate oxidation allowing superior carbon liberation from even the most challenging matrixes. The fusion TOC analyzer is able to achieve unprecedented low-end sensitivity from a non-dispersive infrared detector. TOC analyzer is built on the latest technology and is designed to offer productivity for a wide variety of applications.

B. Treatment Methods

Membrane filter bag method

In this method, palm leaves have been used to treat the wastewater samples. The leaves were first transformed from large solid pieces to soft powder through grinding using electric blade powder grinder "Silver Crest." The palm powder in size of few micrometer (100–200 µm approximately) was kept in closed fabric bags to avoid leakage to the water when

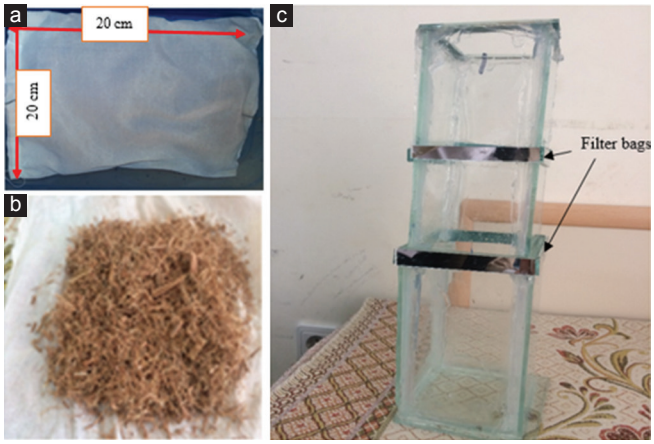

Fig. 3. *A* snapshot of membrane filter bags method: (a) Closed filter bag contain grinded palm leaves, (b) grinded palm leaves in open filter bag, (c) lab scale transparent glass container.

it used as a filter. In this method, two filter bags of grinded palm leaves were used to increase the efficiency of the process. Each bag weighted approximately 250 g, with a size of 20 cm length and 20 cm width. 5 l of each sample were used in this method separately passed through the filters. The bags were fixed in the middle of a transparent glass container (70 cm height and 22 cm width), whereas the water samples were added from the top and the clean water settled in the bottom, with a flow rate of 0.0166 mL/s approximately using stopwatch and measured cylinder. The filter bags were used mainly as a filtration step to remove any solid particles in water samples. The turbidity of water can be decreased using this method as the size of the palm leaves powder was very narrow, so the spaces available for water to move through in the bags are very small. Fig. 3 shows the palm leaves after grinding it in an open filter bag. In addition, the figure shows the lab scale glass container that was used in this method. Fig. 4 shows the schematic diagram of plant membrane system setup with the dimensions of the container and filter bags.

Vine stem method

The second treatment method was carried out using stems of vine tree by putting one head of a stem in the water horizontally. The organic pollution in the water can be removed as a result of vine growing. About 20 vine stems

were fixed in a layer made of cork (30 cm length, 15 cm width, and 4 cm thick). In this method, 5 l of each water samples were added to a separate container, and the vine stems then added to the container. After 2 months, the vines started to grow, and as a result, the water started to become cleaner. After 4 months, samples from each container were taken and tested as the changes in the pH and other properties stopped to appear. As the palm leaves are growing, TOC and hardness levels in water samples will reduce as the plant will use the organic matter and salt in the water to grow. Fig. 5 shows the vines in the plastic container.

VII. Results and Discussion

The following tables demonstrate the results of treating the three types of collected water samples (sewage, ground, and tap water) using both methods (palm leaves and vine stems). In each table, the result of three tests (pH, turbidity, TOC, and hardness) was included to evaluate the effects of the treating methods.

From the test results of groundwater sample in Table IV, it can be clearly seen that the palm leaves method was remarkably reduced the turbidity of wastewater sample from 6.07 NTU to 1.8 NTU after using palm leaves, unlike of the vine stem method that just reduced the turbidity by few NTU from 6.07 NTU to 5.97 NTU. Furthermore, the results obtained showed that the palm leaves method reduced the TOC levels in the groundwater sample from 84 ppm to just 74 ppm; whereas, the vine stem method reduced it from 84 ppm to 26 ppm after the treatment.

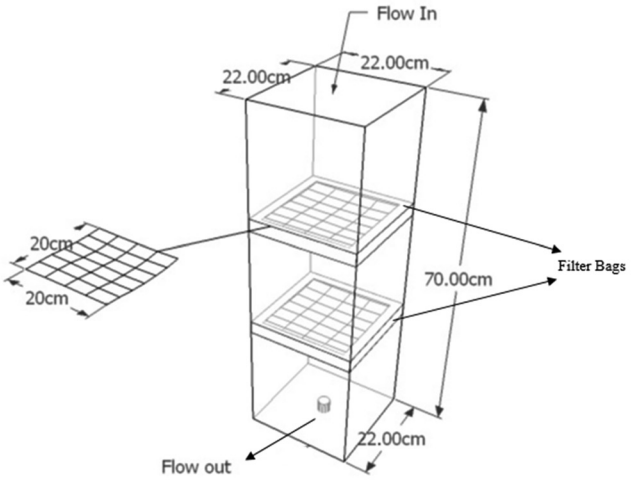

Fig. 4. Schematic diagram of plant membrane system setup.

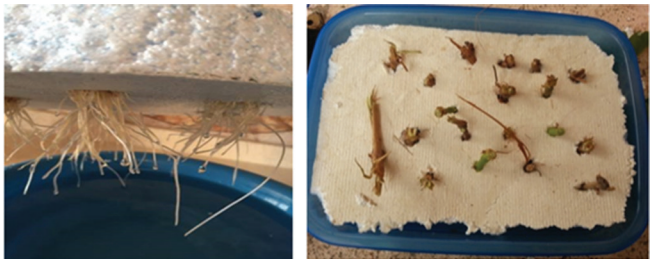

Fig. 5. Vines in lab scale container.

Based on sewage sample treatment results in Table V, its clear that the TOC and hardness were reduced by roughly 50% after using vine stem, whereas the pH was slightly reduced from 8.63 to the normal range of 7.44 and 7.7 after using both methods. However, the yurbidity was considerably decreased from 8.09 NTU to 2.14 NTU after using vine stem and to 1.91 NTU after applying palm leaves.

Regarding the test results of a tap water sample that is shown in Table VI, the turbidity and pH of the sample were slightly reduced after using both methods. However, the hardness of the sample was significantly reduced from 175 mg/L to 93 mg/L after using vine stem; unlike, the palm leaves method where it was slightly decreased the hardness from 175 mg/L to 110 mg/L. According to the results obtained, the TOC of the sample was remarkably reduced from 86.16 ppm to 11.5 ppm after using the vine stem and to 75 ppm after using the palm leaves.

In the following figures, the effects of the treating methods on the property of wastewater (pH, Hardness, TOC, and turbidity) were compared and demonstrated separately.

By comparing Figs. 6 and 7, it can be clearly seen that the pH of all wastewater samples was reduced to the normal range after applying both methods. However, there is a slight variation between the vine stem and palm leaves methods' results. Although there is a variation between the two methods' results, its not quite insignificant and can be ignored.

Figs. 8 and 9 show the changes in the turbidity levels after applying both methods on all water samples. The primary results of turbidity before treatment showed that the

TABLE IV
Test Results of Groundwater Sample (Before and After Treatment).

Test	Before treatment	After treatment	
		Vine stems method	Palm leaves method
Turbidity (NTU)	6.07	5.97	1.8
pH	8.72	7.66	7.53
Hardness (mg/L)	210	95	110
TOC (ppm)	84	26	74

TABLE V
Test Results of Light Sewage Water Sample (Before and After Treatment).

Test	Before treatment	After treatment	
		Vine stems method	Palm leaves method
Turbidity (NTU)	8.09	2.14	1.91
pH	8.63	7.44	7.7
Hardness (mg/L)	320	153	282
TOC (ppm)	87.35	37.9	65.12

TABLE VI
Test Results of Tap Water Sample (Before and After Treatment).

Test	Before treatment	After treatment	
		Vine stems method	Palm leaves method
Turbidity (NTU)	2.4	1.63	1.56
pH	8.63	7.91	7.39
Hardness (mg/L)	175	93	110
TOC (ppm)	86.16	11.5	75

http://dx.doi.org/10.14500/aro.10433

higher and lower turbidity levels were measured in sewage water and tap water samples with 8.09 NTU and 2.4 NTU, respectively. This is because the tap water sample may be treated before being supplied to households. Although both treatment methods had the same effect on sewage and tap water samples, the turbidity of sewage water was considerably reduced compared to tap water sample. From the results, its obvious that the treatment for the light sewage water sample has a higher efficiency than for the tap water sample which can be due to the tap water being clean before treating.

Moreover, the results obtained from treating the groundwater sample showed that the turbidity was considerably reduced from 6.07 NTU to 1.8 NTU when palm leaves used as treatment medium, whereas the turbidity was slightly reduced from 6.07 NTU to 5.97 NTU after treating the groundwater sample with vine stems. This prove that the palm method is more efficient than vine stem for treating groundwater.

From Figs. 10 and 11, the higher levels of hardness were measured in sewage water sample, whereas the lower levels were found in tap water. According to the figures, there is variation in the results of the treatment of sewage and groundwater using vine stem and palm leaves. The vine stem method has significantly reduced the hardness of sewage water from 320 mg/L to 153 mg/L and from 210 mg/L to 95 mg/L for the groundwater. However, the palm leaves method has slightly decreased the hardness of the sewage water from 320 mg/L to 282 mg/L and 210 mg/L to 110 mg/L for the groundwater. Furthermore, both methods have decreased the hardness of tap water from 175 mg/L to 110 mg/L using palm leaves method and to 93 mg/L using vine stem method. This vaiation in results prove that vine stem method is more reliable for a reduction in the hardness of wastewater samples.

By comparing Figs. 12 and 13, the TOC levels before treatment in the three wastewater samples were measured with slightly over 80 ppm. From Figs. 12 and 13, it can be clearly seen that the TOC levels were considerably decreased after using vine stem method; whereas, the TOC levels were slightly reduced after using palm leaves method. The most significant differences between vine stem and palm leave methods results can be noticed in the tap water sample. The vine stem was remarkably reduced the TOC in tap water from 86.16 ppm to 11.5 ppm, whereas the palm leaves were slightly decreased the TOC levels from 86.16 ppm to 75 ppm in the same sample. Furthermore, the TOC levels in the groundwater have considerably decreased after treatment with vine stem in comparison to treatment with palm leaves; whereas, the TOC in groundwater was dropped from 84 ppm to 26 ppm after using vine

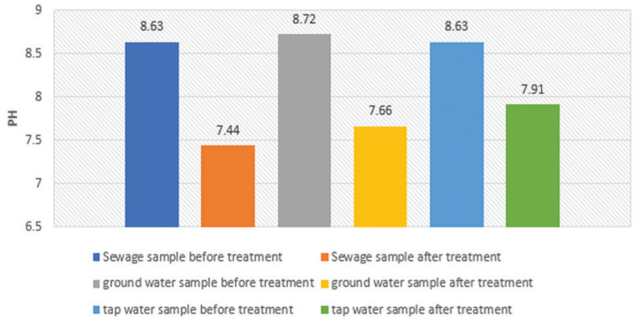

Fig. 6. Change in pH of water samples using vine method.

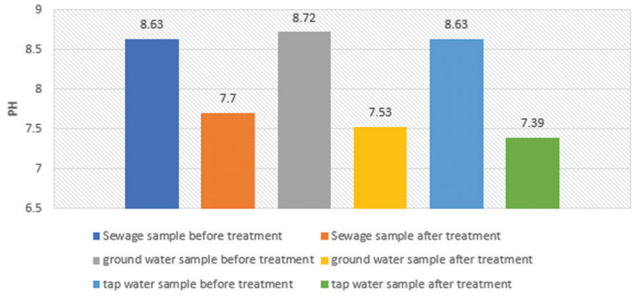

Fig. 7. Change in pH of water samples using palm leaves method.

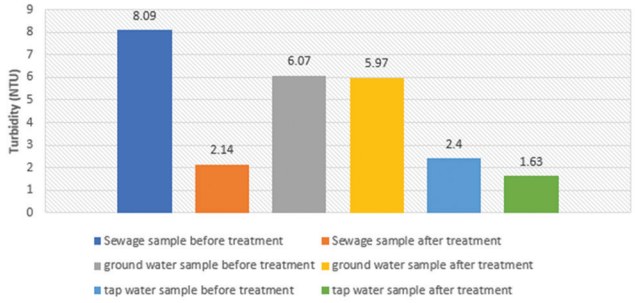

Fig. 8. Change in turbidity of water samples using vine stems method.

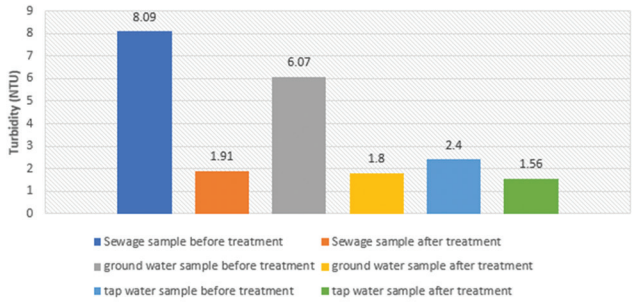

Fig. 9. Change in turbidity of water samples using palm leaves method.

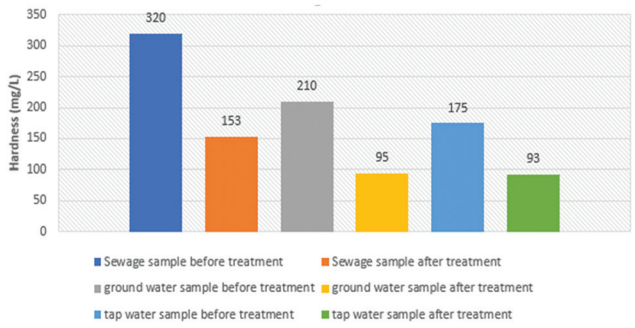

Fig. 10. Change in hardness of wastewater samples using vine stems method.

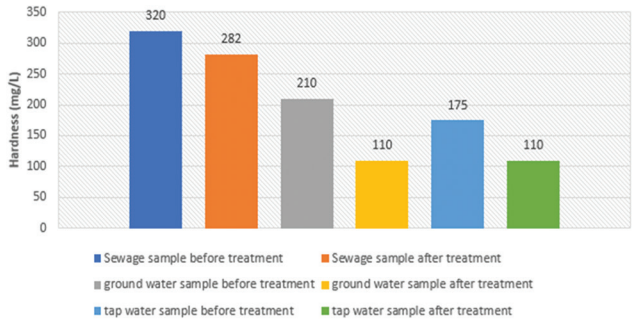

Fig. 11. Change in hardness of wastewater samples using palm leaves method.

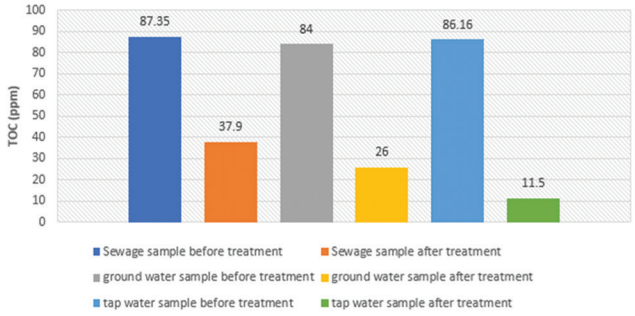

Fig. 12. Change in TOC of wastewater samples using vine stems method.

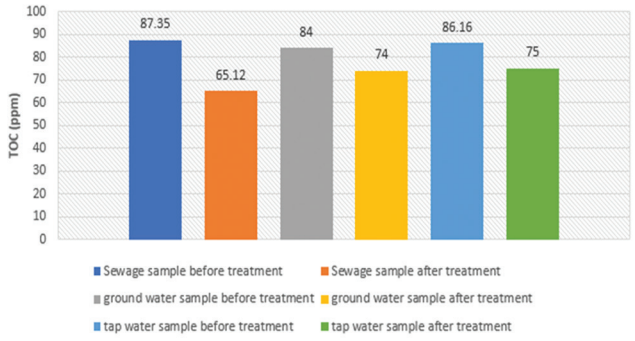

Fig. 13. Change in TOC of wastewater samples using palm leaves method.

stems method and to just 74 ppm after using palm leaves method. Although the TOC levels in sewage water were less decreased after using both methods in comparison to other water samples, the trend still shows that the vine stem method was more effective than palm leaves method. In general, the results proved that the vine stem method was more reliable, unlike the palm leaves method.

VIII. Conclusion

The research was carried out to study the effectiveness of two treatment methods on water samples' pH, turbidity, hardness, and TOC levels. Three different types of water (tap, ground, and light sewage) were used in this study. The first method (plant membrane) involved using two filter bags of palm leaves that showed a great effect on reducing water samples' turbidity. The second method (aquatic plant) includes using vine stems to improve water quality, whereas it showed a reduction in pH, hardness, and TOC levels for all samples.

Before applying the two methods, the highest and lowest levels of TOC, hardness, and turbidity are measured in sewage and tap water samples, respectively. The changes in these levels were measured after 3 days in palm leaves methods (plant membrane) and 4 months in vine stems methods (aquatic method). The results obtained showed that the pH levels were neutralized for all water samples. Furthermore, the turbidly of sewage and tap water was reduced to almost the same levels after applying both methods, except in groundwater where the membrane method was more effective than aquatic plant method. Moreover, the hardness of tap and groundwater samples was noticeably decreased to the same levels after using both methods, except in sewage water sample where the vine stem was more efficient than the other method. The TOC results of all samples after using both methods show that vine stem was very effective compared to the palm leaves method because the TOC levels results were sharply dropped after using vine stems, unlike to the palm leaves.

In general, using palm leaves powder as a membrane was a good method to reduce the turbidity of water as it includes an only physical process to separate the material mixture. However, an aquatic system using vine stem can be used as an effective way to reduce pH, hardness, and TOC levels, as the main purposes of such a system is waste stabilization and nutrient removal.

Acknowledgment

The authors would like to thank PIONEER Pharmaceutical Industries, Sulaymaniyah branch, for performing the tests for collected water samples and also appreciate the effort of Van Mahdy Hama and Hiran Raza in collecting the samples from the sites.

References

Adewumi, J.R., Ilemobade, A.A., and Van Zyl, J.E., 2010. Treated wastewater reuse in South Africa: Overview, potential and challenges. *Resources, Conservation and Recycling*, 55(2), pp.221-231.

Bixio, D., Thoeye, C., De Koning, J., Joksimovic, D., Savic, D., Wintgens, T.1., and Melin, T., 2006. Wastewater reuse in Europe. *Desalination*, 187(1), pp.89-101.

Dobson, R.S., and Burgess, J.E., 2007. Biological treatment of precious metal refinery wastewater: A review. *Minerals Engineering*, 20(6), pp.519-532.

EPA., *2018. 5.5 Turbidity. In Water: Monitoring and Assessment. Available from:*……https://www.archive.epa.gov/water/archive/web/html/vms55.html.

Galan, B., and Grossmann, I.E., 1998. Optimal design of distributed wastewater treatment networks. *Industrial and Engineering Chemistry Research*, 37(10), pp.4036-4048.

Kalra, S.S., Mohan, S., Sinha, A., and Singh, G., 2011. *Advanced Oxidation Processes for Treatment of Textile and Dye Wastewater: A Review*. Vol. 4. In 2nd International Conference on Environmental Science and Development, pp.271-275.

Kanabkaew, T., and Puetpaiboon, U., 2004. Aquatic plants for domestic wastewater treatment: Lotus (*Nelumbo nucifera*) and Hydrilla (*Hydrilla verticillata*) systems. *Aquatic*, 26(5), p.750.

Kurniawan, T.A., Chan, G., Lo, W.H., and Babel, S., 2006. Physico chemical treatment techniques for wastewater laden with heavy metals. *Chemical Engineering Journal*, 118(1), pp.83-98.

Liberatore, L., Bressan, M., Belli, C., Lustrato, G., and Ranalli, G., 2012. Chemical and biological combined treatments for the removal of pesticides from wastewaters. *Water, Air, and Soil Pollution*, 223(8), pp.4751-4759.

Metcalf and Eddy., 2003. *Wastewater Engineering, Treatment Disposal Reuse*. McGraw-Hill, New York.

Muttamara, S., 1996. Wastewater characteristics. *Resources, Conservation and Recycling*, 16, pp.145-159.

Ngo, V.H., Poole, W.D., Hancock, S.J., and France, T.T., 1993. Lemna corp. *Floating Aquatic Plant Water Treatment System with Sprayer System*. U.S. Patent 5,264,127.

Pinnekamp, J., and Friedrich, H., editors., 2006. *Membrane Technology for Waste Water Treatment*. FiW Verlag, New York.

Pokhrel, D., and Viraraghavan, T., 2004. Treatment of pulp and paper mill wastewaterm a review. *The Science of the Total Environment*, 333(1-3), p.37.

Salgot, M., Huertas, E., Weber, S., Dott, W., and Hollender, J., 2006. Wastewater reuse and risk: Definition of key objectives. *Desalination*, 187(1), pp.29-40.

Tchobanoglous, G., Burton, F.L., and Stensel, H.D., 2003. *Wastewater Engineering: Treatment and Reuse*. 4th ed., McGraw-Hill, New York.

Tchounwou, P.B., Yedjou, C.G., Patlolla, A.K., and Sutton, D.J., 2012. Heavy metal toxicity and the environment. *Molecular, Clinical and Environmental Toxicology*. Springer, Basel, pp.133-164.

Timothy, G.E., 2004. Chemistry of Wastewater. Available from: http://www.eolss.net/EolssSampleChapters/C06/E6-13-04-05/E6-13-04-05-TXT.aspx#1._Introduction. [Last accessed on 2017 Mar 22].

U.S. Environmental Protection Agency., 1991. *Constructed Wetlands and Aquatic Plant Systems for Municipal Wastewater Treatment*. U.S. Government Printing Office, Washington, D.C.

Wang, Z., Xue, M., Huang, K., and Liu, Z., 2011. Textile dyeing wastewater treatment. *Advances in Treating Textile Effluent*. Intech, Rijeka, Crotia.

The Economics of Using Solar Energy: School Buildings in Saudi Arabia as a Case Study

Faris A. Alfaraidy, Hassan A. Sulieman

Department of Civil Engineering, Northern Border University, P.O. Box 1321, Arar 91431, Northern Border – KSA

***Abstract*—As a result of increasing population and building of new schools in Saudi Arabia, the demand for electricity is growing rapidly. In this context, the utilization of renewable energy resources such as solar energy appears to goal since it is abundant and holds huge ecological and economic promise. This study aims to provide a new entrance in school buildings' design and construction by studying the current situation of energy consumption, the possibility of using solar cells, and the economics of its exploitation in school buildings. Interviews were conducted in school buildings at different levels in Arar city as a case study to collect data on energy consumption. Furthermore, a base case school building was selected for studying detailed energy consumption, and then, photovoltaic (PV) energy was proposed to use the on-grid system in accordance with governmental regulations. The study concluded that the use of PV energy in school buildings is economically feasible in addition to that more incentive from the government is needed for wide penetration use in Kingdom Saudi Arabia.**

***Index* Terms—Arar, photovoltaic energy, Renewable energy, School building design.**

I. Introduction

School buildings are one of the most important public facilities in our daily social life; it is the main source of education and culture. The growing population in Saudi Arabia leads to the growing demand for new schools. However, it is a rise in the country's school buildings and electricity demands. Therefore, Arar city has the same stress demands. High-energy consumption is one of the most serious problems in the world today. Recently, this topic has encompassed not only economic but also ecological and social importance. School buildings are typical structures, and their optimal energy consumption is a matter of public interest. Renewable energy can be a cost-effective and environmentally friendly in the way to generate energy. Installing a renewable energy project should be carried out in conjunction with energy saving and efficiency measures around buildings. The aim of this study is to assess the current situation of energy consumption in school buildings, to study the possibility of using solar cells in the school buildings, and to study the economics of energy exploitation within school buildings in Arar city, KSA.

ARO-The Scientific Journal of Koya University
Volume VII, No.1(2019), Article ID: ARO.10461, 6 pages
DOI: 10.14500/aro.10461
Received 15 October 2018; Accepted 13 March 2019
Regular research paper: Published 01 May 2019
Corresponding author's e-mail: hassan.abdualrahman@nbu.edu.sa

II. Literature Review

Vast secondary data as a literature review from different sources pertaining to solar energy system were investigated. Brief summary for utilizing solar photovoltaic (PV) as a source of energy is also presented in this study.

Rising energy demand in school buildings can be reduced by improving the efficiency of energy use. There are various methods used in benchmarking energy efficiency in buildings (Mukwaya and Lating, 2014; Harputlugil, 2017). The electric energy consumption may be reduced up to 35.3% and also air condition unit efficiency can also be increased by 31% using some energy-efficient methods which will be beneficial for schools in the management of electric usage and reduce the electric bill by the considerable amount of money (Hani, 2013). Furthermore, 43% reductions in peak cooling load can be achieved by improving envelope insulation, space ventilation, shading, glazing, artificial lighting variation, and evaporative cooling of the structure (Zurigat et al., 2003). In school buildings' microclimate conditions of the city, the location should be considered, for example, in hot regions a need for natural ventilation technique to obtain the thermal comfort conditions. However, in moderate climate regions, the application of the cross natural ventilation technique is necessary to obtain thermal comfort conditions which lead to an efficient energy-saving procedure (Nazhatulzalkis et al., 2017; van Hoof et al., 2010; de Dear and Bragerb, 2002; Givoni, 1992). Saudi Arabia aims to reduce carbon dioxide (CO_2) emissions from 28 to 26 billion standard cubic feet per day by the end of the year 2020 (Saudi

http://dx.doi.org/10.14500/aro.10461

National Transformation Program, 2020). It is clear that climate change is a threat that can only be tackled through the combined efforts of the international community, so the solution must be based on diverse clean, renewable, and environmentally sound sources of energy. Furthermore, Gregory Kats (2006) reported that green schools are less 2% costs than of conventional schools. Besides that, solar water heating can play an economically viable role toward energy security and greenhouse gas emission mitigation (Hafiz and Fahad, 2016).

Renewable energy most importantly, the solar energy source is not depleted, and it is distributed over a wide geographical area. At the end of 2012, the global renewable power capacity was exceeded 1500 GW, and it is expected that renewable energy can cover almost 13% of global energy demand by the year 2020 (Pazheri et al., 2014).

The application of solar energy in Saudi Arabia has been growing since 1960. Systematic major research and development of solar energy technologies were started by King Abdul-Aziz City for Science and Technology (KACST) in 1977. The Saudi Solar Radiation Atlas project was initiated in 1994 as a joint research and development project between the KACST Energy Research Institute and the US National Renewable Energy Laboratory (Said et al., 2008; Pazheri, 2014). Saudi Arabia started a "solar village" program to supply energy for three rural villages using solar power (Pazheri et al., 2011). Saudi Arabia sets a target to install about 54 GW of renewable power capacity by the year 2032, which represents 20% of total electricity production in Saudi Arabia sets a target to install about 54 GW of renewable power capacity by the year 2032, which represents 20% of total electricity production in KSA, and almost 41 GW of the targeted renewable power capacities may be met by solar power (REN21, 2013). The average annual rate of solar radiation is between 100 to 200 W/m2 in Europe, North America, Latin American, and Western Asia, whereas in the Arab countries, including the Gulf Cooperation Council countries, it reaches to about 250 W/m2, so Saudi Arabia is one of the most potentially productive regions and PV technologies may perform well at any Saudi location (Pazheri, 2012, Zell et al., 2015).

III. The Case Study

Arar city is located in the north side of Saudi Arabia, in the heart of a vast rocky limestone plain. It lies about 1100 km northwest of Riyadh, about 60 km from the Iraqi border, and 1451.3 km away from Jeddah town. The climate of Arar is described as a hot desert with annual average temperature varies from 13.75°C to 7.375°C as shown in Table I. Winds generally blow from the east or west, rarely from the south. It is noteworthy that the rainfall in the region has declined gradually over recent years. It is also noted that snow is not uncommon, falling on average every 2–3 years. A PV system is proposed to be connected to operate in parallel with the National Electric Grid.

IV. Materials and Methods

A literature review was cited for PV as a source of energy in different areas and, especially, in school buildings. Previous studies in solar energy and its economy were also cited as explained above. A total of 12 interviews were conducted at the Arar city schools, six schools were girls' schools, whereas the other six schools were boys' schools. On the girls' and boys' schools' side, two schools were elementary schools, two schools were intermediate schools, and two schools were secondary schools. The main reason for this kind of selection was to get a picture and understand the use and need of energy in different school levels in Arar city. In this study, qualitative and quantitative methods were applied to generate valid and reliable data. In particular, an in-depth structured interview sheet was applied in the whole process and the Arabic language was used throughout to generate the data. The data were collected through the interview and direct observation. These data were focused on the historical background of the school buildings aiming energy consumption. A typical school building was selected in Arar city. All the building details were used as an input for later examinations of software and simulation. The details include building drawings as plans, elevations, and perspectives. In addition, it includes the building structure details alongside with most common external walls and thermal insulations. The building case study is representative of a major school building style in the city. It is considered a low rise building which comprises mainly from three floors, with 1200 m^2 each floor area. The roof has a skylight gross area of 200 m^2. All elements which affect heat flow in the space are described including walls, windows, doors, roofs, skylights, floors, occupants, lighting, electrical equipment, miscellaneous heat sources, infiltration, and partitions as shown in school plan in Fig. 1. The government regulates

TABLE I
Annual average temperature

Parameter	Annual average temperature, °C
Mean dry bulb temperature	13.75
Mean coincident wet bulb temperature	7.375

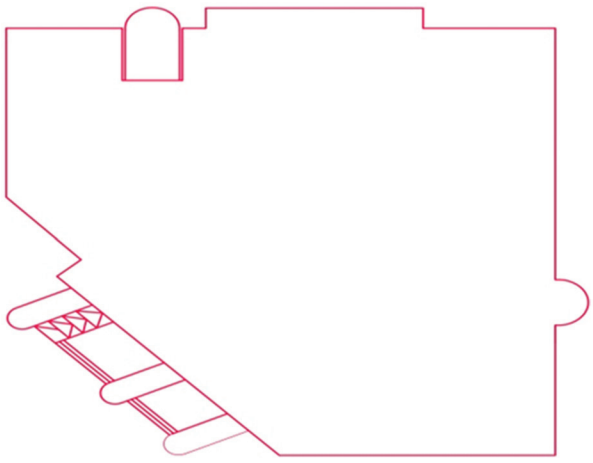

Fig. 1. School building layout.

that the use of PV system in the grid should be in the zone of 15% of the transformer capacity, and hence, the use of 150 kW is proposed to be used in the base case school building.

V. Results and Discussion

A. Conventional School Interview

The interview sheet was designed to explore the existing data of energy consumption of different conventional school types in Arar city. The sheet consists of two parts, the first part concentrated on general data such as school name, location, number of students, number of administration, number of teachers, and volume of school, and hence, the second part concentrated in various type sources of energy consumption such as lighting and air condition systems. This sheet gave results that the main source of energy consumption is air condition, lighting, and other appliances such as computers. Furthermore, the main type of air conditioning type used is window type of two-tone (24000 British Thermal Unit, BTU) and the main lighting type is fluorescent, whereas the window materials are the aluminum type with single glass layer and the material of the door is a steel type. Furthermore, Al interviewed school buildings are heat insulated but not well insulated. Then, the energy consumption varies from 36,000 kWh in small school buildings to 155,000 kWh in large school buildings and, in average, varies from 6,250 kWh, 81,500 kWh, and 116,500 kWh in intermediate, secondary, and primary schools, respectively, as presented in Table II.

B. Base Case School Building

The base case school building is an intermediate school located in Arar city 30.90 N and 43.48 W; it is front elevation facing southwest and has a rectangular shape with one corner cut a triangle. The building has three floors each of 3.5 m height of overall height 10.5 m. The building floor dimension is 41 × 37 m and the whole building is occupied by 500 students in addition to teaching and administrative staff. The external wall area of each floor is approximately 1625 m^2 structured as 25-mm thickness external marble particle plaster, hollow concrete blocks with 50-mm extruded polystyrene, and 25-mm thickness internal cement sand plaster. The floor structure is 100-mm thickness slab on grade and roof structure is composed of 10-mm ceramic tiles, 20-mm thickness cement sand mortar, 50-mm thickness aggregate sand, 50-mm extruded polystyrene, 200-mm thickness horde slab, and 25-mm thickness internal roof plaster. The type of windows is aluminum frame with 6-mm thickness unclear glass, 12-mm air gap, and 6-mm thickness glass and without thermal breaks with no curtains. The general characteristics of power density in the building are described in Table III.

Applying Hourly Analysis Program version 4.99 (HAP 4.99) software for the above characteristics, it is found that the absorptivity and overall U-Value for wall and roof are listed in Table IV.

The base case building is characterized as a low-rise building which falls in zone 2 (SBC601), The base case building is characterized as a low-rise building which falls in zone 2 (SBC601), and hence its heat transfer coefficient is listed in Table V.

Using ASHRAE standards for the above characteristics, it is found that the heat transfer coefficient for wall, skylight, windows, doors, and roof were listed in Table VI.

The actual heat transfer coefficients compared with the SBC601 code are illustrated in Table VII.

To predict the school energy consumption, some assumptions were drawn as illustrated in Table VIII.

Using the HVAC assumption that illustrated in Table VIII, the consumption of energy in the school building was set in Table IX.

C. Design of Solar PV Plant

A solar PV system was planned to be installed at intermediate school. The technical specifications of the PV system planned to be installed are included in Table X.

TABLE II
School buildings' average energy consumption

Energy consumption	School type		
Average	Primary	Intermediate	Secondary
Energy (kWh)	116,500	61,250	81,500

TABLE III
Summary of power density in base case

Characteristic	Description of base case school building
Solar absorbance	0.55 external walls, MC 0.35 for the roof, LC
Lighting power density	3 W/m^2 ground floor 2 W/m^2 1st floor 2 W/m^2 2nd floor
Equipment power density	2.0 kW ground floor 1.0 kW 1st floor 1.0 kW 2nd floor
Infiltration	0.5 ACH
HVAC System type	2 tons in classrooms and 25 tons central system
Thermostat setting	24°C for cooling 20°C for heating
Coefficient of performance	2.87
Weather file	IWEC2

MC: Medium color, LC: Light color, ACH: Air volume change per hour, IWEC2: Internal weather for energy calculations, V2.0.

TABLE IV
Overall u-value and absorptivity

Wall	The wall outside surface color	Medium external color
	Absorptivity	0.675
	Overall U-value	1.21 W/(m².°C)
Roof	The wall outside surface color	Light external color
	Absorptivity	0.675
	Overall U-value	0.764

TABLE V
The base case building heat transfer coefficient

Component	Area, m²	Heat transfer coefficient (W/m².°C)
Wall	1625	1.21
Roof	1000	0.764
Skylight	196	6.975
Windows	158	4.082
Doors (metal)	10	5.93

 http://dx.doi.org/10.14500/aro.10461

TABLE VI
THE BASE CASE BUILDING ENERGY TEFFICIENT REQUIREMENT

Wall and roof: Overall heat transfer coefficient (W/m^2.°C)	Wall: 0.387 For zone 2 Roof: 0.238 For zone 2
Door overall heat transfer coefficient (W/m^2. °C)	2.839
Window overall heat transfer coefficient (W/m^2. °C)	2.668 for all zones
Solar heat gain coefficient, SHGC	For all zones≥0.25
SRI for envelope color	SRI≥50
Water absorption for insulation materials	≤0.3%
Continuous insulation	Insulation shall be continuous across all structural members without thermal bridges other than fasteners and service openings.
Ventilation	qv=0.05*A+3.5*Noc Where, qv=Ventilation required flow rate, L/s, A=Conditioned floor area m^2 and, Noc=Number of occupants
Infiltration in fenestration	Fenestration and skylights should not exceed 1.5 L/s/m^2
Infiltration in doors	a. Air leakage for sliding doors should not exceed 1.5 L/s/m^2 b. Air leakage for swinging doors should not exceed 2.5 L/s/m^2
Vertical fenestration area	≤25% of the air-conditioned area for all zones
Skylight fenestration area	≤3% of the gross roof area for all zones
Interior lighting power allowance	≤10 W/m^2 for all zones
Energy efficiency ratio, EER	EER ≥11, for cooling capacities 12,000–240,000BTU/h, and EER≥10 for cooling capacities ≥240000 BTU/h.

SRI: Surface reflectance index

TABLE VII
ANNUAL HEAT TRANSFER COEFFICIENT COMPARED TO SBC601 REQUIREMENT

Component	Area, (m^2)	Building heat transfer coefficient (W/m^2.°C)	SBC601 heat transfer coefficient (W/m^2.°C)
Wall	1625	1.21	0.387
Roof	1004	0.764	0.238
Skylight	196	6.975	2.668
Windows	158	4.082	2.668
Doors	10	5.93	2.839

TABLE VIII
ASSUMPTIONS OF HVAC CONSUMPTION (KWH)

Assumptions	Parameters
Energy efficiency ratio, EER (BTU/h)/kW	10
Number of months per semester	4
Number of semesters	2
Weekends	Friday and Saturday
HVAC running hours per day	3–7

HVAC

D. Economic Evaluation of PV System

The economics of PV are related to their efficiency as well as to their optics. The cost of PV materials is often expressed on a per-unit-area basis, but the modules are often sold based on cost per watt that potentially generated under peak solar illumination conditions. A 150 kW solar PV system is installed of 607,666.50 SAR total cost, that is, 4.051 SAR/watt. The electricity bill is decreased by the solar-generated energy as illustrated in Table XI.

TABLE IX
THE SCHOOL ENERGY AVERAGE MONTHLY CONSUMPTION

Item	Power, kW	Consumption, kWh/month
HVAC	217	8,554
Lighting and other appliances	65.2	3,459
Average predicted electrical consumption	282.7	12,013

HVAC

TABLE X
TECHNICAL SPECIFICATIONS OF PV SYSTEM

Description	Measurement
Present connected load	282.70 kW
Installed PV system	151.20 kW
Number. of panels	577
Peak power capacity per panel	260 Watt
Solar PV module capital cost	607,666.50 SAR
Module efficiency	17%
Lifetime	25 years

PV: Present value

Assumptions:

1. Price of electricity from grid 0.32 SAR/kWh.
2. The electric load of the building (282.7 kW) exceeds the system size (150 kW).

The prospective owner of a solar system may have many reasons for purchase. They may wish to do their part for the investment or to lead others by example. However, one criterion that is likely to be high on the list of most individuals is the financial benefit of the investment. Several economic criteria have been proposed to do this job. Some useful criteria used for economic analysis of PV projects are reviewed: Payback period and net present value (NPV) methods.

E. Payback Period

Payback period is simply the number of years it takes to recoup an investment, and it can be calculated using equation (1) as shown below:

Payback period = investment/income or savings (1)

From the table, the investment is calculated as 720,000 SAR and the income or savings annually is 73,584 SAR, then

Payback period = 607,666.50/73,584 = 8.26 years.

F. NPV

The most broadly used economic evaluation tool for capital projects, for example, a solar system is the NPV, since it provides the actual value of completing a project. This is, however, more detail and complex than the payback strategy; in addition, it gives the best results since it considers the time value of money. NPV can be calculated using the formula in equation (2).

$$NPV = \sum_{t=0}^{n} \frac{C_i}{(1+r)^t} \quad (2)$$

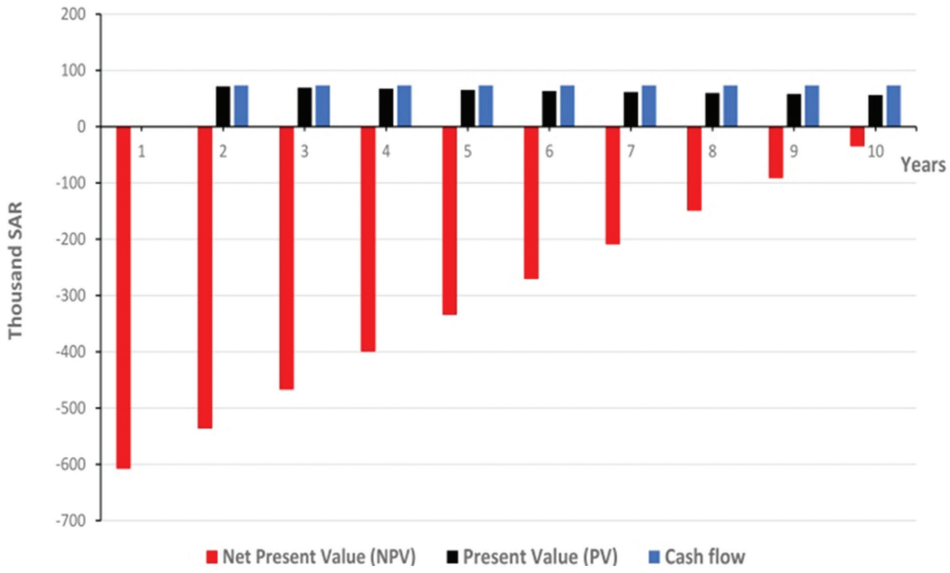

Fig. 2: Net present value calculations.

TABLE XI
MONTHLY SAVINGS AFTER PV INSTALLATION

Parameter	Amount/Year in SAR
Annual electricity bill before PV	138,681.3
Annual electricity bill after PV	39,480.3
Net savings	99,201

PV: Present value

TABLE XII
NET PRESENT VALUE CALCULATION

Year	Cash flow	Discount rate	PV	NPV
0		1.000000000		(607,666.50)
1	73584	0.970873786	71440.7767	(536,225.70)
2	73584	0.942595909	69359.9774	(466,865.70)
3	73584	0.915141659	67339.7839	(399,525.90)
4	73584	0.888487048	65378.4309	(334,147.51)
5	73584	0.862608784	63474.2048	(270,673.30)
6	73584	0.837484257	61625.4415	(209,047.86)
7	73584	0.813091511	59830.5258	(149,217.34)
8	73584	0.789409234	58087.8891	(091,129.45)
9	73584	0.766416732	56396.0088	(034,733.44)
10	73584	0.744093915	54753.4066	020,109.97

PV: Present value, NPV: Net present value

Where,
S = Initial cost of the system,
t = Time for cash flow,
N = The total time of the project,
R = The discount rate, and C_i = the net cash flow at time t.

Then, S = 607,666.50 SAR and the NPV are calculated in Table XII and Fig. 2, assuming that the constant cash flow with a fixed tariff of power during the coming years in addition to the constant discount rate of 3%.

VI. Conclusion

The objective of this paper is to understand the economic impact of increasing deployment of PV energy at significant scale in the KSA. The economics of solar PV can be a challenging problem to get a handle on; however, the costs of solar cells are expected to continue to decline. The value of solar PV installation is expected to be beneficial when solar PV may become economically feasible. This analysis was carried out for Arar city school buildings when PV system proposed to be on grid connection. The expected value of solar will continue to be dominated by radiation and the cost of electricity in the KSA. This type of quantification of financial value for solar cells and related technologies should play a vital role in the decisions made by the system user. The regions where solar PV shows economic feasibility are expanding and this analysis predicts that there is an ability to host a profitable PV installation. Finally, it is recommended that, for this system to be widely used toward sustainable energy systems, innovation and more government incentives should be made so as to increase the system economic feasibility.

Acknowledgment

The authors gratefully acknowledge the approval and the support of this research study by the grant No. ENG-20171-7-F-7150 from the Deanship of Scientific Research at Northern Border University, Arar, K.S.A.

References

de Dear, R.J. and Bragerb, G.S., 2002. Thermal comfort in naturally ventilated buildings: Revisions to ASHRAE standard 55. *Energy and Building*, 34(6), pp.549-561.

Givoni, B., 1992. Comfort climate analysis and building design guidelines. *Energy and Building*, 11(1), pp.11-23.

Hafiz, M.A. and Fahad, A.A.,2016. Optimum selection of solar water heating (SWH) systems based on their comparative techno-economic feasibility study for the domestic sector of Saudi Arabia. *Renewable and Sustainable Energy Reviews*, 62, pp.336-349.

Hani, H.S., 2013. Auditing and analysis of energy consumption of an educational building in a hot and humid area. *Energy Conversion and Management*, 66, pp.143-152.

Harputlugil, T., 2017. *Energy Efficient Building Design Development: A Retrospective Approach*. International Symposium on Energy Efficiency in Buildings, Ankara, Turkey, pp.296-303.

Kats, G., 2006. *Greening America's Schools: Costs and benefits*. A Capital E Report. Available from: https://www.usgbc.org/drupal/legacy/usgbc/docs/Archive/General/Docs2908.pdf.

Mukwaya, N.I. and Lating, P.O., 2014. *Benchmarking Energy Efficiency of Commercial Office Buildings in Kampala.* 2nd. International Conference on Advances in Engineering Sciences and Applied Mathematics, Istanbul, Turkey.

Nazhatulzalkis, J., Nurul, I.M., Mohd, F.K. and Suriani, N.A.W., 2015. Thermal comfort of a residential building in Malaysia at different micro-climates. *Procedia Social and Behavioral Sciences*, 170, pp.613-623.

Pazheri, F.R., 2014. Solar power potential in Saudi Arabia. *International Journal of Engineering Research and Applications*, 4(9), pp.171-174.

Pazheri, F.R., Malik, N.H., Al-Arainy, A.A., Essam, A.A., Ahmed, I. and Safoora, O.K., 2011. *Smart Grid Can make Saudi Arabia Megawatt Exporter*. IEEE Asia-Pacific Power and Energy Engineering Conference (APPEEC), Wuhan, China, pp.1-4.

Pazheri, F.R., Malik, N.H., Othman, M.F. and Babar, M., 2012. Optimum power dispatch problems: An overview. *International Journal of Engineering Inventions*, 1(6), pp.49-54.

Pazheri, F.R., Othman, M.F., Malik, N.H., Al-Arainy, A.A. and Khan, Y., 2014. *Optimum Power Dispatch Management in Presence of Renewable Energy and Energy Storage*. Energy and Power, Science and Technology Publishing Inc., Available from: https://www.researchgate.net/publication/264971511.

REN21, 2013. *MENA Renewables Status Report*. Renewable Energy Policy Network for the 21st Century.

Said, S.A.M., El-Amin, I.M. and Al-Shehri, A.M., 2008. Renewable Energy Potentials in Saudi Arabia (Lecture). Workshop. American university of Beirut, Faculty of Engineering and Architecture, Beirut.

van Hoof, J., Mazej, M. and Hensen, J.L.M., 2010. Thermal comfort: Research and practice. *Frontiers in Bioscience*, 15, pp.765-788.

Zell, E., Gasim, S., Wilcox, S., Katamoura, S., Stoffel, T., Engel-Coxa, J. and AlSubie, M., 2015. Assessment of solar radiation resources in Saudi Arabia. *Energy and Building*, 119(1), pp.422-438.

Zurigat, Y.H., Al-Hinai, H., Jubran, B.A. and Al-Masoudi, Y.S., 2003. Energy efficient building strategies for school buildings in Oman. *International Journal of Energy Research*, 27(3), pp.241-253.

Physicochemical Quality and Genotoxic Potential of Wastewater Generated by Canteen Complex

Ebenezer O. Dada, Chioma M. Agu and Modupe O. Akinola

Department of Cell Biology and Genetics, Environmental Biology Unit, Faculty of Science, University of Lagos, Akoka, Yaba, Lagos, Nigeria

Abstract—Canteens generate high volumes of wastewater that should constantly be subjected to physicochemical and genotoxicity screening. In this study, the wastewater generated by a canteen complex was screened for physicochemical properties and genotoxic potential using standard procedures and *Allium cepa* chromosome assay. Results showed that the wastewater had total suspended solids, total dissolved solids, and total hardness concentrations of 120.70 mg/l, 554.50 mg/l, and 500.00 mg/l, respectively. The chloride concentration of the wastewater (7873.60 mg/l) was much higher than the recommended limit of 250 mg/l. The wastewater inhibited root growth in *A. cepa* at 0.1%, 1%, 10%, 25%, 50%, and 100% concentrations but promoted root growth at 2% and 5% concentrations. The wastewater was highly mitodepressive, with mitotic inhibition generally increasing with rising concentrations. The major chromosomal aberrations observed in *A. cepa* exposed to different concentrations of canteen wastewater were vagrant, sticky, and bridged chromosomes. No chromosomal aberration was observed in onion roots exposed to water (control). The differences in total chromosomal aberrations across wastewater concentrations were not statistically significant ($P > 0.05$). In view of these results, the practice of discharging untreated canteen wastewater into drainage canals may not be environmentally sustainable.

***Index Terms*—Chromosomal aberration, Environment, Mitodepressive, Pollution.**

I. Introduction

Catering or food service is an essential but complex system that provides food and beverages away from home (Davies et al., 1998; Fusi et al., 2016). A component part of the catering system is the canteen service. A canteen prepares and serves food and drink to its customers. In canteen services, meals are usually cooked and served on premise, but many canteens also offer takeaway and food delivery services.

Canteen wastewater is the water that has been used for cleaning meats and vegetables, washing dishes and cooking utensils, or cleaning the floor and other associated substances. Canteens use high volumes of water in food preparation and generate correspondingly high volumes of contaminant-bearing wastewater. Canteen wastewater can be both a useful resource and an environmental burden. Canteen wastewater contains plant growth-promoting nutrients and may possibly be used for farming irrigation to aid crop production after undergoing preliminary treatments to reduce fats, oils, and greases and other pollutants. However, in most situations, canteen wastewater negatively impacts communities and ecosystems. Even if canteen wastewater is used for irrigation, the nutrients may leach down the soil to pollute groundwater after sometime (Mahmood and Maqbool, 2006). Canteen wastewater is typically associated with contaminants and other environment-polluting parameters such as organic compounds, biological oxygen demand (BOD), suspended solids, oil and grease, chemical oxygen demand (COD), proteins, carbohydrates, and a host of others (Mohamed et al., 2015; Ying et al., 2011).

Since the services that canteens and other catering services provide are crucial to basic and daily human needs, a huge number of canteens and food outlets are usually found in cities and towns. In many countries, wastewaters from catering and food services constitute the largest source of domestic wastewater (Mohamed et al., 2015). The wastewater generated and discharged, on daily basis, by these vast number of canteen and other food outlets usually constitutes an enormous burden to the environment and public health (Chen et al., 2000). The wastewater composition of canteens varies from culture to culture and from one ethnic group to another. Even for a particular canteen, the composition of wastewater generated may vary from time to,time because the food served for breakfast, lunch, and dinner may vary.

Unlike in many developed countries, where catering service is effectively and efficiently regulated such that canteens and cafeteria must, of necessity, install wastewater treatment facilities to reduce fats, oils, and greases in wastewater (Rainwater, 2004; Mohamed et al., 2015), in Nigeria and some other developing countries, canteens are less regulated, do not

ARO-The Scientific Journal of Koya University
Volume VII, No.1(2019), Article ID: ARO.10463, 8 pages
DOI: 10.14500/aro.10463
Received 26 October 2018; Accepted 14 April 2019
Regular research paper: Published 01 May 2019
Corresponding author's e-mail: eodada@unilag.edu.ng

 http://dx.doi.org/10.14500/aro.10463

install any wastewater treatment facility, and consequently dispose of their wastewater untreated in gutters and drainage canals. Such direct discharge of wastewater down the drain by canteens constitutes enormous extra load to the receiving environment. Among other adverse effects, the oil and grease components of the wastewater may aggregate and break down to generate unpleasant odor. Although studies have shown that some physicochemical qualities of canteen wastewater such as organic compounds, BOD, suspended solids, oil and grease, COD, proteins, carbohydrates, and metals are capable of inducing environmental pollution (Chen et al., 2000; Mahmood and Maqbool, 2006; Ying et al., 2011; Mohamed et al., 2015; Fusi et al., 2016), more research attention needs to be focused on the genotoxic potential of these wastewaters.

Genotoxicity is the ability of a substance to interact with the DNA and/or the cellular mechanisms that maintain the stability of the genome. Genotoxicity tests are used for the prediction of carcinogenicity, and their outcomes are often reliable in interpreting carcinogenicity studies. Onions (*Allium cepa*) are among the plants that are used for short-term environmental mutagen studies. *A. cepa* assay is sensitive and reliable short-term chemical mutagen-induced chromosomal aberration tests. *A. cepa* tests are cheap, and the results can easily be analyzed, unlike other short-term tests (Feretti et al., 2007; Leme and Marin-Morales, 2009). This study aimed to assess the genotoxic potential of wastewater generated by a canteen complex.

II. Materials and Methods

A. Collection of Samples

The approximately equal sized and healthy looking bulbs of *A. cepa* (onions) used for this study were purchased from Oyingbo Market (latitude 6º45'N and longitude 3º.39'E), Lagos Mainland Local Government Area of Lagos State, Nigeria. The canteen complex whose wastewater was used for the study is located within the main campus of the University of Lagos, Nigeria. There are 12 canteens that make up this complex, with each serving different foods to under- and post-graduate students. The wastewater was collected from the drainage canal into which every canteen in the complex discharged its effluent. The wastewater was collected in a 5-L plastic container in the morning at about 9.00 am local time, when cooking activities were always at its peak, and was immediately taken to the laboratory for physicochemical analyses and genotoxicity test.

B. Physicochemical Analyses of Canteen Wastewater

Canteen wastewater was analyzed for physicochemical properties including color, pH, electrical conductivity, turbidity (nephelometric turbidity unit [NTU]), total suspended solids (TSS), total dissolved solids (TDS), nitrate (NO_3^-P), phosphate (PO_4^{3-}P), dissolved oxygen (DO), BOD, COD, total alkalinity, total acidity, total hardness, and metals (Zn, Pb, Cd, and Cr). The tests were carried out using the methods described by the American Public Health Association (1998) and as done by Dada et al. (2017). Some of the tests are briefly described.

Color

The color of wastewater was determined using HACH DR 2000 direct reading spectrophotometer method 8025. Each sample was first filtered and measured against previously filtered deionized water as blank at a wavelength of 455 nm.

Test for pH

The pH of the wastewater was estimated using test-2 pH meter. The meter was first standardized against buffer solutions pH 4, 7, and 9.2 after which samples were tested in turn.

Electrical conductivity (EC) and TDS

The electrical conductivity and TDS of the wastewater were measured using portable combined electrical conductivity/TDS/temperature meter (HM Digital COM-100). The meter was standardized with 342-ppm sodium chloride calibration solution testing.

Turbidity (NTU)

The turbidity of the wastewater was measured using HACH DR 2000 direct reading spectrophotometer method 8237. The turbidity of the sample was estimated against deionized water as a blank at a wavelength of 450 nm.

TSS

TSS was measured using HACH DR 2000 direct reading spectrophotometer method 8006. The TSS of each sample was estimated against deionized water as blank at a wavelength of 810 nm.

Nitrate (NO_3^- N)

The nitrate concentration of the wastewater was determined using the HACH DR 2000 direct reading spectrophotometer method 8039. The HACH NitraVer 5 Nitrate Pillow was used in 25 ml of water sample against the sample not treated with NitraVer 5 reagent as blank at a wavelength of 500 nm.

Phosphate (PO_4^{3-} P)

The phosphate concentration of the wastewater was determined using the HACH DR 2000 direct reading spectrophotometer method 8048. The HACH PhosVer 3 Phosphate Powder Pillow reagent was used in 25 ml of the water sample against deionized water as blank at a wavelength of 890 nm.

DO

The DO of each water sample was determined using a portable Orion-3 DO meter. The DO meter was calibrated with water saturated with air after which the different water samples were tested in turn.

BOD_5^{20}

The BOD of the wastewater sample was determined using the Winkler method. The method involves estimating the DO content of the water sample on day 0 (day of sampling) and then the 5th day of the 5-day incubation, at 20°C in the dark against a blank.

COD

To determine the COD of wastewater sample, 0.4 g of $HgSO_4$ was placed in a reflux flask and 20 ml of water

sample was added and mixed properly. Thereafter, 10 ml of 0.25 N $K_2Cr_2O_7$ solution, four seeds of anti-bumping granules, and 30 ml of H_2SO_4-Ag_2SO_4 reagent were added. The flask was then connected to the condenser and slowly heated. The mixture was refluxed for 2 h and then cooled. The walls of the condenser were washed down into the flask with distilled water. The resulting mixture was diluted to 150 ml and titrated with 10 N ferrous ammonium sulfate (FAS) solution using ferroin as an indicator. A color change from blue green to wine red indicated the end point. A blank experiment with distilled water in place of sample was also performed. The procedure was repeated for each sample and the COD value computed is given below.

$$\text{COD in mg / l} = \frac{(V1 - V2) \times N \times 800}{X} \quad (1)$$

Where,
V1 = Volume of FAS for blank
V2 = Volume of FAS for water
N = Normality of FAS
X = Volume of sample taken.

Alkalinity

The alkalinity of the wastewater sample was determined by the acid-base titrimetric method. Aliquot portion of each water sample was titrated with standard solution of sulfuric acid (0.05 M) using methyl orange as indicator.

Acidity

Two drops of phenolphthalein indicator was added to 50 cm^3 of each wastewater sample. Each was then titrated with 0.02 N NaOH until the color changed to faint pink, characteristic of pH 4.5.

$$\text{Acidity as Mg / l}CaCO_3 = \frac{A \times N \times 500 \times D}{\text{Volume of sample}} \quad (2)$$

Where,
A = Volume of NaOH used at end point
N = Normality of NaOH
D = Dilution factor.

Total hardness

To determine the acidity of the wastewater sample, 100 cm^3 of the sample was measured into a 250 cm^3 conical flask and 2.0 ml buffer solution was added and mixed properly. Eight drops of Eriochrome black T indicator were introduced, followed by titration with 0.01 M EDTA solution. A color change from wine red to pure blue indicated the end point. The entire procedure was carried out for each of the water samples. Total hardness for each sample was then computed.

$$\text{Total hardness in mg / L } CaCO_3 = \frac{\text{ml of EDTA} \times M \times 100 \times 1000}{\text{ml of sample}} \quad (3)$$

C. Determination of Metals

To determine the concentrations of metals, the wastewater sample was first digested. Wastewater sample was first thoroughly shaken, after which 100 ml was transferred into a beaker and 5 ml of concentrated nitric acid was added. The beaker was placed on a hot plate and evaporated to dryness. It was then cooled and another 5 ml concentrated nitric acid was added. Heating was continued until a light-colored residue was observed. Then, 1 ml of concentrated nitric acid was added and the beaker was warmed slightly to dissolve the residue. The walls of the beaker were then washed with distilled water. The volume was adjusted to 50 ml. Zinc, Pb, Cd, and Cr were determined in the digested samples using the atomic absorption spectrophotometer.

D. Procedure for A. cepa Genotoxicity Assay

Genotoxicity test was adapted from Adegbite and Olorode (2002), Olorunfemi et al. (2011), and Dada et al. (2017; 2018). The onions used for this test were first sun-dried for 1 week, after which the dry ones were selected for the test. The outer scales and the dried roots present at the base of the sun-dried onions were carefully peeled off with a sharp razor blade to expose the fresh meristematic tissues (primordial). The peeled bulbs were placed in distilled water during the cleaning procedure to prevent the fresh meristematic tissues (primordial) from drying up. The onions were thereafter grown in distilled water at room temperature (25–31°C) for 24 h. When the roots were about 1–2 cm long, they were exposed to eight concentrations of canteen wastewater (0.1%, 1%, 2%, 5%, 10%, 25%, 50%, and 100%) prepared using distilled water as diluents and control, for 24, 48, and 72 h. The test substrates were changed daily. Six onion bulbs were set up for each concentration, of which the best five were selected for morphological (root growth inhibition) and cytological (chromosomal aberration) evaluations.

To determine the root growth inhibition by canteen wastewater, the root lengths of the onions exposed to each wastewater concentration and the ones exposed to distilled water (control) were measured at 24, 48, and 72 h of exposure. Mean root length, percentage root length, and percentage root length inhibition were calculated according to the equations indicated below.

$$\text{Mean root length (cm)} = \frac{\text{Summation of root lengths}}{\text{Total number of root lengths counted}} \quad (4)$$

$$\%\,\text{Root length} = \frac{\text{Root length in test solution}}{\text{Root length in control}} \times 100 \quad (5)$$

$$\%\,\text{Root length inhibition} = \frac{\text{Root lenth in control} - \text{Root length in test solution}}{\text{Root length in control}} \times 100 \quad (6)$$

Chromosomal aberration study was carried out by the squash technique for onion root as described by Adegbite and Olorode (2002). At the end of the exposure periods, the roots of onion bulbs with the best growth at each concentration were removed with forceps and fixed in 1:3 aceto-alcohol. Chromosome samples were taken from the root tips containing actively growing cells. One root tip was squashed on each slide and stained with acetocarmine for 10 min. Coverslips were carefully lowered onto the slide to exclude air bubble. To prevent the possible drying out

http://dx.doi.org/10.14500/aro.10463

of the preparation, the coverslips were sealed on the slides with clear fingernail polish. Each prepared slide was viewed under the ×40 objective of the light microscope (Leica 2000 Phase Contrast Microscope) to observe its mitotic stages. Data on total cells, total dividing cells, and cells carrying chromosomal aberrations were taken from five microscope fields for each of the different concentrations and the control (Fiskesjo, 1985).

The mitotic index was calculated by expressing the number of dividing cells as a percentage of total cells counted for each of the treatments and the control.

$$\text{Mitotic index} = \frac{\text{Number of dividing cells}}{\text{Total number of cells}} \times 100 \quad (7)$$

$$\%\,\text{Mitotic inhibition} = \frac{\text{Mitotic index in control} - \text{Mitotic index in test solution}}{\text{Mitotic index in control}} \times 100 \quad (8)$$

The frequency of chromosomal aberrations was calculated by expressing the number of aberrant cells as a percentage of total dividing cells for each treatment. Scoring of chromosomal aberrations was taken from five microscopic fields for each of the different wastewater concentrations (Fiskesjo, 1985).

$$\%\,\text{Chromosomal aberration} = \frac{\text{Number of total chromosomal aberrations}}{\text{Total number of dividing cells}} \times 100 \quad (9)$$

E. Statistical Analysis of Data

The total number of chromosomal aberrations across all canteen wastewater concentrations was analyzed by one-way analysis of variance. Mean differences were compared for significance by the least significant difference *post hoc* test. All analyses were carried out by SPSS (Version 22).

III. Results

A. Physicochemical Properties of Canteen Wastewater

The result of the physicochemical analysis of canteen wastewater as presented in Table I showed that the wastewater had TSS, TDS, and total hardness concentrations of 120.70 mg/l, 554.50 mg/l, and 500.00 mg/l, respectively. The DO and BOD of the wastewater were 19.00 mg/l and 110.20 mg/l, respectively. The chloride concentration of the wastewater (7873.60 mg/l) was much higher than the recommended limit of 250 mg/l set by the Lagos State Environmental Protection Agency. All the metals assessed were present in lower concentrations than the recommended limits except Zn whose concentration of 27.10 mg/l was higher than the recommended limit of 5.0 mg/l.

B. Effect of Canteen Wastewater on the Root Growth of A. cepa

At the end of 24-h test period, there was no visible damage to the root tips of onions in the control and in test solutions.

TABLE I
Physicochemical Properties of Canteen Wastewater

Canteen wastewater qualities	Concentrations	
	Canteen wastewater	LASEPA limits
Physical		
Temperature (0°C)	26.80	na
pH	4.54	5.5–9.0
Color	Cloudy	na
Turbidity (NTU)	109.72	na
Conductivity(μS/cm^3)	1109.00	na
Total suspended solids mg/l	120.70	100.0
Total dissolved solids mg/l	554.50	2,100.0
Chemical		
Total hardness mg/l	500.00	na
Total alkalinity mg/l	25.00	na
Total acidity mg/l	50.00	na
BOD mg/l	110.20	50.0
COD mg/l	180.00	na
Dissolved Oxygen mg/l	19.00	2.0
Chloride mg/l	7,873.60	250.0
Nitrate mg/l	29.50	na
Sulfate mg/l	2.00	na
Phosphate mg/l	12.10	na
Metals		
Zinc mg/l	27.10	5.0
Lead mg/l	0.024	0.1
Cadmium mg/l	0.001	0.02
Chromium mg/l	0.004	0.036
Biological		
Bacteria	3.40×10^5	na
Coliform	1.10×10^2	na
Yeast	nd	Na

LASEPA: Lagos State Environmental Protection Agency, nd: Not detected, na: Not available. NTU: Nephelometric turbidity unit, BOD: Biological oxygen demand, COD: Chemical oxygen demand

At 48 h and 72 h, there was a slight darkening in the root tip of onions in 50% and 100% canteen wastewater. However, canteen wastewater inhibited root growth in *A. cepa* at 0.1%, 1%, 10%, 25%, 50%, and 100% concentrations. Canteen wastewater of 100% concentration induced the highest root growth inhibition of 34.82% and 59.56% in *A. cepa*, respectively, at 24 and 72 h of exposure. Canteen wastewater of 50% concentration induced the highest onion root growth inhibition of 44.95% at 48 h of exposure. Canteen wastewater of 1% concentration induced the least root growth inhibition of 12.83%, 14.80%, and 16.04% at 24, 48, and 72 h of exposure, respectively.

On the other hand, canteen wastewater also promoted root growth in *A. cepa* at 2% and 5% concentrations. Relative to the control, canteen wastewater of 2% concentration induced more growth in *A. cepa* roots by 27.23%, 40.82%, and 49.01% at 24, 48, and 72 h of exposure, respectively (Table II).

C. Mitotic Activity in A. cepa Exposed to Canteen Wastewater

The mitotic activity in *A. cepa* exposed to different concentrations of canteen wastewater showed that the number of dividing cells and the percentage mitotic index decreased with increasing concentrations at 24, 48, and 72 h of

exposure, whereas the percentage mitotic inhibition increased with rising concentrations. The number of dividing cells and percentage mitotic index also decreased with increasing period of exposure, whereas percentage mitotic inhibition increased with period of exposure. At 24 h of exposure, 100% canteen wastewater induced the highest percentage mitotic inhibition of 91.52%. At 48 and 72 h of exposure, the lowest percentage mitotic inhibitions of 87.31% and 91.03%, respectively, were induced by 2% canteen wastewater (Table III).

C. Chromosomal Aberrations Induced by Canteen Wastewater

The chromosomal aberrations observed in *A. cepa* exposed to different concentrations of canteen wastewater in this study were vagrant, sticky, and bridged chromosomes. Sticky chromosomes were the most frequent (370). C-mitosis was observed only in one root cell. No chromosomal aberration was observed in onion roots exposed to water (control). Canteen wastewater of 5% concentration induced the highest chromosome aberration of 99, whereas canteen wastewater of 2% concentration induced the least, 44. However, the differences in total aberrations across wastewater concentrations were not statistically significant ($P > 0.05$).

The percentage chromosome aberration induced by canteen wastewater in onion roots increased with rising concentrations except for 2% wastewater that deviated from this pattern by inducing the least percentage aberration of 29%. Canteen wastewater of 100% induced the highest aberration of 96.1%, whereas 0.1% wastewater induced percentage aberration of 34. 0%. Canteen wastewater of 10% and 50% concentrations induced 61.0% and 76.7% chromosomal aberrations, respectively (Table IV). Representative photomicrographs of normal and aberrant chromosomes are shown in Figures 1-8.

IV. Discussion

Nutrition is a basic biological function of life. The increasing human population has brought about global awareness for the need to create more raw and cooked foods but with only little attention paid to the environmental impact of rising food production. This is more so in developing countries, where food outlets, including cafeteria and canteens, may be set up without installing any wastewater treatment facility and without carrying out an adequate environmental impact assessment.

Some physicochemical parameters of the canteen wastewater under the study, including conductivity, BOD, and chloride, were high or above regulatory limits but were relatively lower than those assessed in some previous studies (Chen et al., 2000; Mohamed et al., 2015). However, some other parameters of the wastewater (including pH, TSS, BOD) were not only lower than those assessed in previous studies but were also below or within regulatory limits. The very high conductivity of the canteen wastewater must have been occasioned by the equally very high chloride concentration. The high chloride concentration in the wastewater may indicate greater use of table salt and salt-containing spices in different canteens contained within the complex.

TABLE II
Effect of Canteen Wastewater on The Root Growth Of *A. cepa*

Canteen W/water conc.	Mean root growth			% Root growth			% Root growth inhibition		
	24 h	48 h	72 h	24 h	48 h	72 h	24 h	48 h	72 h
Ctr	2.6±1.06	2.6±1.29	3.0±1.44	100	100	100	0	0	0
0.1%	1.8±0.84	2.0±1.26	1.9±1.98	69.63	77.04	61.98	30.37	23.00	38.02
1%	2.2±0.88	2.2±0.88	2.2±1.07	87.17	85.20	83.96	12.83	14.80	16.04
2%	3.2±1.33	3.7±1.72	4.6±2.30	127.23	140.82	149.01	−27.23	−40.82	−49.01
5%	2.7±0.97	2.7±1.15	4.0±2.77	105.76	102.81	130.54	−5.76	−2.81	−30.60
10%	1.9±0.83	1.9±0.92	1.7±1.11	72.51	71.43	56.70	27.49	28.57	43.30
25%	1.9±0.86	1.7±1.00	1.8±0.74	72.51	65.82	57.80	27.49	34.18	42.20
50%	1.9±48	1.4±0.66	1.3±0.69	74.35	55.05	41.75	25.64	44.95	58.24
100%	1.7±0.85	1.7±0.85	1.2±0.80	65.18	63.52	40.44	34.82	36.48	59.56

W/water: Wastewater, Conc: Concentration, Ctr: Control, Hrs: Hours, *A. cepa: Allium cepa*

TABLE III
Mitotic Activity in *A. cepa* Exposed to Canteen Wastewater

CW conc	Total cells counted			Number of dividing cells			Mitotic index (%)			Mitotic inhibition (%)		
	24 h	48 h	72 h	24 h	48 h	72 h	24 h	48 h	72 h	24 h	48 h	72 h
Ctr	1000	1000	1000	513	513	513	51.30	51.30	51.30	0	0	0
0.1%	965	932	921	57	52	41	5.91	5.58	4.45	88.50	89.12	91.33
1%	942	918	873	68	46	36	7.22	5.01	4.12	85.93	90.23	91.97
2%	948	875	848	53	57	39	5.59	6.51	4.60	89.10	87.31	91.03
5%	916	887	832	51	39	24	5.57	4.40	2.89	89.14	91.43	94.37
10%	903	852	809	46	33	21	5.09	3.87	2.60	90.08	92.46	94.93
25%	885	831	783	43	35	16	4.86	4.21	2.04	90.53	91.79	96.02
50%	874	828	765	40	29	17	4.58	3.50	2.22	91.07	93.18	95.67
100%	851	813	741	37	27	13	4.35	3.32	1.75	91.52	93.53	96.59

CW: Canteen wastewater, Conc: Concentration, Ctr: Control, Hrs: Hours, *A. cepa: Allium cepa*

 http://dx.doi.org/10.14500/aro.10463

TABLE IV
CHROMOSOMAL ABERRATIONS INDUCED IN *A. CEPA* ROOT CELLS EXPOSED TO DIFFERENT CONCENTRATIONS OF CANTEEN WASTEWATER

CW conc.	Chromosomal aberration type										
	Sticky			Vagrant			Bridged anaphase			Total Abr.	% Abr.
	24 h	48 h	72 h	24 h	48 h	72 h	24 h	48 h	72 h		
0.1%	5	8	11	3	11	3	6	3	1	51	34.0
1%	17	15	17	5	2	2	0	1	0	59	39.3
2%	11	11	15	7	0	0	0	0	0	44	29.5
5%	23	18	13	2	5	7	15	13	3	99	86.8
10%	14	15	20	1	7	1	3	0	0	61	61.0
25%	23	21	18	0	0	0	7	4	1	74	78.7
50%	18	19	14	4	7	2	0	2	0	66	76.7
100%	25	10	9	11	15	4	0	0	0	74	96.1
Total		Sticky			Vagrant			Bridged anaphase		528	
		370			99			59			

CW Conc: Canteen wastewater concentration, Abr: Aberration. The differences in total aberrations across wastewater concentrations were not significant ($P>0.05$). *A. cepa: Allium cepa*

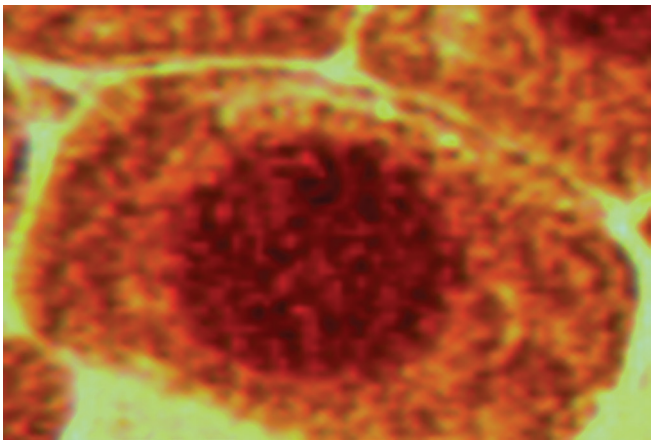

Fig. 1. Normal prophase.

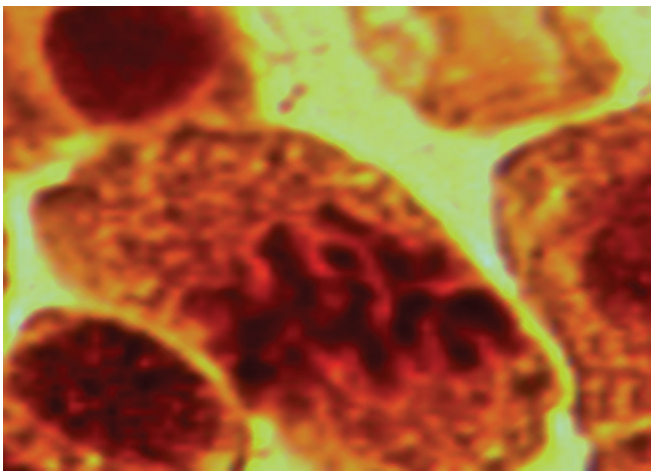

Fig. 2. Normal metaphase.

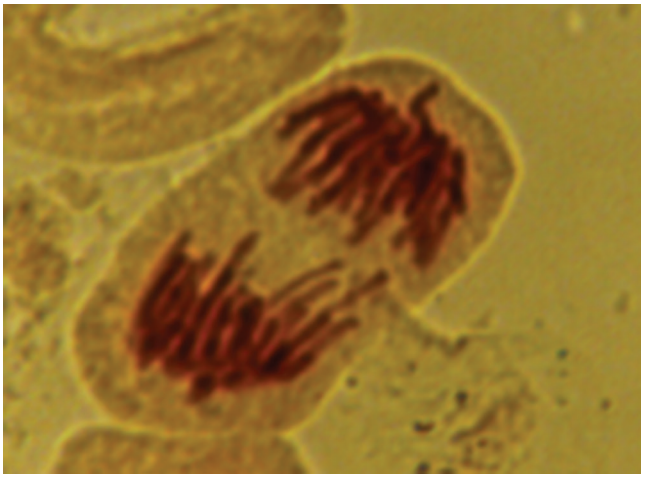

Fig. 3. Normal anaphase.

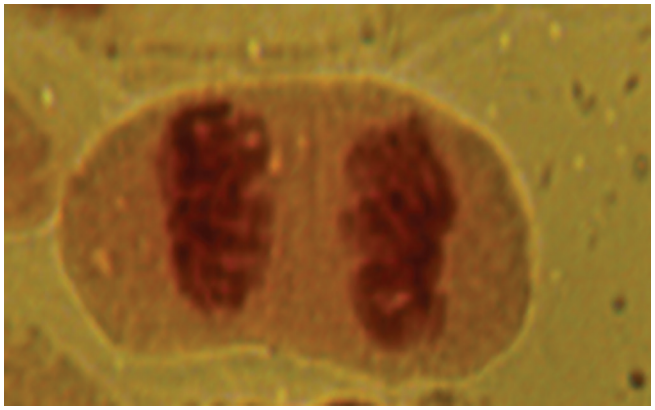

Fig. 4. Norma telophase.

The effects produced on the root growth of *A. cepa* in this study require attention. First, root growth inhibition was neither directly nor inversely proportional to increasing wastewater concentration. Second, although the canteen wastewater inhibited root growth at most of its concentrations, it also promoted root growth at 2% and 5% concentrations. The inhibition in root growth of *A. cepa* by some concentrations of canteen wastewater implies that the metals and other parameters such as BOD, total hardness, and conductivity in the wastewater were harmful to *A. cepa* roots at those concentrations. On the other hand, the fact that canteen wastewater promoted root growth at 2% and 5% concentrations, suggesting that it contains some nutrients that may promote plant growth at appropriate concentrations. Such growth-promoting nutrients may likely include organic compounds such as proteins, carbohydrates, and essential micronutrients such as Zn and Cu (Yasin et al., 2017).

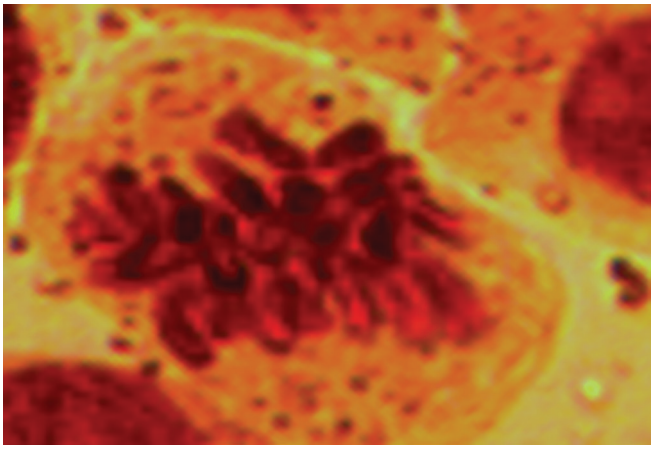

Fig. 5. Sticky anaphase.

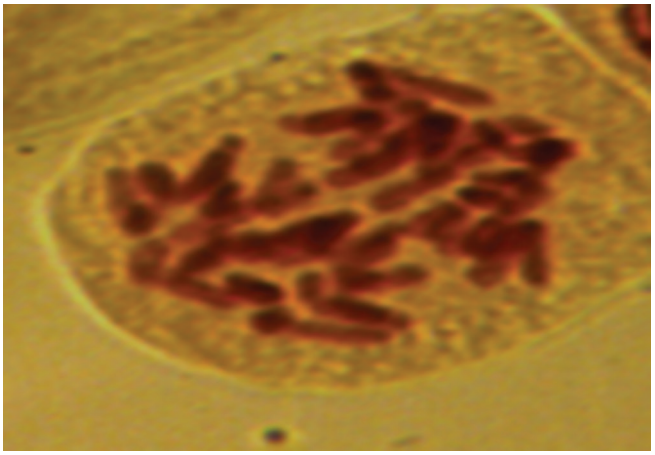

Fig. 6. Vagrant anaphase.

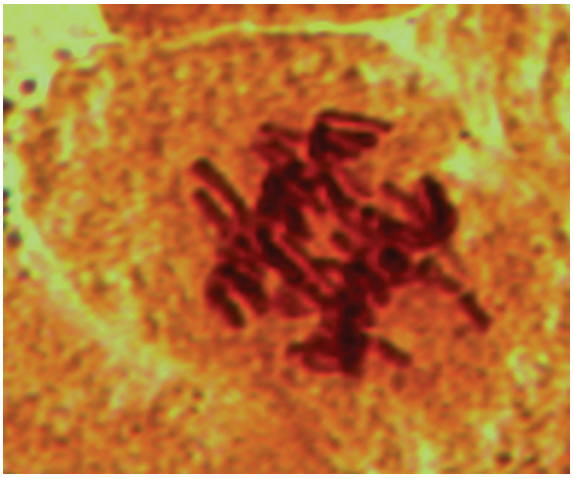

Fig. 7. Bridged anaphase.

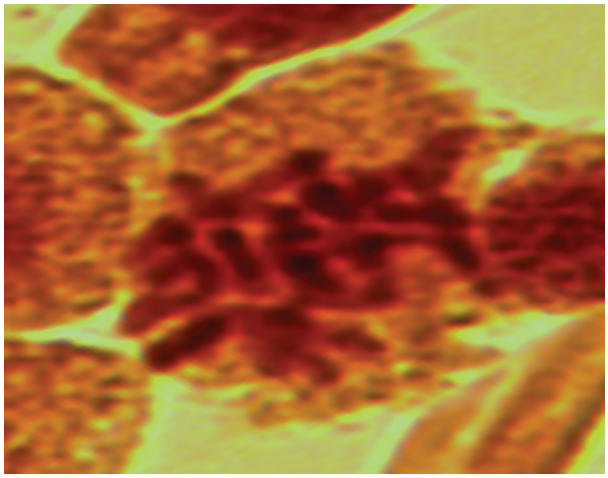

Fig. 8. C-mitosis.

Canteen wastewater was observed to be highly mitodepressive in *A. cepa* roots with mitotic inhibition increasing with rising concentrations. Mitotic index is considered a reliable indicator for the presence of cytotoxic pollutants (Kaymak and Goc-Rasgele, 2009). The decreased mitotic index and increased mitotic inhibition are also likely associated with the presence of metals and other parameters such as BOD, total hardness, conductivity, and perhaps, other parameters are not assessed in this study. These contaminants must have either disrupted DNA synthesis or completely halted metabolic activities, thereby preventing the cells from entering mitosis (Metin and Burun, 2008).

Only few chromosomal aberrations (mainly sticky, vagrant, and bridged) were observed. Nevertheless, chromosomal aberrations, irrespective of types or numbers, are generally signs of toxicity resulting from the presence of genotoxic materials. Chromosome bridges result from chromosome and/or chromatid breaks, indicating clastogenic effect (Leme and Marin-Morales, 2009). C-mitosis, the least frequent aberration in this study indicate a risk of aneuploidy. Sticky and vagrant chromosomes, which were the most frequent aberrations observed, result from chromatin dysfunction or spindle failure. Chromosome stickiness may result from improper folding of chromatin fiber into single chromatid and chromosome, which consequently hinder free chromosome separation (Klasterska et al., 1976). Prominent stickiness of the chromatin matrix is indicative of toxicity which often results in abnormal metaphases and anaphases. Sticky chromosomes are associated with a disturbance in the balance of the quantity of histones or other proteins responsible for controlling the proper structure of nuclear chromatin. Stickiness is considered a common sign of toxic effects on chromosomes that may lead to cell death (Kuras, 2004; Metin and Burun, 2008).

Typical of most non-corporate canteens in Nigeria, the canteens that generated the wastewater under study are not fitted with wastewater treatment facilities. Rather, untreated wastewaters are discharged through a drain channel. In view of the pollutant load and the genotoxic potential of canteen wastewater as found in this study and the fact that canteens generate high volumes of wastewater, the practice of discharging untreated canteen wastewater may not be environmentally sustainable. Such untreated wastewater eventually increases the pollution loads of the receiving soil and water environments. In addition, increasing volumes of untreated canteen wastewater may also constitute pollution threat to groundwater.

V. Conclusion

As found in this study, canteen wastewater has genotoxic properties likely brought about by its substantially high pollutant load. The practice of discharging untreated canteen wastewater into drainage canals may not be environmentally sustainable. Nevertheless, canteen wastewater also promoted root growth at low concentrations. Where and when possible, canteen wastewaters that have undergone proper treatment may be converted to productive uses like farm irrigation.

References

Adegbite, A.E., and Olorode, O., 2002. Karyotype studies of three species of *Aspilia thouar* (Heliantheae-Asteraceae) in Nigeria. *Plant Science Research Communication*, 3, pp.11-26.

American Public Health Association, APHA, 1998. *American Standard Methods for Examinations of Water and Wastewater.* 19th ed. American Public Health Association (APHA)-American Water Works Association (AWWA)-American Pollution Control Federaation (WPCF), Washinghton, DC.

Chen, X., Chen, G., and Yue, P.O., 2000. Separation of pollutants from restaurant wastewater by electrocoagulation. *Separation Purification Technique*, 19, pp.65-76.

Dada, E.O., Akanni, A.R., and Akinola, M.O., 2017. Comparative physico-chemical and genotoxicity assessments of textile mill company effluent and local Tie-and-Dye textile wastewater. *Journal of Applied Science and Environmental Management*, 21(5), pp.877-882.

Dada, E.O., Akinola, M.O., and Haruna, R., 2018. Physico-chemical and genotoxicity assessments of palm oil mill effluent generated by a corporate refinery in Nigeria. *Pollution*, 4(1), pp.83-92.

Davies, B., Lockwood, A., and Stone, S., 1998. *Food and Beverage Management*. 3rd ed. Butterworth-Heinemann, Oxford.

Feretti, D., Zerbini, I., Zani, C., Ceretti, E., Moretti, M., and Monarca, S., 2007. *Allium cepa* chromosome aberration and micronucleus tests applied to study genotoxicity of extracts from pesticide-treated vegetables and grapes. *Food Additives and Contaminants*, 6, pp.561-572.

Fiskesjo, G., 1985. *Allium* test on river water from bran and sexan before and after closure of a chemical factory. *Ambiologia*, 14, pp.99-103.

Fusi, A., Guidetti, R., and Azapagic, A., 2016. Evaluation of environmental impacts in the catering sector: The case study of pasta. *Journal of Cleaner Production*, 132, pp.146-160.

Kaymak, F., and Goc-Rasgele, P., 2009. Genotoxic effects of raxil on root tips and anthers of *Allium cepa* L. *Caryologia*, 62(1), p.1-9.

Klasterska, I., Natrajan, A.T., and Ramel, C., 1976. An investigation of the origin of chromatid aberrations and chromosome stickiness as a category of chromatid aberrations. *Hereditas*, 83, p.153.

Kuras, L., 2004. Characterization of protein–DNA association *in vivo* by chromatin immunoprecipitation. In: Dickson, R.C., and Mendenhall, M.D., editors. *Signal Transduction Protocols, Methods in Molecular Biology*. Humana Press, Totowa, pp.147-162.

Leme, D.M., and Marin-Morales, M.A., 2009. *Allium cepa* test in environmental monitoring: A review on its application. *Mutation Research/Reviews in Mutation Research*, 682, pp.71-81.

Mahmood, S., and Maqbool, A., 2006. Impacts of wastewater irrigation on water quality and on the health of local community in Faisalabad. *Pakistan Journal of Water Resources*, 10, pp.230-270.

Metin, M., and Burun, B., 2008. Cytogenetic effects of *Urginea maritima* L. Aqueous extracts on the choromosomes by using allium test method. *Caryologia*, 61(4), pp.342-348.

Mohamed, R.M.S., Apandi, N.M., Peralta, H.M.M., and Kasim, A.H.M., 2015. Removal of nutrients from cafeteria wastewater using varying concentrations of microalga *Scenedesmus* sp. *Proceedia Environmental Sciences*, 2015, pp.2-6.

Olorunfemi, D.I., Ogieseri, U.M., and Akinboro, A., 2011. Genotoxicity screening of industrial effluents using onion bulbs (*Allium cepa* L.). *Journal of Applied Science and Environmental Management*, 15(1), pp.211-216.

Rainwater, K., 2004. Review of Systems for Restaurant Wastewater Pre-Treatment. Paper Submitted to Texas On site Wastewater Treatment Research Council, Austin, Texas.

Yasin, Z.A.M., Mahmood, M., and Shaharudiin, N.A., 2017. Effects of micronutrients (Cu, Zn, Mn, and Fe) on the growth of spathoglottis plicata plantlets. *Journal of Biotechnology, Computational Biology and Bionanotechnology*, 98(1), pp.5-13.

Ying, L., Li-Kun, Y., and Jing, Z., 2011. Study the way to forecast the discharge of restaurant wastewater in Beijing. *Proceedia Environmental Sciences*, 11, pp.850-857.

Theoretical Calculations for the Acidity of Cyanopolyynes $HC_{2n+1}N$ (n = 0–5) in Gas and Aqueous Phases Using Ab initio Methods

Hassan H. Abdallah

Department of Chemistry, College of Education, Salahaddin University-Erbil,
Kurdistan Region - F.R. Iraq

***Abstract*—Cyanopolyynes have been found in the interstellar medium, cold dust cloud Taurus Molecular Cloud-1, and the Titan's atmosphere. Theoretical calculations are carried out to predict gas and aqueous phase acidities of a series of cyanopolyynes acids. Two levels of theory were used in this study, with the combination of density functional theory, and Møller–Plesset perturbation (MP2) theory, MP2 methods with two types of basis set, namely, Pople's 6–311++g (d, p) basis set and Dunning's aug-cc-pVTZ basis set. The calculations of these molecules reveal that pKa values varying from 12.25 to 17.25 and indicate that the acidity of these molecules in aqueous phase increases whereas the acidity in gas phase decreases with an increasing chain length of these acids.**

***Index Terms*—Ab initio, Acidity, Cyanopolyynes, Density functional theory, Møller–Plesset perturbation.**

I. Introduction

Cyanopolyynes with the general formula, $HC_{2n+1}N$ (n = 0–5), have been detected in the interstellar medium. The larger $HC_{11}N$ was observed in cold dust cloud Taurus molecular cloud (TMC)-1 (Bell et al., 1997). Cyanopolyynes are also discovered in the Titan's atmosphere, which is rich in elements such as carbon, hydrogen, and nitrogen (Kunde et al., 1981). The origin of these large carbon chains with alternating single and triple carbon-carbon (C-C) bonds is still unclear but ion-molecule reactions especially those involving C+ are presumed to be the main source. However, recent studies indicate that neutral-neutral reactions may also lead to such carbon chains (McCarthy and Thaddeus, 2001; Mendoza et al., 2018; and Skomorowski et al., 2018).

The detection of long linear carbon-chain molecules in interstellar and circumstellar clouds has come as a surprise. Ab initio calculations show that long linear species are usually more energetic than their ring or ring-chain counterparts and were observed to be less stable in the earthbound environment. In contrast, many linear chains such as the cyanopolyynes $HC_{2n+1}N$ were found to be widespread and abundant in the cold circumstellar and interstellar clouds (Kunde et al., 1981 and McCarthy and Thaddeus, 2001). The abundance of these long chains and the scarcity of their ring counterparts in the cold ultraviolet-shielded clouds yield keys to the formation of large molecules in interstellar space and can potentially help us in understanding the origin of diffuse interstellar bands (Botschwina, 2003).

Carbon chain molecules can be classified into several families, depending on a few factors such as the structure of their linear backbone (acetylenic backbone with alternating single and triple C-C bonds, or cumulenic backbone with double bonds), their electronic ground state (open shell or closed shell) and the groups at the end of the chain (H, CN, CH_2, or CH_3). The two most widespread families are the polyynes ($HC_{2n+1}N$ and $CH_3C_{2n+1}H$) and the polyacetylene radicals (C_nH). The most abundant is presumably the family of polyacetylenes ($HC_{2n}H$), which unfortunately are non-polar and hence not detectable at radio wavelengths. Note, however, that these species have been detected in mid-infrared spectrum with the infrared space observatory (Botschwina and Horn, 1997).

It has been proposed that the polyynes and carbon-chain radicals formed directly in the gas phase through reactions of CCH with polyynes, polyacetylenes, and/or polyacetylene ions (for example, $HC_{2n+1}N + CCH \rightarrow HC_{2n+3}N + H$) (Botschwina et al., 1997). Such reactions tend to insert two triply bonded carbon atoms into the carbon backbone, uncoupling the formation of chains with an odd number of C-atoms from those with an even number, which could explain the alternating high and low abundances observed as the length of the C backbone increases. For example, in the molecular shell around IRC+10216 and the dark cloud TMC-1, the two main astronomical sources of carbon chain molecules, the abundance of the C_nH radicals with an even number of C-atoms is about 30 times larger than that of radicals of similar size with an odd number of carbon atoms. In contrast, the decrease in abundance between successive species within the even (or odd) number of C-atoms families,

ARO-The Scientific Journal of Koya University
Volume VII, No.1(2019), Article ID: ARO.10484, 7 pages
DOI: 10.14500/aro.10484
Received 24 December 2018; Accepted 17 April 2019
Regular research paper: Published 01 May 2019
Corresponding author's email: hassan.abdullah@su.edu.krd

$C_nH/C_{n+2}H$, is found to be only 4–6 (Botschwina, 2003 and McCarthy and Thaddeus, 2001).

Electronic structure calculations in cyanopolyynes were also reported and guided the discovery of some cyanopolyynes in the interstellar medium (McCarthy and Thaddeus, 2001). The HC_9N molecule was already investigated with the Coupled Cluster Theory, at the CCSD (T)/cc-pVTZ level of theory (Botschwina et al., 1997), and the results were employed to determine cyanopolyyne column densities in TMC-1 (Bell et al., 1997). This CCSD (T)/cc-pVTZ study presents the equilibrium geometry and the dipole moment for HC_9N (Botschwina et al., 1997). Another study compares dipole moments obtained for small cyanopolyynes with perturbation theory, Møller–Plesset perturbation (MP2), and density functional theory (DFT), through the BP86 functional, using a small basis set, 6–31G*. The results showed that MP2 yields more accurate dipole moment values than BP86 (Moliner et al., 1996). More recent articles also deal with the electronic structure of some cyanopolyynes using DFT and CCSD (T) (Botschwina, 2003, Qi et al., 2009, Woon and Herbst, 2009, and Scemama et al., 2002). Other works deal only with the stretching modes of a few cyanopolyynes such as HCN, HC_3N (Botschwina et al., 1995), HC_5N (Botschwina et al., 1997), and HC_7N (Botschwina et al., 1997) using the CCSD (T) method with triple-zeta basis sets or some combined treatment.

Moreover, DFT calculations also indicated that the alternation between C-C bonds that maintain characteristics of single and triple bonds persists in polyynes as large as $HC_{30}H$ (Scemama et al., 2002). Interestingly, the difference between the bond lengths for either single and triple C-C bonds near the center of polyynes ($HC_{2n}H$) and cyanopolyynes are predicted as being equal to only 0.1 Å. Another interesting characteristic of these molecules has large molecular dipole moments that facilitate their detection (Arnau et al., 1990). Unfortunately, the experimental values of this quantity are only limited to the smallest cyanopolyynes.

The deprotonation energies of organic acids and the proton affinities of the corresponding conjugate bases are widely used for the prediction of gas phase and aqueous phase Bronsted acidities (Smith and March, 2007, Dewar and Dieter, 1986, Siggel et al., 1988, Kass, 1990, Burk and Koppel, 1993, Koppel et al., 1994, and Burk et al., 1996). Strong acids have small values of deprotonation energy (that is, the release of the proton is easier) whereas strong bases have large values of proton affinity (that is, the binding to the proton is stronger). Several works on the prediction of the acidity of organic and inorganic acids can be found in literature. For instance, Smith and Radom (Smith and Radom, 1995 and Smith and Radom 1995) have shown that the G2 and G2 (MP2) methods provide excellent results for both deprotonation enthalpies and proton affinities of small molecules.

Catalan and Palomar (Catalan and Palomar, 1998) have investigated gas-phase acidities of a number of species and have shown that the calculations at B3LYP/6–311+G (d) and 6–311+G (3df, 3pd) level of theory correlate well with the experimental data. Good correlations have been obtained between experimental pKa values of a wide range of organic Bronsted acids and their calculated gas-phase deprotonation enthalpies (Choho et al., 1996). Correlations between theoretical results and gas-phase acid-base equilibrium constants of organic compounds have been reported for amines, alcohols, and thiols (Yang and Mortier, 1986, Contreras et al., 1999, and Pérez et al., 2000). An excellent correlation was obtained between the aqueous-phase acidity calculated with the HF/3–21G (d) method and experimental pKa values for a series of nitrogen bases (D'Souza et al., 2000).

Recently, a reasonable correlation was obtained between the deprotonation energies of the compounds calculated at the HF/3–21G and B3LYP/6–31G (d) levels of theory and their aqueous pKa values (Rezende, 2001 and Rezende 2001). The ability to predict acidity using a coherent, well-defined theoretical approach, without external approximation or fitting to experimental data would be very useful to chemists. Due to the rapid development of computational chemistry, the acidity of small molecules in the gas phase can be calculated with equivalent or greater accuracy than can be obtained experimentally. However, the current situation is less satisfactory in solution, mostly due to the difficulty of calculating solvation energies with adequate accuracy.

In this study, the acidy of six cyanopolyynes acids is predicted in the gas and aqueous phases using DFT and MP2 methods with two basis sets, 6–311++g (d, p) and aug-cc-pVTZ. The charge distribution and the effect of the length of the cyanopolyynes on the acidy of these compounds are elucidated.

II. Computational Methods

A. Gas-phase Acidity Calculations

Calculations are performed with the Gaussian 09 W software package (Frisch et al., 2009). The geometries of the neutral and deprotonated species are fully optimized using DFT and MP2 theory, MP2 level of theory at the 6–311++G (d, p) and aug-cc-pVTZ basis sets. Frequency calculations are performed at the same level of theory to characterize the stationary points obtained. The gas-phase Gibbs free energy change (ΔG°_{gas}) of Scheme 1 is calculated using Eq. (1). For ΔG°_{gas} (H^+) the experimental value of −6.28 kcal/mol is used (Liptak et al., 2002).

$$AH_{(\mathrm{gas})} \rightarrow A^{-}_{(gas)} + H^{+}_{(gas)}$$

$$\Delta G^{\circ}_{gas} = G^{\circ}_{gas}\left(A^{-}\right) + G^{\circ}_{gas}\left(H^{+}\right) - G^{\circ}_{gas}(AH) \qquad (1)$$

B. Aqueous-phase Acidity Calculations

Solvent effects are taken into account by means of the polarizable continuum model (PCM) (Miertuš et al., 1981, Miertuš and Tomasi, 1982, and Cossi et al., 1996) through the full optimization calculations at the B3LYP/6–311++G (d, p) level of theory (using the gas-phase optimized geometries). The PCM calculations employ the UAHF atomic

radii when constructing the solvent cavity for the calculation of the Gibbs free energy of solvation. A common practice to calculate the aqueous Gibbs free-energy change of an acid dissociation (ΔG°_{aq}), see Eq. (2) is by combining the ΔG°_{gas} of the deprotonation process with the change in Gibbs free energy of solvation $\Delta\Delta G^{\circ}_{solv}$ using the thermodynamic cycle of Scheme 1 and Eq. (3). For ΔG°_{solv} (H^+) the experimental value of −264.61 kcal/mol is used (Liptak et al., 2002). The aqueous pKa is calculated according to Eq. (5). All the calculations and experimental data reported in this paper are at 298.15 K.

$$\Delta G^{\circ}_{aq} = G^{\circ}_{aq}\left(A^{-}\right) + G^{\circ}_{aq}\left(H^{+}\right) - G^{\circ}_{aq}(AH) \quad (2)$$

$$\Delta G^{\circ}_{aq} = \Delta G^{\circ}_{gas} + \Delta\Delta G^{\circ}_{solv} \quad (3)$$

$$\Delta G^{\circ}_{aq} = G^{\circ}_{gas}(A^{-}) + G^{\circ}_{gas}(H^{+}) - G^{\circ}_{gas}(AH) + \Delta G^{\circ}_{solv}(A^{-}) + \Delta G^{\circ}_{solv}(H^{+}) - \Delta G^{\circ}_{solv}(AH) \quad (4)$$

$$\mathrm{pK_a} = \frac{\Delta G^{\circ}_{aq}}{RT\ln 10} \quad (5)$$

Charif and his group (Charif et al., 2007) have found a correlation between these two Gibbs free energy changes with

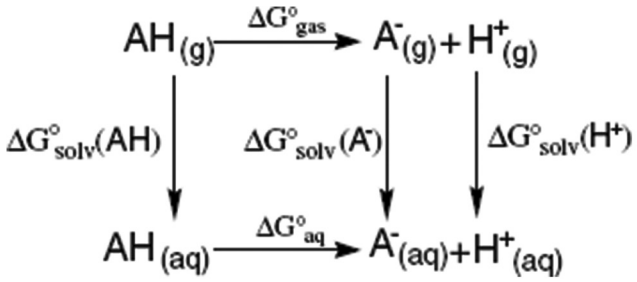

Scheme 1. G°_{solv} (X) represents the Gibbs free energy of solvation of species X.

R^2 = 0.947 that might be very helpful to be used as a scale factor to get values closer to the experimental results. They found a correlation between the experimental and calculated aqueous pKa values. The regression equation with the corresponding standard deviation and correlation coefficient (R^2) values is given in Eq. (6).

$$pK_a = 0.8755\ pKa\ (calc.) - 1.7563 \quad (R^2 = 0.934,\ SD = 4.80) \quad (6)$$

III. Results and Discussion

A. Optimized Geometry

The molecules under study were optimized to obtain their ground state structures, with the levels of theory aforementioned in the methods of calculations. Fig. 1 shows the optimized geometry of the studied cyanopolyynes. The optimized structures were at the ground state with no imaginary frequencies. The bond lengths of the studied molecules are listed in Table I.

The vibrational modes of the optimized structures were carefully examined. The most important vibrational mode belongs to the CH stretching. The frequencies of the stretching vibration are listed in Table II. In addition, the values of the dipole moment of these compounds are also listed. It is clear that the value of the stretching frequency is increasing from HCN to the HC_5N, whereas for the molecules beyond that the value is constant. This indicates that the strength of the CH bond increases with the length of the chain, resulting in difficulty for the proton to dissociate as the chain becomes longer until it becomes constant at a certain length. On the other hand, the dipole moments of the molecules show a different trend whereby the dipole moment is increasing as the length of the molecule increases.

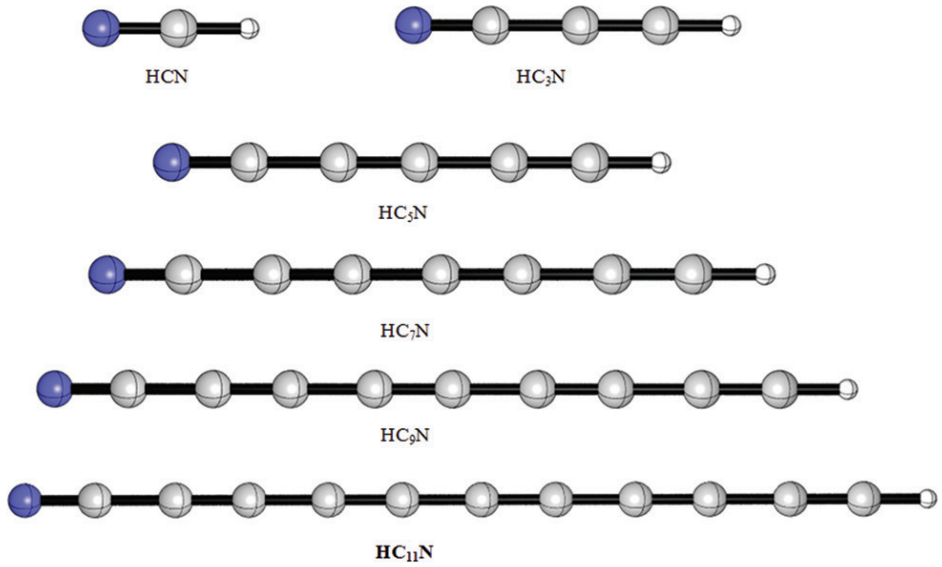

Fig. 1. The optimized structures of the studied cyanopolyynes.

 http://dx.doi.org/10.14500/aro.10484

TABLE I
BOND LENGTHS IN A OF THE OPTIMIZED STRUCTURES OF THE STUDIED CYANOPOLYYNES IN THE GAS-PHASE AND THE VALUES BETWEEN BRACKETS ARE FOR THE AQUEOUS PHASE

Bond	HCN	HC_3N	HC_5N	HC_7N	HC_9N	$HC_{11}N$
H–C	1.078 (1.081)	1.076 (1.078)	1.066 (1.068)	1.066 (1.068)	1.066 (1.068)	1.066 (1.068)
$C_1 \equiv C_2$		1.236 (1.236)	1.226 (1.227)	1.228 (1.228)	1.229 (1.229)	1.229 (1.229)
$C_2–C_3$		1.386 (1.385)	1.363 (1.363)	1.360 (1.360)	1.358 (1.358)	1.358 (1.358)
$C_3 \equiv C_4$			1.232 (1.232)	1.238 (1.238)	1.241 (1.241)	1.242 (1.242)
$C_4–C_5$			1.368 (1.367)	1.352 (1.352)	1.347 (1.347)	1.344 (1.344)
$C_5 \equiv C_6$				1.236 (1.236)	1.243 (1.243)	1.247 (1.246)
$C_6–C_7$				1.365 (1.364)	1.348 (1.347)	1.341 (1.341)
$C_8 \equiv C_9$					1.238 (1.238)	1.246 (1.246)
$C_9–C_{10}$					1.364 (1.363)	1.346 (1.345)
$C_{10} \equiv C_{11}$						1.239 (1.239)
$C_{11}–C_{12}$						1.364 (1.362)
C≡N	1.183 (1.181)	1.193 (1.192)	1.184 (1.183)	1.186 (1.184)	1.186 (1.185)	1.186 (1.185)

TABLE II
DIPOLE MOMENT (M) AND THE STRETCHING FREQUENCIES IN THE GAS AND AQUEOUS PHASES

Bond	HCN	HC_3N	HC_5N	HC_7N	HC_9N	$HC_{11}N$
μ (gas) (debye)	3.333	4.273	5.021	5.657	6.186	6.636
μ (aq) (debye)	4.103	5.560	6.599	7.395	7.978	8.412
C-H str. (gas) (cm^{-1})	3452.76	3472.67	3487.72	3486.33	3486.02	3486.25
C-H str. (aq) (cm^{-1})	3428.35	3450.98	3467.33	3466.35	3466.01	3466.14

TABLE III
DENSITY FUNCTIONAL THEORY RESULTS OF THE GIBBS FREE ENERGY IN (KCAL/MOL), PKA VALUES IN THE GAS AND AQUEOUS PHASES AND THE SCALED VALUES OF PKA IN THE AQUEOUS PHASE

Bond	Basis set	ΔG°_{gas}	ΔG°_{aq}	pK_a-gas	pK_a-aq	pK_a-aq-sc
HCN	6–311++g (d, p)	341.993	21.963	250.705	16.000	12.251
	aug-cc-pVTZ	340.110	20.708	249.577	15.096	11.460
HC_3N	6–311++g (d, p)	339.483	29.493	248.917	21.694	17.236
	aug-cc-pVTZ	337.600	28.238	247.560	20.540	16.226
HC_5N	6–311++g (d, p)	333.208	29.493	244.563	21.853	17.376
	aug-cc-pVTZ	331.953	28.865	243.453	20.956	16.591
HC_7N	6–311++g (d, p)	329.443	30.120	241.570	21.890	17.408
	aug-cc-pVTZ	328.188	28.865	240.446	21.128	16.741
HC_9N	6–311++g (d, p)	326.305	30.120	239.229	22.075	17.570
	aug-cc-pVTZ	325.050	28.865	238.275	21.276	16.871
$HC_{11}N$	6–311++g (d, p)	324.423	30.120	237.953	22.246	17.720
	aug-cc-pVTZ	323.168	29.493	236.877	21.710	17.251

A. Gas-phase Acidities

The calculated gas-phase ΔG°_{gas} of the acid dissociation and aqueous pK_a values (relative to water) at 298.15 K is reported in Tables III and IV. Besides that, the last column is for the scaled values which were calculated according to the Equation (6).

A satisfactory linear correlation is obtained showing that the gas-phase Gibbs free energy change of deprotonation generally increases when the acidity of these compounds decreases. It should be noted that very accurate aqueous pK_a values (relative to water) can only be obtained for acids weaker than the hydronium ion (pK_a = −1.74) and stronger than water (pK_a = 15.74) (Bell et al., 1997). It is well known that in the gas phase, acidity orders may be much different than in aqueous solution for certain families of compounds. Simple alcohols are an example of this: Whereas tertiary alcohols are more acidic than secondary and primary alcohols in the gas phase, in aqueous solution the acidity order is reversed because the much bulkier tertiary anion is poorly solvated. A similar pattern is found in simple aliphatic carboxylic acids and when analyzing the basicity order of amines (Bell et al., 1997).

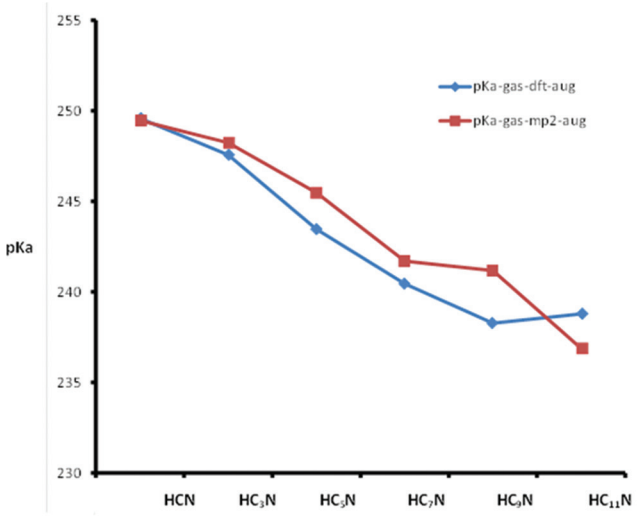

Fig. 2. The correlation between the pK_a values and chain length of the cyanopolyynes in the gas phase.

From the results we have obtained, we can infer that the aqueous phase acidity order of the family of cyanopolyynes acids is very similar to that in the gas phase. Hence, it might be possible to use gas-phase calculations to predict the aqueous pK_a values of carbon acids.

As shown in Fig. 2, the pK_a values of the studied cyanopolyynes are generally decreasing with the increase of the chain length in the gas phase in parallel behavior with the values of the ΔG°_{gas}. Fig. 2 shows that the calculated pK_a values using DFT method are lower than the MP2 method. The general behavior of the plot may be attributed to the

effect of the solvent molecules on the acidity of these compounds. In conclusion, in the gas phase, the acidity of these compounds increases with increasing chain length; however, this may be attributed to the method and the type of the basis set used in the calculations.

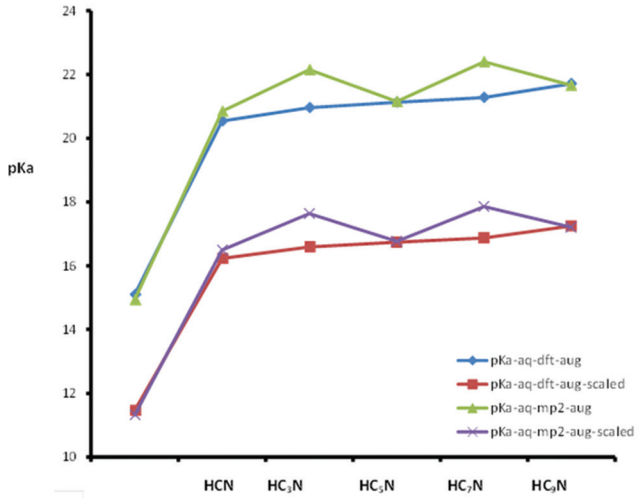

Fig. 3. The correlation between the pK_a values and chain length of the cyanopolyynes in the aqueous phase.

B. Aqueous-phase Acidities

The calculated aqueous phase ΔG°_{aq} of the acid dissociation and pK_a values of the compounds under study (using Eq. 4 and 5) at 298.15 K are reported in Tables III and IV using DFT and MP2 methods, respectively. According to both

TABLE IV
MØLLER–PLESSET PERTURBATION RESULTS OF THE GIBBS FREE ENERGY IN (KCAL/MOL), PKA VALUES IN GAS AND AQUEOUS PHASES AND THE SCALED VALUES OF PKA IN THE AQUEOUS PHASE.

Bond	Basis set	ΔG°_{gas}	ΔG°_{aq}	pK_a-gas	pK_a-aq	pK_a-aq-sc.
HCN	6–311++g (d, p)	343.875	23.845	252.213	17.409	13.485
	aug-cc-pVTZ	340.110	20.080	249.457	14.935	11.319
HC_3N	6–311++g (d, p)	342.620	32.631	251.424	23.704	18.997
	aug-cc-pVTZ	338.228	28.238	248.235	20.844	16.493
HC_5N	6–311++g (d, p)	338.228	33.258	248.084	24.333	19.547
	aug-cc-pVTZ	334.463	30.120	245.472	22.150	17.636
HC_7N	6–311++g (d, p)	334.463	33.258	245.198	24.407	19.612
	aug-cc-pVTZ	329.443	28.865	241.699	21.154	16.764
HC_9N	6–311++g (d, p)	332.580	33.886	244.002	24.724	19.890
	aug-cc-pVTZ	328.815	30.748	241.178	22.400	17.855
$HC_{11}N$	6–311++g (d, p)	330.698	33.886	242.468	24.730	19.895
	aug-cc-pVTZ	325.678	29.493	238.788	21.659	17.206

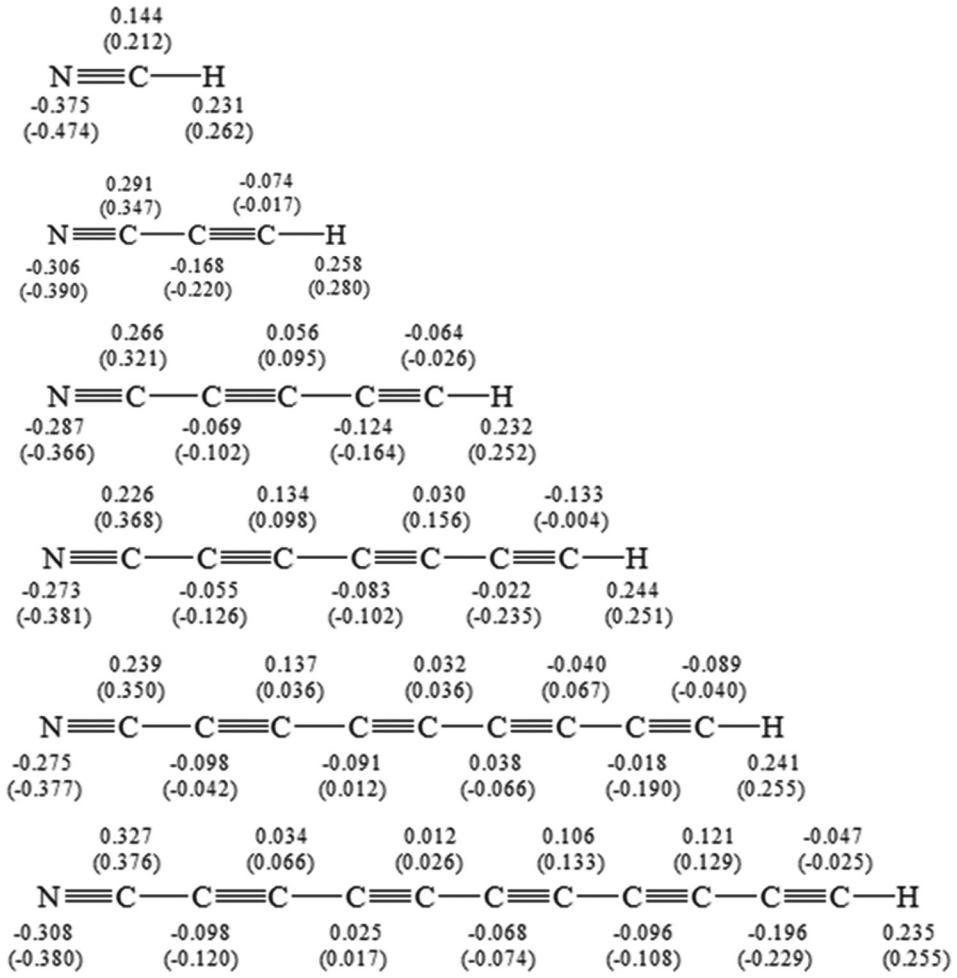

Fig. 4: The charge distribution on atoms in the gas and aqueous phases as found in the natural bond orbital analysis.

methods, the values have an opposite trend to the values in the gas phase in which the change in Gibbs free energy increases with the increase in the length of the molecule. Tables III and IV also show the results of the scaled values of the pK_a. The scaled values are smaller than those calculated with Equation (6) which indicates that the calculated change in Gibbs free energy of solvation might be slightly overestimated. The reason for this lies in the inadequacy of continuum solvation models to accurately calculate solvation energies since explicit solute–solvent interactions are ignored. The inclusion of continuum solvent effects in the geometry optimizations and frequency calculations might improve these results slightly. The plot of the pK_a values versus the studied molecules is displayed in Fig. 3.

A satisfactory correlation is obtained between the length of the carbon chain and the values of pK_a. However, there are some points to be highlighted. The scaled values are lower than the calculated raw values. Furthermore, the DFT method has shown lower values of pK_a than the MP2 method. Finally, the pK_a values are slightly increasing with the increase of the chain length starting from HC_3N and beyond and hence the acidity is decreasing with increasing the chain length.

For more understanding to the properties of these molecules, natural bond orbital method was used to calculate the charge distribution on each atom of the molecules and shown in Fig. 4 at the gas and solution phases. As shown in Fig. 4, there is no single trend for the charge distribution on the atoms. However, in general, the N and H atoms have the highest negative and positive charges, respectively.

IV. Conclusions

In the present work, we have shown satisfactory values of aqueous pK_a values of cyanopolyynes in the gas and aqueous phases through the calculation of the change in Gibbs free energy for these molecules and their deprotonated form. The correlation equation between the experimental aqueous pK_a values and the calculated values was used to predict better pK_a values. To assess the validity of our results, further experimental work is required. The difference in the acidity of the compounds studied can be interpreted through the charge distribution and conjugation effects. In the gas phase, the pK_a values decrease and the acidity increase with the increase of conjugation or the molecule length, whereas, in the aqueous phase, the pKa values increase and the acidity decrease with increasing the chain length.

References

Arnau, A., Tu˜non, I., Silla, E., and Andres, J.M., 1990. HC_nN: The largest molecules in the interstellar medium. *Journal of Chemical Education*, 67, pp.905-906.

Bell, M., Feldman, P., Travers, M., McCarthy, M., Gottlieb, C., and Thaddeus, P., 1997. Detection of $HC_{11}N$ in the Cold Dust Cloud TMC-1. *The Astrophysical Journal*, 483(1), pp.L61-L64.

Botschwina, B., Horn, M., and Oswald, K., 1997. Coupled cluster calculations for HC7N, HC7NH+ and C7N, molecules of interest to astrochemistry. *Molecular Physics*, 92(3), pp.381-392.

Botschwina, P., 2003. Spectroscopic properties of interstellar molecules: Theory and experiment. *Physical Chemistry Chemical Physics*, 5(16), pp.3337-3348.

Botschwina, P., and Horn, M., 1997. Accurate equilibrium structure and electric dipole moment of HC9N: Predictions on the basis of large-scale coupled cluster calculations. *Journal of Molecular Spectroscopy*, 185(1), pp.191-193.

Botschwina, P., Heyl, Ä., Oswald, M., and Hirano, T., 1997. Ab initio anharmonic force fields and spectroscopic properties for HC5N and HC5NH+, molecules of interest to astrochemistry. *Spectrochimica Acta Part A: Molecular and Biomolecular Spectroscopy*, 53(8), pp.1079-1090.

Botschwina, P., Schulz, B., Horn, M., and Matuschewski, M., 1995. Ab initio calculations of stretching vibrational transitions for the linear molecules HCN, HNC, HCCF and HC3N up to high overtones. *Chemical Physics*, 190(2-3), pp.345-362.

Burk, P., and Koppel, I., 1993. Critical test of PM3 calculated gas-phase acidities. *Theoretica Chimica Acta*, 86(5), pp.417-427.

Burk, P., Koppel, I., Koppel, I., Yagupolskii, L., and Taft, R., 1996. Super acidity of neutral Bronsted acids in gas phase. *Journal of Computational Chemistry*, 17(1), pp.30-41.

Catalan, J., and Palomar, J., 1998. Gas-phase protolysis between a neutral Brønsted acid and a neutral Brønsted base. *Chemical Physics Letters,* 293, pp.511-514.

Charif, I., Mekelleche, S., Villemin, D., and Mora-Diez, N., 2007. Correlation of aqueous pKa values of carbon acids with theoretical descriptors: A DFT study. *Journal of Molecular Structure: THEOCHEM*, 818(1-3), pp.1-6.

Choho, K., Van Lier, G., Van de Woude, G., and Geerlings, P., 1996. Acidity of hydro fullerenes: A quantum chemical study. *Journal of the Chemical Society, Perkin Transactions II*, pp.1723-1732.

Contreras, R., Fuentealba, P., Galván, M., and Pérez, P., 1999. A direct evaluation of regional Fukui functions in molecules. *Chemical Physics Letters*, 304(5-6), pp.405-413.

Cossi, M., Barone, V., Cammi, R., and Tomasi, J., 1996. Ab initio study of solvated molecules: A new implementation of the polarizable continuum model. *Chemical Physics Letters*, 255(4-6), pp.327-335.

D'Souza, F., Zandler, M., Deviprasad, G., and Kutner, W., 2000. Acid base properties of fuller opyrrolidines: Experimental and theoretical investigations. *The Journal of Physical Chemistry A*, 104(29), pp.6887-6893.

Dewar, M., and Dieter, K., 1986. Evaluation of AM1 calculated proton affinities and deprotonation enthalpies. *Journal of the American Chemical Society*, 108(25), pp.8075-8086.

Frisch, M.J., Trucks, G.W., Schlegel, H.B., Scuseria, G.E., Robb, M.A., Cheeseman, J.R., Scalmani, G., Barone, V., Mennucci, B., Petersson, G.A., Nakatsuji, H., Caricato, M., Li, X., Hratchian, H.P., Izmaylov, A.F., Bloino, J., Zheng, G., Sonnenberg, J.L., Hada, M., Ehara, M., Toyota, K., Fukuda, R., Hasegawa, J., Ishida, M., Nakajima, T., Honda, Y., Kitao, O., Nakai, H., Vreven, T., Montgomery, J.A Jr., Peralta, J.E., Ogliaro, F., Bearpark, M., Heyd, J.J., Brothers, E., Kudin, K.N., Staroverov, V.N., Kobayashi, R., Normand, J., Raghavachari, K., Rendell, A., Burant, J.C., Iyengar, S.S., Tomasi, J., Cossi, M., Rega, N., Millam, J.M., Klene, M., Knox, J.E., Cross, J.B., Bakken, V., Adamo, C., Jaramillo, J., Gomperts, R., Stratmann, R.E., Yazyev, O., Austin, A.J., Cammi, R., Pomelli, C., Ochterski, J.W., Martin, R.L., Morokuma, K., Zakrzewski, V.G., Voth, G.A., Salvador, P., Dannenberg, J.J., Dapprich, S., Daniels, A.D., Farkas, Ö., Foresman, J.B., Ortiz, J.V., Cioslowski, J., and Fox, D.J., 2009. Gaussian 09, Revision E.01. Gaussian, Inc., Wallingford CT.

Kass, S.R., 1990. Hydrocarbon acidities calculated with MINDO/3, MNDO, and AM1. *Journal of Computational Chemistry*, 11, pp.94-104.

Koppel, I.A., Taft, R.W., Anvia, F., Zhu, S.Z., Hu, L.Q., Sung, K.S., DesMarteau, D.D., Yagupolskii, L.M., and Yagupolskii, Y.L., 1994. The gas-phase acidities of very strong neutral Bronsted acids. *Journal of the American Chemical Society*, 116, pp.3047-3057.

Kunde, V., Aikin, A., Hanel, R., Jennings, D., Maguire, W., and Samuelson, R., 1981. C_4H_2, HC_3N and C_2N_2 in Titan's atmosphere. *Nature*, 292(5825), pp.686-688.

Liptak, M., Gross, K., Seybold, P., Feldgus, S., and Shields, G., 2002. Absolute pKa determinations for substituted phenols. *Journal of the American Chemical Society*, 124(22), pp.6421-6427.

McCarthy, M., and Thaddeus, P., 2001. Microwave and laser spectroscopy of carbon chains and rings. *Chemical Society Reviews*, 30(3), pp.177-185.

Mendoza, E., Lefloch, B., Ceccarelli, C., Kahane, C., Jaber, A.A., Podio, L., Benedettini, M., Codella, C., and Viti, S., 2018. A search for Cyanopolyynes in L1157-B1. *Monthly Notices of the Royal Astronomical Society*, 475(4), pp.5501-5512.

Miertuš, S., and Tomasi, J., 1982. Approximate evaluations of the electrostatic free energy and internal energy changes in solution processes. *Chemical Physics*, 65(2), pp.239-245.

Miertuš, S., Scrocco, E., and Tomasi, J., 1981. Electrostatic interaction of a solute with a continuum. A direct utilizaion of AB initio molecular potentials for the prevision of solvent effects. *Chemical Physics*, 55(1), pp.117-129.

Moliner, V., Andrés, J., Arnau, A., Silla, E., and Tuñón, I., 1996. Rotational constants and dipole moments of interstellar polyynes: A comparative MP2 and density functional (BP86) study. *Chemical Physics*, 206(1-2), pp.57-61.

Pérez, P., Simón-Manso, Y., Aizman, A., Fuentealba, P., and Contreras, R., 2000. Empirical energy density relationships for the analysis of substituent effects in chemical reactivity. *Journal of the American Chemical Society*, 122(19), pp.4756-4762.

Qi, J., Chen, M., Wu, W., Zhang, Q., and Au, C., 2009. Parity alternation of interstellar molecules cyanopolyynes HCnN (n=1–17). *Chemical Physics*, 364(1-3), pp.31-38.

Rezende M.C., 2001. The acidity of carbon acids in aqueous solutions: Correlations with theoretical descriptors. *Tetrahedron*, 57, pp.5923-5930.

Rezende, M., 2001. A theoretical HSAB study of the acidity of carbon acids CH3Z. *Journal of the Brazilian Chemical Society*, 12(1), pp.73-80.

Scemama, A., Chaquin, P., Gazeau, M., and Bénilan, Y., 2002. Theoretical study of the structure and properties of polyynes and monocyano and dicyanopolyynes: Predictions for long chain compounds. *The Journal of Physical Chemistry A*, 106(15), pp.3828-3837.

Siggel, M.R., Thomas, T.D., and Saethre, L.J., 1988. Ab initio calculation of Broensted acidities. *Journal of the American Chemical Society,* 110, pp. 91-96.

Skomorowski, W., Gulania, S., and Krylov, A., 2018. Bound and continuum-embedded states of cyanopolyyne anions. *Physical Chemistry Chemical Physics*, 20(7), pp.4805-4817.

Smith, B., and Radom, L., 1995. Calculation of proton affinities using the G2 (MP2, SVP) Procedure. *The Journal of Physical Chemistry*, 99(17), pp.6468-6471.

Smith, B., and Radom, L., 1995. Gas-phase acidities: A comparison of density functional, MP2, MP4, F4, G2 (MP2, SVP), G2 (MP2) and G2 procedures. *Chemical Physics Letters*, 245(1), pp.123-128.

Smith, M.B., and March, J., 2007. March's Advanced Organic Chemistry. 6th ed. John Wiley, New York, pp.359-364.

Woon, D., and Herbst, E., 2009. Quantum chemical predictions of the properties of known and postulated neutral interstellar molecules. *The Astrophysical Journal Supplement Series*, 185(2), pp.273-288.

Yang, W., and Mortier, W., 1986. The use of global and local molecular parameters for the analysis of the gas-phase basicity of amines. *Journal of the American Chemical Society*, 108(19), pp.5708-5711.

http://dx.doi.org/10.14500/aro.10471

Assessment of Natural Radioactivity Levels and Radiation Hazards of Soils from Erbil Governorate, Iraqi Kurdistan

Zakariya A. Hussein

Department of Physics, Faculty of Science and Health, Koya University,
Koya KOY45, Kurdistan Region - F.R. Iraq

***Abstract*—In this work, the activity concentrations of natural radionuclides ^{226}Ra, ^{232}Th, and ^{40}K in soil samples from Erbil Governorate, Iraqi Kurdistan were investigated by a gamma-spectroscopy system based on high-purity germanium detector. This is to assess the dose of radionuclides exposure to the population, knowing the health risks and to have a baseline for future changes in the environmental radioactivity. It was found that the activity concentrations of ^{226}Ra, ^{232}Th, and ^{40}K were ranged from 14.6 ± 1.6 to 38.2 ± 2.8 Bq/kg, 4.5 ± 1.4 to 52.4 ± 5.8 Bq/kg, and 302.8 ± 12.6 to 388.6 ± 12.8 Bq/kg, respectively. The measured activity concentrations for these radionuclides were compared with the reported data of other countries and with the worldwide average activity of soil. Radium equivalent activities, absorbed dose rate, excess lifetime cancer risk, and the values of hazard indices were calculated for the measured samples to assess the radiation hazard of the natural radioactivity in all samples to the people. It was concluded that the radium equivalent activities of the studied samples are below the internationally accepted values. These results show that annual effective dose absorbed through occupant from activity construction of soil samples used in the under place is below 1.0 mSv/y. It is concluded that the assessment radioactivity of soil is within acceptable levels and does not pose any health hazard to the population.**

***Index Terms*—Gamma-ray spectroscopy, Radioactivity, Soil, Erbil Governorate.**

I. Introduction

The natural radioactivity present in the environment is the main source of radiation exposure of humans and constitutes the background radiation level (Amrani and Tahtat, 2001). The principle characteristic supporters of outer introduction from gamma beams are ^{226}Ra, ^{232}Th, and ^{40}K. Since these radionuclides are not consistently disseminated, the information of their dispersion in soil assumes a critical part in radiation security (Aziz et al., 2014). Natural radionuclides in soil represent the significant component of population background exposure. The specific levels of terrestrial environmental radiation are related to the geological composition of each lithological separated area, and to the content of natural radionuclides in rocks from which the soils originate in each area (Snežana et al., 2012). The relatively more abundant naturally occurring radionuclides belong to uranium and thorium decay series (Zakariya et al., 2013). Humans are exposed to both internal and external radiation from the natural sources. Internal exposure occurs through the intake of terrestrial radionuclides through inhalation or ingestion. Inhalation exposure dose results from the existence of dust particles in air, including radionuclides from ^{238}U and ^{232}Th decay series (Hammood and Khalifa, 2011). The radioactivity concentrations in soil give information on both natural and manmade sources which are important in radiological monitoring and assessment of radiation dose for public (Eissa, et al., 2010).

Also literature showed that studies on radionuclide concentrations in mines have been extensively in national studies (Hussein, 2018; Azeez et al., 2018; Ahmed and Samad, 2014; Dashty and Ali, 2013; Makki et al., 2014; Hussain and Hussain, 2011; Hussain and Abbas, 2010; Ali, 2011; Kamal et al., 2015). Mining activities have not been subjected to radiological regulatory control and so there is generally little or no awareness and knowledge of the radiological hazards. In addition, ^{137}Cs is the most important fission product released to the environment as a result of nuclear activities, because this radionuclide rapidly passes through soil to vegetables and creates a dose effect (Hammood and Khalifa, 2011. p. 22). Several studies have been measured and evaluated values for the level of natural radioactivity in worldwide national studies; such as, in Malaysia (Alzubaidi et al., 2016; Salih, 2018), India (Sureshgandhi et al., 2014; Punniyakotti and Ponnusamy, 2017), Nigeria (Fasae, 2013: Jibiri and Biere, 2014), Brazil (Veiga et al., 2006), Egypt (Darwish et al., 2015), and Saudi Arabia (El-Taher and Abdelhalim, 2013: Al-Zahrani, 2012).

ARO-The Scientific Journal of Koya University
Volume VII, No.1(2019), Article ID: ARO.10471, 6 pages
DOI: 10.14500/aro.10471
Received 11 November 2018; Accepted 16 April 2019
Regular research paper: Published 01 May 2019
Corresponding author's e-mail: zakariya.Hussein@koyauniversity.org

Natural occurring radioactive material when the is processed, the concentration of the radionuclides became higher in the wastes, so the radionuclides have a very long half-life, when concerning about the public safety (Hassan et al., 2013).

The goal of this study decides the concentration of activity ^{226}Ra, ^{232}Th, and ^{40}K in the soil from Erbil Governorate, Iraq. Assessment of natural radioactivity of the soil samples for some regions in Kurdistan region considers as the main objective of this research. The radium equivalent activity (Ra_{eq}), absorbed gamma dose rate (D), external hazard (H_{ex}), internal hazard (H_{in}), gamma radiation representative level index (I_{γ}), and the outdoor and indoor annual effective dose rate annual effective dose equivalent (AEDE) were calculated and compared with the standard values and other references values.

II. Research Methodology

A. Study Area

Erbil Governorate is the capital of Kurdistan Region Government – Iraq, the oldest city with continuous residentially. This city is regarded as one of the most deep-rooted Governorates in the area. The Erbil Governorate is located at the height of 418 m from sea level. The geographic area of the study place is located northwest to Sulaymaniyah Governorate and it is only 350 km from Baghdad. The city is surrounded by Nineveh from West, and Kirkuk city from East, and Iran and Turkey from North. The total area of the Erbil Governorate is 15214 Km^2 (Kamal and Ali, 2004), as shown in Fig. 1.

B. Sample Collection and Preparation

In the current study, 54 soil samples taken from top soil to a depth of 15 cm were collected from 15 different locations in Erbil Governorate. The samples had been desiccated in an oven at about 100°C for 24 h to remove the moisture content material then pulverized and closely sealed in cylindrical plastic chambers (13 cm diameter and 14 cm height). The samples have been saved for 30 days before counting so as to confirm up to expectation^{238}U attains radioactive equilibrium including their daughters. In average 500 g of soil is used per each sample (Jayasheelan et al., 2013).

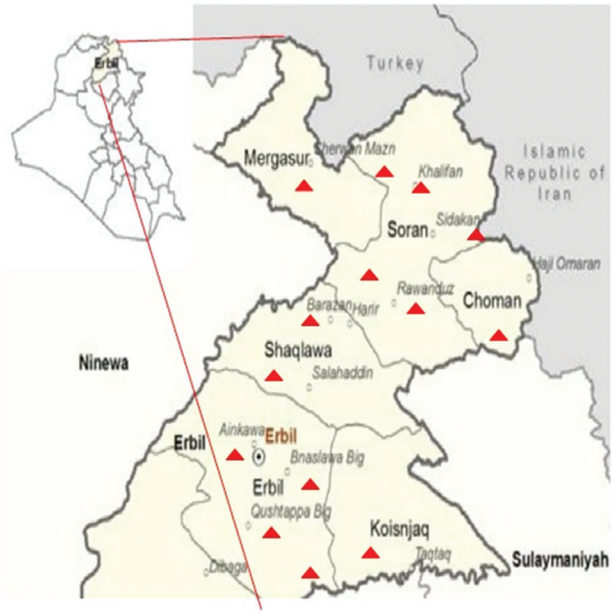

Fig. 1. Map of samples location samples in study area.

C. Gamma-ray Spectrometry

The activity natural radionuclides concentration of ^{226}Ra, ^{232}Th, and ^{40}K in soil was found using gamma-ray spectrometer system at the Biophysics Laboratory, Physics Department, USM-Malaysia. After the equipoise, the sample was kept on up of the germanium detector and calculated for a duration of 54,000 s. In the present work, we are used^{152}Eu,^{137}Cs, and^{60}Co standard sources and ^{226}Ra standard source and its progenies were used in energy calibration. The concentration of radium-226 was determined from photopeak 609.3 keV of a^{214}Bi peak, whereas the 911.2 keV photopeak of^{228}Ac peak and 583.4 keV of^{208}TI applied to fined. Thorium-232 and photopeak at 1461.6 keV were used to fine the concentration of potassium-40. To determine radionuclide concentrations for each soil sample, the total net counts below the chosen photopeaks after subtracting convenient background counts were used and by applying convenient factors for photopeak effectiveness (Kumar et al., 2001).

D. Calculation of Radiological Parameters

The gamma-ray radiation risks due to the particular radionuclides ^{226}Ra, ^{232}Th, and ^{40}K were estimated through various points. The activity concentrations of the samples have been calculated using the net area below photopeaks by (Lu and Xiaolan, 2006).

$$A_s\,(Bq/kg)=C_a/\varepsilon P_\tau\, M_s \quad (1)$$

Where A_s is the radio nucleus activity concentration of the sample, C_a is the net count rate below the corresponding peak, P_τ is the absolute transition probability of the specific ɣ ray, M_s is the mass of the sample (kg), and ε is the detector efficiency at the specific ɣ ray energy.

The ultimate widely available used radiation hazard index Ra_{eq} is called the radium equivalent activity Ra_{eq}. Radium equivalent activity is a weighted sum of activities of the up three radionuclides primary based on the determination that 370 Bq/kg of ^{226}Ra, 259 Bq/kg of ^{232}Th, and 4810 Bq/kg of ^{40}K produce the same γ-ray dose rates. Ra_{eq} is given through formula (Aziz et al., 2014).

$$Ra_{eq}=A_{Ra}+(A_{Th}\times 1.43)+(A_K\times 0.077) \quad (2)$$

Where A_k, A_{Th}, and A_{Ra} are the activity concentrations of ^{40}K, ^{232}Th, and ^{226}Ra, in Bq/kg, respectively. The equation is based on the presumption that 370 Bq/kg, 259 Bq/kg, and 4810 Bq/kg of ^{226}Ra, ^{232}Th, and ^{40}K, respectively, make the same gamma-ray dose rate.

To limit the outer gamma-radiation dose from the soil sample, an extensively used hazard index, the internal hazard index (H_{in}) and the external hazard index (H_{ex}) and were determined by the formula (Eissa et al., 2010).

$$H_{in}=A_{Ra}/185+A_{Th}/259+A_K/4810 \quad (3)$$

 http://dx.doi.org/10.14500/aro.10471

$$H_{ex}=A_{Ra}/370+A_{Th}/259+A_{K}/4810 \quad (4)$$

Where A_{Ra}, A_{Th}, and A_k the activities of ^{226}Ra, ^{232}Th, and ^{40}K in Bq/Kg.

Radiation risks related with the natural radionuclides of soil samples were estimated through radioactivity level index, $I_{\gamma r}$. The following formula was used to determine $I_{\gamma r}$ for soil below realization (Hussein, 2011).

$$I_{\gamma r}=(C_{Ra}/150)+(C_{Th}/100)+(C_{K}/1500) \quad (5)$$

Where C_{Ra}, C_{Th}, and C_K are the specific activities of ^{226}Ra, ^{232}Th, and ^{40}K in Bq/kg, respectively.

To determine average absorbed gamma dose in air D_R (nG/h) at 1 m above the ground for regular distribution of radionuclides using the formula provided through UNSCEAR (UNSCEAR, 2000).

$$D_R \text{ (nG/h)}=0.427C_{Ra}+0.623C_{Th}+0.043C_{K} \quad (6)$$

Where 0.427, 0.623, and 0.043 activities to indoor dose rate diversion factors in nG/h/Bq/kg for, ^{226}Ra, ^{232}Th, and ^{40}K, respectively. The absorbed dose rate expresses the received dose in the open air from the radiation emitted from radionuclides concentration in environmental materials. The absorbed dose used to calculate the AEDE by applying the occupancy factor of 0.2 for outdoor and 0.8 for indoor with an dose conversion factor of 0.7 Sv/Gy (Al-Hamarneh, and Awadallah, 2009).

$$(AEDE)_{outdoor}=D \text{ (nG/h)}\times 8760 \text{ (h/y)}\times 0.7 \times(103 \text{ mSv/nGy } 10^{9})\times 0.2 \quad (7)$$

$$(AEDE)_{indoor}=D \text{ (nG/h)}\times 8760 \text{ (h/y)}\times 0.7 \times(103 \text{ mSv/nGy } 10^{9})\times 0.8 \quad (8)$$

III. Results and Discussion

The results of the present work on the three types of samples are abridged in the following parts.

A. Activity Concentration in Active Soil Samples

The activity concentration of the natural radionuclides of the ^{226}Ra, ^{232}Th, and ^{40}K has been calculated in the soil samples from Erbil Governorate using gamma-ray spectrometer. The measured specific activities of ^{238}U, ^{232}Th, and ^{40}K in Becquerel per kilogram in soil samples were determined by Equation (1) and the results for the same are shown in Table I. The activity of ^{226}Ra in the soil ranged from 14.6 ± 1.6 Bq/kg (Erbil Central) to 38.2 ± 2.8 Bq/kg (Choman) with a mean of 25.61 Bq/kg, ^{232}Th ranged from 4.5 ± 1.4 Bq/kg (Erbil Central) to 38.2 ± 4.5 Bq/kg (Shaqlawa) with a mean of 20.15 Bq/kg, and ^{40}K ranged from 302.8 ± 12.6 Bq/kg (Erbil Central) to 388.6 ± 12.8 Bq/kg (Mergasur) with a mean of 326.64 Bq/kg.

The appointed activity due to ^{40}K is the biggest contributor to the total activity for all the samples. The mean activity concentration values of ^{226}Ra, ^{232}Th, and ^{40}K in the soil samples from different locations in Erbil Governorate, are shown in Fig. 2.

Table II shows the comparison for different regions of soil samples of the mean activity concentrations values. The difference in the radioactivity concentrations in the soil of the different area of the world, depending to the range of fertilizer utilized to the soil and geological status of the area (SEAM, 2005, Azeez et al., 2018).

TABLE I
The Average Activity Concentrations of Radionuclides in Soil used in Erbil Governorate

Location	Number of samples	^{226}Ra (Bq/kg)	^{232}Th (Bq/kg)	^{40}K (Bq/kg)
Erbil central	5	14.6±1.6	4.5±1.4	302.8±12.6
Koya	5	20.8±1.5	22.8±2.3	319.5±14.2
Soran	5	29.6±2.2	45 6±2.8	320.2±11.2
Rawanduz	4	30.8±2.2	26.2±2.5	322.4±12.6
Xabat	4	19.2±1.4	52.4±5.8	317.2±12.8
Shaqlawa	4	28.6±2.1	38.2±4.5	325.6±14.5
Choman	4	38.2±2.8	25.6±2.7	364.2±14.8
Khalifan	4	26.8±1.8	16.4±1.5	318.6±12.2
Hiran	4	24.5±1.7	8.6±4.2	316.4±15.6
Mergasur	3	34.5±2.9	18.5±2.4	388.6±12.8
Salahaddin	3	18.6±1.5	9.2±1.6	308.4±14.2
Sidakan	3	32.6±2.4	21.8±2.6	342.8±11.6
Bnslawa	3	17.2±1.2	11.6±1.4	310.4±12.5
Dibaga	3	22.6±1.7	6.2±2.6	315.9±11.7

TABLE II
Comparison of Activity Concentration of ^{226}Ra, ^{232}Th, and ^{40}K with Other Countries and Present Study

Country	Mean activity concentration (Bq/kg)			References
	^{226}Ra	^{232}Th	^{40}K	
Turkey	37	40	667	(Tufan and Disci, 2013)
Syria	23	20	270	(UNSCEAR, 2000)
Iran	28	22	640	(UNSCEAR, 2000)
Qatar	23.2	45.2	127.1	(UNSCEAR, 2000)
Jordan	49	27	291	(Al-Hamarneh and Awdallah, 2009)
Oman	29.7	15.9	225	(Goddard, 2001)
India	32.4	48.2	312.5	(Jayasheelan, et al., 2013)
Japan	29	28	310	(UNSCEAR, 2000)
China	38.5	54.6	584	(Lu and Xiaolan, 2006)
Pakistan	25.8	49.2	561.6	(Aziz et al., 2014)
Sweden	34	42	680	(UNSCEAR, 2000)
United State	40	35	370	(UNSCEAR, 2000)
Iraq	25.61	20.1`5	326.64	Present study

B. Radiological Indices

Estimate the health risks, the radium equivalent activity (Ra_{eq}), internal hazard index (H_{in}), external hazard index (H_{ex}), and representative level index ($I_{\gamma r}$), have been measured from the activity concentrations of ^{226}Ra, ^{232}Th, and ^{40}K by Equations (2), (3), (4), and (5), respectively, and the values are shown in Table III.

The results are shown in Table III describe that the radium equivalent activity varied from 86.4 to 188.2 Bq/kg with an average value of 141.4 Bq/kg. However, all the values for radium equivalent activity obtained here away under the limit of 370 Bq/kg (IAEA, 1989).

The internal radiation hazard index (H_{in}) ranged from 0.32 to 0.62 with an average value of 0.45 for external radiation hazard index (H_{ex}) ranged from 0.22 to 0.53 with an average value of 0.376, which all values are under the critical value of unity. Thus, established on these results of external hazard

TABLE III
AVERAGE RADIOLOGICAL HAZARDS (H_{EX}, H_{IN}, I_{TR}, AND RA_{EQ}) IN SOIL FROM ERBIL GOVERNORATE IRAQI KURDISTAN

Location	Number of samples	Radium equivalent activity Ra_{eq} (Bq/kg)	External hazard index H_{ex}	Internal hazard index H_{in}	Representative level index $I_{\gamma r}$
Erbil central	5	86.4	0.22	0.32	0.54
Koya	5	134.5	0.32	0.43	1.14
Soran	5	158.4	0.42	0.52	1.46
Rawanduz	4	168.4	0.44	0.54	1.48
Xabat	4	128.6	0.32	0.42	1.16
Shaqlawa	4	124.8	0.29	0.38	0.56
Choman	4	172.6	0.46	0.55	1.51
Khalifan	4	145.7	0.39	0.48	1.21
Hiran	4	138.2	0.35	0.44	1.17
Mergasur	3	188.2	0.52	0.62	1.88
Salahaddin	3	128.6	0.32	0.39	0.58
Sidakan	3	176.8	0.48	0.56	1.54
Bnslawa	3	115.8	0.28	0.36	0.57
Dibaga	3	112.8	0.26	0.34	0.55
	Minimum	86.4	0.22	0.32	0.54
	Maximum	188.2	0.52	0.62	1.88
	Average	141.4	0.36313	0.455625	1.110625

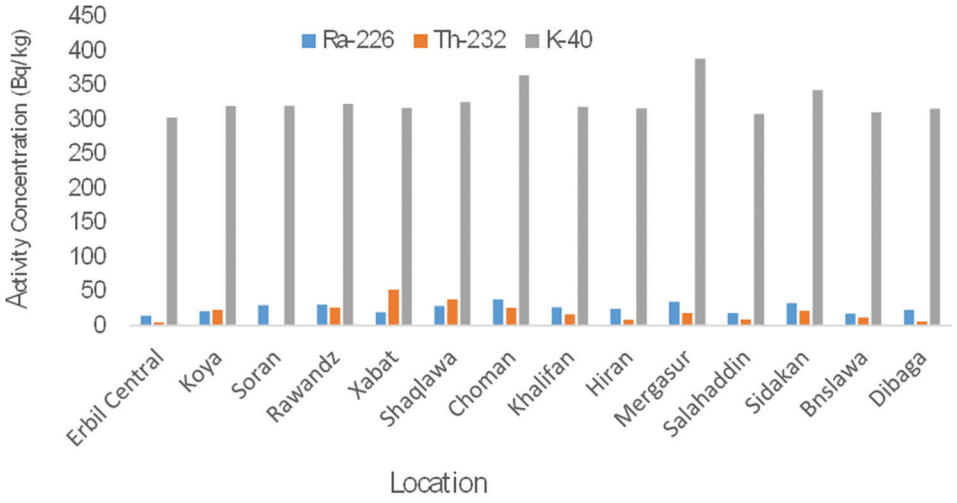

Fig. 2. Average activity of radionuclides in soil from different locations in Erbil Governorate, Iraqi Kurdistan.

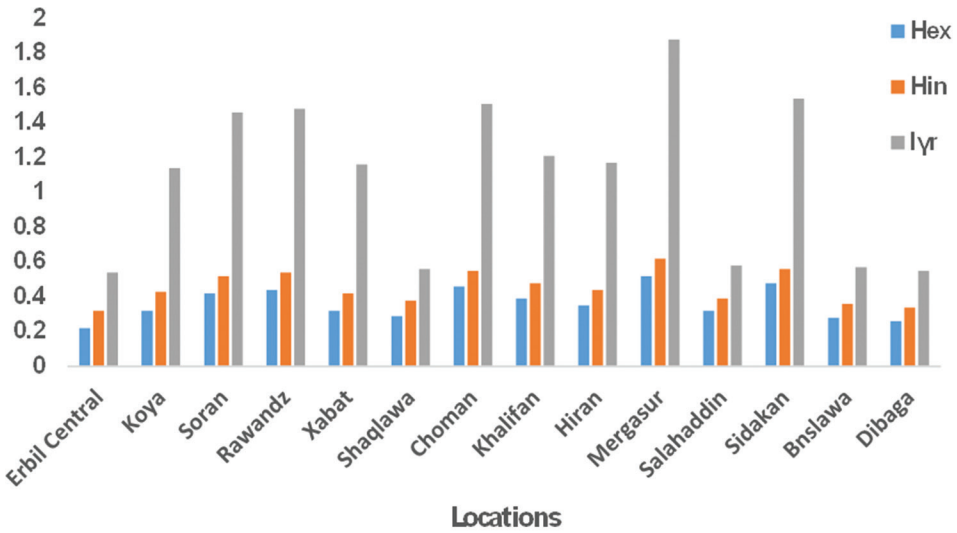

Fig. 3. The main representative level index, Iγr and hazard index (H_{ex}, H_{in}).

 http://dx.doi.org/10.14500/aro.10471

TABLE IV
AIR-ABSORBED DOSE RATES AND ANNUAL EFFECTIVE DOSES IN SOIL SAMPLES OF ERBIL GOVERNORATE

Location	Number of samples	Absorbed dose (nGh^{-1})				Annual effective dose (mSv/y)	
		^{226}Ra	^{232}Th	^{40}K	Total	$(AEDE)_{outdoor}$	$(AEDE)_{indoor}$
Erbil Central	5	6.87	2.25	9.15	18.27	0.04	0.14
Koya	5	10.22	11.54	10.12	31.88	0.05	0.18
Soran	5	15.48	22.86	10.24	48.58	0.07	0.24
Rawanduz	4	18.46	14.24	10.82	43.52	0.08	0.25
Xabat	4	9.24	26.74	9.28	45.26	0.05	0.19
Shaqlawa	4	17.82	18.92	10.64	47.38	0.07	0.22
Choman	4	26.72	13.84	11.56	52.12	0.09	0.32
Khalifan	4	16.92	8.58	10.56	36.06	0.08	0.28
Hiran	4	13.54	4.56	10.42	28.52	0.06	0.16
Mergasur	3	25.66	9.64	11.48	46.78	0.08	0.24
Salahaddin	3	9.86	4.98	9.28	24.12	0.06	0.18
Sidakan	3	23.55	10.86	11.32	45.73	0.07	0.23
Bnslawa	3	8.94	5.78	9.15	23.87	0.05	0.18
Dibaga	3	12.48	3.46	10.28	26.22	0.06	0.17
Average		15.41	11.30	10.30	37.02	0.065	0.21

AEDE: Annual effective dose equivalent

indices and radium equivalent activity, one can conclude that there are no health risks from the soil in Erbil Governorate region. Representative level index ($I_{\gamma r}$) varies from 0.54 to 1.88 with an average value of 1.11 as shown in Table III. The main representative level index, $I_{\gamma r}$, and hazard index (H_{ex}, H_{in}) are shown in Fig. 3.

C. Absorbed Dose and Annual Effective Dose

Using Equations (6), (7), and (8) measured total absorbed gamma dose rates, AEDE for indoor and outdoor, respectively, and the values are shown in Table IV. It is spotted that the activity concentration of ^{226}Ra, ^{232}Th, and ^{40}K from the absorbed dose rate varies from 6.87 to 26.72, 2.25 to 26.74, and 9.15 to 11.56 nGh^{-1}, respectively. The average dose absorbed in the work location range from 18.27 nGh^{-1} (Erbil Central) to 52.12 nGh^{-1} (Choman) a mean value 37.02 nGh^{-1}, which is lower than the limits recommended by ICRO report (ICRP, 1993).

The corresponding outdoor and indoor annual effective doses range from 0.04 to 0.09 mSv/y and 0.14 to 0.32 mSv/y, with an average value of 0.06 and 0.21 mSv/y, respectively. The worldwide mean annual effective dose is approximately 0.5 mSv/y, and the results for person countries are generally between the 0.3 and 0.6 mSv/y range for indoors recommended by UNSCEAR (UNSCEAR, 2000). Thus, the study area is still in the zones of simple radiation level which leaves the soil radioactivity there below a threat to the environment and body risks.

IV. Conclusion

Natural radioactivity levels in the soil samples for some locations in Erbil governorate have investigated using high pure germanium detector. It was found that the estimated levels were low compared with the standard levels. The mean value of total absorbed dose rate is 37.02 $nGyh^{-1}$, which is under than the world average value of 55 $nGyh^{-1}$ (ICRP, 1993). The determined average radium equivalent activity (Ra_{eq}) values for all the soil samples examined were lower than the recommended maximum level of radium equivalent of 370 Bq/kg^{-1}. The score obtained from internal and external hazard index are under than unity. The annual effective doses for indoor and outdoor are below than the action level of ICRP. The values obtained in the study are within the recommended safety limit, showing that the soil does not discompose any significant radiation risks.

Acknowledgments

The authors would like to thanks to all staff working in Biophysics Laboratory, Physics Department, USM-Malaysia for offering the use of their gamma spectrometer system.

References

Ahmed, A.H., and Samad, A.I., 2014. Measurement of radioactivity levels in daily intake foods of Erbil city inhabitants. *Journal of Zankoy Sulaimani Part A*, 16(4), pp.111-121.

Ali, M.M., 2011. Measurement of radon-222 concentration in soil samples of some sulfuric spring in hit city using CR-39 detector. *Baghdad Science Journal*, 8(4), pp.972-975.

AL-Zahrani, J.H., 2012. Natural radioactivity and heavy metals in milk consumed in Saudi Arabia and population dose rate estimates. *Life Science Journal*, 9(2), pp.651-656.

Alzubaidi, G., Hamid, F.B., and Abdul, R.I., 2016. Assessment of natural radioactivity levels and radiation hazards in agricultural and virgin soil in the state of Kedah, North of Malaysia. *The Scientific World Journal*, 2016, p.9.

Amrani, D., and Tahtat, M., 2001. Natural radioactivity in Algerian building materials. *Applied Radiation and Isotopes*, 54, pp.687-689.

Azeez, H.H., Ahmad, S.T., and Hanna, H., 2018. Assessment of radioactivity levels and radiological-hazard indices in plant fertilizers used in Iraqi Kurdistan region. *Journal of Radioanalytical and Nuclear Chemistry*, 317, pp.1273-1283.

Aziz, A.Q., Ishtiaq, A.K., Jadoon, A.A., Wajid, A.A., Adil, M.M., Anees, S.M., Abdul, W., and Aneela, T., 2014. Study of natural radioactivity in Mansehra

granite, Pakistan: Environmental concerns. *Radiation Protection Dosimetry*, 158(4), pp.466-478.

Darwish, D.A.E., Abul-Nasr, K.T.M., and El-Khayatt, A.M., 2015. The assessment of natural radioactivity and its associated radiological hazards and dose parameters in granite samples from South Sinai, Egypt. *Journal of Radiation Research and Applied Sciences*, 8(1), pp.17-25.

Dashty, T.A., and Ali, H.A., 2013. Measurement of radioactivity for ^{226}Ra radionuclide in soil samples from Bekhma region using gamma ray spectrometry. *Journal of Concepts in Pure and Applied Science*, 1(1), pp.44-48.

Eissa, H.S., Medhat, M.E., Said, S.A., and Elmaghraby, E.K., 2010. Radiation dose estimation of sand samples collected from different Egyptian beaches. *Radiation Protection Dosimetry*, 147, pp.533-540.

EL-Taher, A., and Abdelhal, M.A.K., 2013. Elemental analysis of phosphate fertilizer consumed in Saudi Arabia. *Life Science Journal*, 10(4), pp.701-708.

Fasae, K.P., 2013. Natural radioactivity in locally produced building materials in Ekiti state, Southwestern Nigeria. *Civil and Environmental Research*, 3(11), pp.99-112.

Goddard, C.C., 2002. Measurement of outdoor terrestrial gamma radiation in the Sultanate of Oman. *Health Physics*, 82(6), pp.869-874.

Hammood, H.A., and Al-Khalifa, I.J.M., 2011. Radon concentration measurement in water of Dhi-Qar governorate in Iraq using emanometer. *Journal of Basrah Researches (Sciences)*, 37(5), pp.22-29.

Hassan, N.M., Mansour, N.A., and Hassan, M.F., 2013. Evaluation of radionuclides concentration and association radiological hazard indexes in building materials used in Egypt. *Radiation Protection Dosimetry*, 157, pp.214-220.

Hussain, R.O., and Abbas, E.K., 2010. Measurement of natural occurring radio nuclides (NORMs) in soil using gamma- ray spectrometry. *Journal of Kufa Physics*, 2(2), pp.15-22.

Hussain, R.O., and Hussain, H.H., 2011. Investigation the natural radioactivity in local and imported chemical fertilizers. *Brazilian Archives of Biology and Technology*, 54(4), pp.777-782.

Hussein, A., 2011. Successive uranium and thorium adsorption from Egyptian monazite by solvent impregnated foam. *Journal of Radioanalytical and Nuclear Chemistry*, 289, pp.321-329.

Hussein, A.M., 2018. Natural radioactivity and radon exhalation in the sediment river used in Sulaymaniyah governorate, Iraq, dwellings. *ARO-The Scientific Journal of Koya University*, 6(2), pp.7-12. Available from: http://www.aro.koyauniversity.org/article/view/ARO.10471. [Last accessed on 2019 Mar 18].

IAEA., 1989. Measurement of Radionuclides in Food and the Environment. IAEA Technical Report Series No. 295, Vienna.

ICRP., 1993. International Commission on Radiological Protection ICRP Publication 65, Annals of the ICRP 23(2). Pergamon Press, Oxford.

Jayasheelan, A., Manjunatha, S., Yashodhara, I., and Karunakara, N., 2013. Study of natural radioactivity and estimation of radiation dose in the environment of Tumkur, Karnataka, India. *Radiation Protection Dosimetry,* 158(1), pp.73-78.

Jibiri, N.N., and Biere, P.E., 2011. Activity concentrations of232Th, 226Ra and 40K and gamma radiation absorbed dose rate levels in farm soil for the production of different brands of cigarette tobacco smoked in Nigeria. *Iranian Journal of Radiation Research*, 8(4), pp.201-206.

Kamal, O.A., Salar, Z.M., and Adil, M.H., 2015. Assessment of Rn and U concentrations in the soil of Qadafery, Kalar and Zarayan located in Sulaimani governorate of Kurdistan region-Iraq. *American Journal of Environmental Protection*, 4(1), pp.40-44.

Kamal, H.K., and Ali, M.S., 2004. Geological formation in Iraqi Kurdistan. *Kurdistan Academicians Journal Part A*, 4(1), pp.19-39.

Kumar, A., Singh, B., and Singh, S., 2001. Uranium, radium and radon exhalation studies in some soil samples from Una district, Himachal Pradesh, India using track-etching technique. *Indian Journal of Pure and Applied Physics*, 39, pp.761-764.

Lu, X., and Xiaolan, Z., 2006. Measurement of natural radioactivity in sand samples collected from the Baoji Weihe Sands Park, China. *Environmental Geology*, 50, pp.977-982.

Makki, N.F., Kadhim, S.H.A., Alasadi, A.H., and Almayahi, B.A., 2014. Natural radioactivity measurements in different regions in Najaf city, Iraq. *Journal of Computer Trends and Technology*, 9(6), pp.286-289.

Punniyakotti, J., and Ponnusamy, V., 2017. Radionuclides of238U, 232Th and 40K in beach sand of southern regions in Tamilnadu State, India (Post-Tsunami). *Indian Journal of Pure and Applied Physics*, 55, pp.218-230.

Salih, N.F., 2018. Determination of natural radioactivity and radiological hazards of ^{226}Ra, ^{232}Th, and ^{40}K in the grains available at Penang Markets, Malaysia, using high-purity germanium detector. *ARO-The Scientific Journal of Koya University*, 6(1), pp.71-77. Available from: http://www.aro.koyauniversity.org/article/view/ARO.10327. [Last accessed on 2019 Mar 18].

SEAM Programme., 2005. Damietta Governorate Environmental Profile, Ministry of State for Environmental Affairs. Egyptian Environmental Affairs Agency, UK.

Snežana, N., Nenadovic, M., Kljajević, L.M., Vukanac, I., Spahić, M.P., Radosavljevic-Mihajlovic, A.S., and Pavlovic, V.B., 2012. Vertical distribution of natural radionuclides in soil: Assessment of external exposure of population in cultivated and undisturbed areas. *Science of the Total Environment*, 429, pp.309-316.

Sureshgandhi, M., Ravisankar, R., Rajalakshmi, A., Sivakumar, S., Chandrasekaran, A., and Pream, A.D., 2014. Measurements of natural gamma radiation in beach sediments of north east coast of Tamilnadu, India by gamma ray spectrometry with multivariate statistical approach. *Journal of Radiation Research and Applied Sciences*, 7(1), pp.7-17.

Tufan, M.C., and Disci, T., 2013. Natural radioactivity measurements in building materials used in Samsun, Turkey. *Radiation Protection Dosimetry*, 156, pp.87-92.

UNSCEAR., 2000. Report to General Assembly, with Scientific Annexes, Sources and Effects of Ionizing Radiation, United Nations, New York.

Veiga, R., Sanches, N., Anjos, R.M., Macario, K., Bastos, J., Iguatemy, M., Aguiar, J.G., Santos, A.M., Mosquera, B., Carvalho, C., Filho, M.B., and Umisedo, N.K., 2006. Measurement of natural radioactivity in Brazilian beach sands. *Radiation Measurements*, 41, pp.189-196.

Zakariya, A.H., Jaafar, S.M., and Asaad, H.I., 2013. Measurement of radium content and radon exhalation rates in building material samples using passive and active detecting techniques. *International Journal of Scientific and Engineering Research*, 4(9), pp.1827-1831.

http://dx.doi.org/10.14500/aro.10460

Synthesis and Characterization of New Schiff Base Ligand Type [N_4O_4] from 3-(Ethoxymethylene) Pentane-2.4-dione and its Ni^{II} Complex

Eman I. Alsalihi

Department of Chemistry, Faculty of Science and Health, Koya University,
Koya KOY45, Kurdistan Region – F.R. Iraq

Abstract–**The Schiff base reaction plays an important role in the condensation reaction between 3-(ethoxymethylene) pentane-2.4-dione and 3,3'-diaminobenzidine in the presence of calculated amounts of KOH as a catalyst. This reaction has been carried out in the ethanol under reflux and overnight stirring condition. All syntheses were carried out under an atmosphere of hydrogen forming a new ligand [3,3',3'',3'''-(1E,1'E,1''E,1'''E)-(biphenyl-3,3',4,4'-tetrayltetrakis (azan-1-yl-1-ylidene)) tetrakis (methan-1-yl-1-ylidene) tetrakis (4-methoxybut-3-en-2-one)] type [N_4O_4]. The ligand and its Ni^{II} complex of the general formula [$Ni_2(L)$] have been characterized by spectroscopic methods (Fourier transform infrared and ultraviolet-visible), elemental analysis (C.H.N), metal content, magnetic susceptibility measurement, thin-layer chromatography, mass spectrometry, X-ray powder diffraction powder diffraction, ^{1}H-nuclear magnetic resonance, molar conductance, and biological activity. The ligand and its Ni complex were exposed to two types of bacteria (Staphylococcus aureus and Bacillus subtilis), using the agar disc diffusion method, and the ligand and its Niɪ complex exhibited significant activities against these two types of bacteria. Our study revealed the formation of a new ligand type [N_4O_4] and four-coordinate tetrahedral structure around Ni^{II} metal ion with the ratio of 1:2 (ligand:metal) stable compounds which can be used in many fields, such as medicine and industry.**

***Index Terms*—3-(Ethoxymethylene) pentane-2.4-dione, Four-coordinate tetrahedral complex, Nickel(II) acetate hydrate-99+%, Structural study, Schiff bases.**

I. Introduction

3-(Ethoxymethylene) $C_8H_{12}O_3$ Average mass 156.179 Da Boiling Point 140–142°/15 mm is a chemical that can be prepared by triethoxymethane and pentane-2,4-dione. This reaction is a kind of substitution. 3-(ethoxymethylene) can be used to produce (2-acetyl-3-oxo-but-1-enyl)-phosphonic acid diethyl ester with phosphonic acid diethyl ester, sodium salt (Anne-Louise et al., 2005). Nickel(II) acetate hydrate-99+% with the formula $Ni(CH_3COO)_2{\bullet}H_2O$ and formula weight 176.97 (hydrate), soluble in water, alcohol ambient temperatures is used in synthesis of polynuclear-nickel polyoxotungstate cluster compounds that are ideal for the design of molecular magnets. 3,3'-Diaminobenzidine (DAB) (Yang et al., 2016) is an organic compound with the formula $(C_6H_3(NH_2)_2)_2$. This derivative of benzidine is a precursor to polybenzimidazole, which forms fibers that are renowned for their chemical and thermal stability (Hans and Dieter, 2005). DAB is symmetric about the central carbon bond between both ring structures. In the crystal, the rings of each molecule are co-planar, and the amine units connect molecules to form an intermolecular 3-dimensional hydrogen bond network (Qian and Huang, 2010). Schiff bases have played an important role in the development of coordination chemistry as they readily form stable complexes with most of the transition metals. The chemistry of Schiff base ligands species has been gaining considerable interest primarily due to their fascinating structural diversities (Asadi et al., 2011; Monfared et al., 2011; Chamayou et al., 2011). The electrophilic carbon atoms of aldehydes and ketones can be targets of nucleophilic attack by amines. The end result of this reaction is a compound in which the C=O double bond is replaced by a C=N double bond. This type of compound is known as an imine, or Schiff base with the general formula $R_1R_2C{=}NR_3$, where R is an organic side chain. In this definition, the Schiff base is synonymous with Azomethine. Many Schiff base complexes show excellent catalytic activity in various reactions and the presence of moisture (Abu-Dief and Mohamed, 2015). The Schiff bases are widely used for industrial purposes and also exhibit a broad range of biological activities. This short review compiles examples of the most promising antimalarial, antibacterial, antifungal, and antiviral Schiff bases. An overview of synthetic methodologies used for the preparation of Schiff bases is also described (Da Silva et al., 2011). In this manuscript, we describe the synthesis and physical characterization of 3,3',3'',3'''-(1E,1'E,1''E,1'''E)-(biphenyl-3,3',4,4'-tetrayltetrakis(azan-1-yl-1-ylidene))tetrakis(methan-1-yl-1-ylidene) tetrakis(4-methoxybut-3-en-2-one) type [N_4O_4] ligand in the ratio of 1:4 (DAB) and 3-(Ethoxymethylene),

ARO-The Scientific Journal of Koya University
Volume VII, No.1 (2019), Article ID: ARO.10460, 7 pages
DOI: 10.14500/aro.10460
Received 07 October 2018; Accepted 02 May 2019
Regular research paper: Published 30 May 2019
Corresponding author's e-mail: eman.ibraheem@koyauniversity.org

and its new monomeric metal complex with a range of divalent transition metal ion Ni^{n}, in the ratio of 2:1 metal ligands, forming new compound of M-N and M-O new bands by condensation reaction, and it has been supported by the most important techniques.

II. Materials and Technique

A. Materials

The chemical reagents (3-(Ethoxymethylene), DAB, KOH, methanol, ethanol, and nickel acetate hydrate) were commercially available and used without purification. Solvents were distilled from appropriate drying agents immediately before use.

B. Physical Measurements

Reagents were purchased from Fluka and Redial–Dehenge Chemical Co. Melting points were obtained on a Buchi SMP-20 capillary melting point apparatus and are uncorrected. Fourier transform infrared (FT-IR) spectra were recorded as FT-IR spectrophotometer in the range 4000–400 cm−0. Electronic spectra of the prepared compounds were measured in the region 200–900 nm for 10−0 M solutions in dimethyl sulfoxide (DMSO) and distilled water at 25°C using a Shimadzu160 spectrophotometer with 1.000 ± 0.001 cm matched quartz cell. Elemental microanalyses were performed on a C.H.N. analyzer, whereas metal contents of the complexes were determined by atomic absorption (A.A.) technique using a Shimadzu A.A. 680G A.A. spectrophotometer. Electrical conductivity measurements of the complexes were recorded at room temperature for 10−f M solutions of the samples in DMSO and distilled water using a PW 9526 digital conductivity meter. Magnetic measurements were recorded on a Bruker BM6 instrument at room temperature following the Faraday's method. The mass spectrum for the ligand was obtained by electron-impact on (Shimadzu GCMSQPA 1000), and proton one-nuclear magnetic resonance (1H-NMR) spectrum were acquired in (DMSO-d6) solutions using (Jeol Lambda 400 MHz) spectrometer with tetramethylsilane.

III. Synthesis of $[N_4O_4]$ Ligand

A. Preparation of [3,3',3",3"'-(1E,1'E,1"E,1"')E)-(biphenyl-3,3',4,4'-tetrayltetrakis(azan-1-yl-1-ylidene))tetrakis(methan-1-yl-1-ylidene)tetrakis(4-methoxybut-3-en-2-one)] Type $[N_4O_4]$ Ligand. Scheme 1

All syntheses were carried out under an atmosphere of hydrogen. To a solution of DAB (2 g, 9.33 mmol) in ethanol (20 mL) was added 3-(ethoxymethylene) (3.4 mL) in ethanol (1.5 mL) in one portion in the ratio of 1:4, respectively. The solution was stirred for (24 h) overnight reaction at room temperature. After this time the mustard precipitate was filtered off, recrystallized with some drops of methanol, and dried in vacuum Yield: (1.2 g, 72%) m.p. (120°C).

B. Synthesis of the Ni^{n} Complex $[Ni_2(L)]$

$[N_4O_4]$ ligand complex was prepared by the general methods Scheme 2, and as follows:

A suspension of nickel (II) acetate hydrate (0.44 g, 2.49 mmol) and $[N_4O_4]$ (0.8 g, 1.52 mmol) in methanol (20 mL) with calculated amount of KOH was heated at reflux for (2 h). After cooling, a pale mustard precipitate was obtained that was collected, washed with methanol (5 mL) and dried in vacuum Yield: (0.52 g, 65%) m.p. (175°C). The [Ni2(L)] metal ion complex has been prepared in the ratio of 2:1 metal-ligand. Elemental analysis data, colors, and yields for the complexes are given in Table I.

IV. Results and Discussion

The $[N_4O_4]$ ligand was achieved from the reaction of DAB and 3-(ethoxymethylene) in the ratio of 1:4 in alkaline medium. The general synthetic method for the preparation of the ligand and its Ni^{n} complex is according to Scheme 2. The ligand was obtained in almost a quantitative yield, and the metal complex of the ligand with Ni^{n}, metal ion was obtained in moderate yields. The compounds were characterized by elemental analysis, I.R, ultraviolet-visible (U.V-Vis.), magnetic susceptibility, melting point, thin-layer chromatography (T.L.C.), X-ray powder diffraction (X-RD), mass spectrophotometer,1H-NMR, and conductivity measurements.

A. The IR Spectrum of the Ligand

The bands are at 3400 and 3200 cm^{-1} due to the $\upsilon(NH_2)$ primary amine group (Anto et al., 2009 and Varghese et al., 2006) of DAB Fig. 1-b. The strong band is at 1200–1250 cm^{-1} due to the υ(C-O-C) group (Devi and Mohamed, 2012) of 3-(Ethoxymethylene) Fig. 1-a. These two bands disappeared in the spectrum of the $[N_4O_4]$ ligand (Fig. 1-c), as a result of the replacement of the hydrogen atoms of the imine group by 3-(ethoxymethylene) and the formation of a new $[N_4O_4]$ ligand. This causes the appearance of new band at 1579.6 cm^{-1} due to the υ(C=N) group, which indicates Schiff base reaction. In the spectrum of 3,3'-Diaminobenzidine (Fig. 1-b), the band is at 3000 cm^{-1},which, due to the υ(C-H ring) (Shayma et al.,

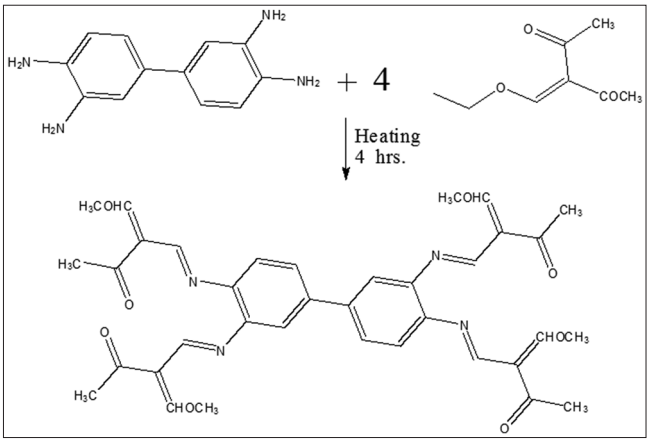

Scheme 1: Synthetic route for ligand $[N_4O_4]$.

 http://dx.doi.org/10.14500/aro.10460

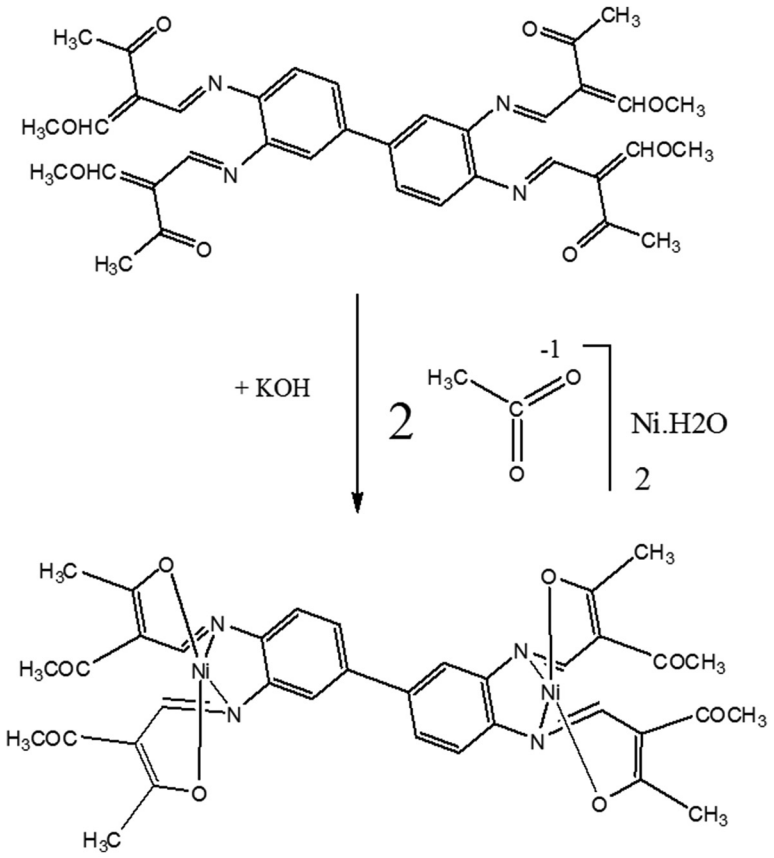

Scheme 2: The general structure for suggested [Ni_2(L)] metal ion complex.

TABLE I
THE PHYSICAL PROPERTIES OF THE LIGAND AND ITS [Ni_2(L)] METAL ION COMPLEX

Molecular formula	M.Wt	Yield%	Color	m.pc^o	Found, (calc%)					ξM(Ω^{-1} cm^2 mol^{-1})
					Ni	C	H	H	O	
$[N_4O_4]$ $C_{36}H_{38}N_4O_8$	654.71	72	Musterd	120	-	66.04	5.85	5.85	19.55	-
					-	50.54	4.21	4.21	17	-
$C_{36}H_{35}N_4Ni_2O_8$	769.07	65	Pale musterd	175	15.26	56.22	4.59	4.59	16.6414.71	19
					13.33	48.31	3.06	3.06		

TABLE II
FT-IR SPECTRA FOR THE LIGAND AND ITS PRECURSORS WITH ITS [Ni_2(L)] METAL ION COMPLEX

Χομπουνδ	ν(−NH_2)	ν(X−H) Ρινγ	ν(X=O)	ν(−NH)	CH3	ν(X−O−X)	ν(X=N)	ν(M−N)	ν(M−O)
3-(ethoxymethylene)	-	-	1650	-	1390	1200-1250	-	-	-
3,3'-Diaminobenzidine	3400-3200	3000	-	-	-	-	-	-	-
$[N_4O_4]$ $C_{36}H_{38}N_4O_8$	-	2900	1600	-	1273	-	1579.6	-	-
$C_{36}H_{35}N_4Ni_2O_8$	-	2951	1773	-	1371	-	1598	598.6	600

2016) has been shifted to higher frequency for the ligand at (2900 cm^{-1}), whereas the υ(C=O) band at 1650 cm^{-1} (Baran et al., 2007 and Roeges, 1994) of 3-(Ethoxymethylene) Fig. 1-a is shifted to the lower frequency at (1600 cm^{-1}) in comparison with that of the spectrum of the free ligand (Fig. 1-c), as a result of the coordination between DAB and 3-(Ethoxymethylene) starting materials Table II.

B. The UV-Vis Spectrum of the Ligand

The UV-Vis spectrum of the ligand exhibits a high intense absorption peak at (210 nm) (47619 cm^{-a}) (ϵ_{max}=1421 molar^{-1}. cm^{-}), assigned for (π→ π*) transition (Anuradha and Rajarel, 2011) Table III.

C. The IR Spectrum of the [Ni_2(L)] Metal Ion Complex

In the spectrum of the free ligand Fig. 1-c, there are important bands at 1579.7 cm^{-1}, 1600 cm^{-1}, and 2900 cm^{-1} due to the υ(C=N), υ(C-O), and υ(C-H) ring, respectively. All these bands have been shifted to higher frequencies in comparison with that of the spectrum of Ni^{II} complex Fig. 1-d, as a consequence of the coordination of the ligand with the metal ion, whereas the characteristic new formed

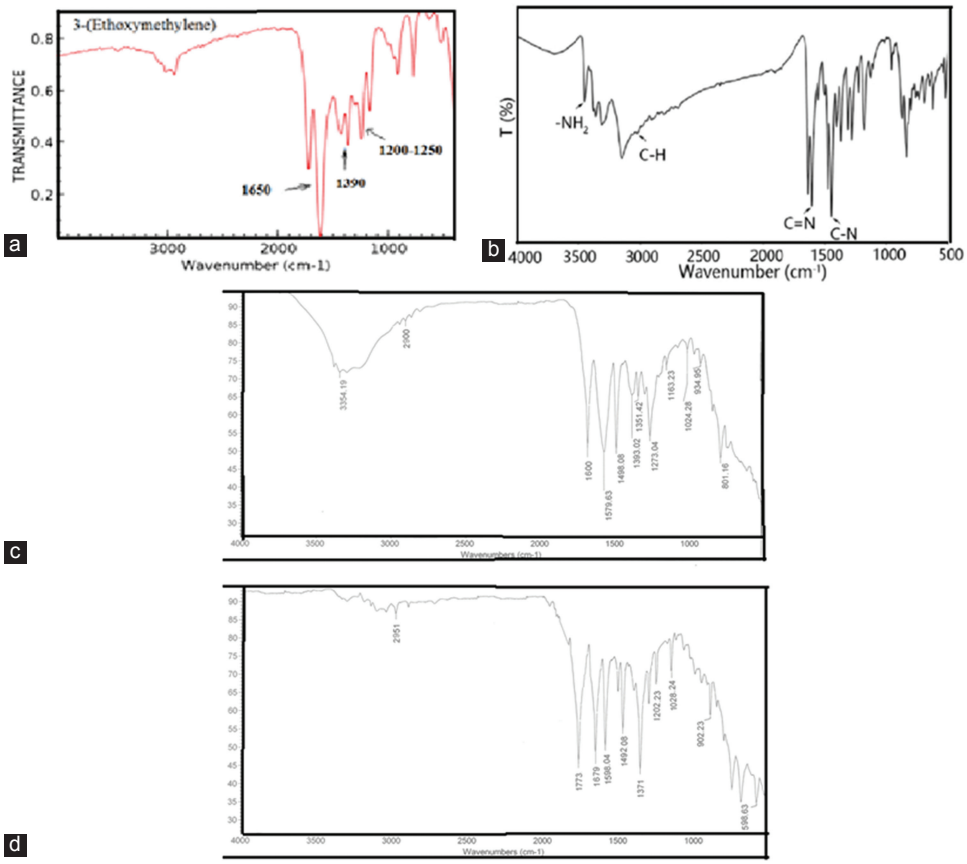

Fig. 1. (a-d) The Fourier transform infraredspectrum for the [N_4O_4] ligand and its starting materials with its [Ni_2(L)] metal ion complex.

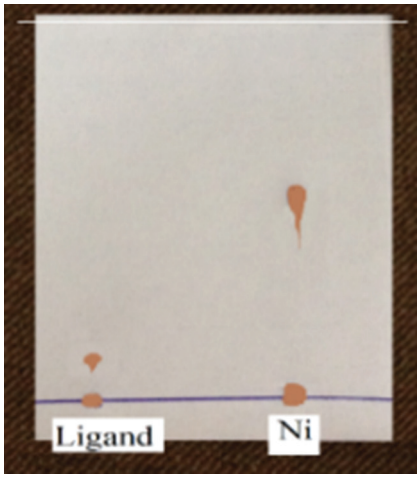

Fig. 2. The thin-layer chromatography measurements for the [N_4O_4] ligand and its [Ni_2(L)] metal ion complex.

bands at 598.6 cm^{-1} and 600 cm^{-1} range are assigned to the υ(Ni-N) and υ(Ni-O) (Ali et al., 2001), respectively, for all the formed complex Table II.

D. The UV-Vis Spectrum of the Ni^n Complex

The UV-Vis spectra of Ni^n complex showed two intense absorption peaks in the range at 285 nm (35087 cm^{-1}) (ϵ_{max}=1560 $molar^{-1}$. cm^{-1}) and (300 nm) (33333 cm^{-1}) (ϵ_{max}=90 $molar^{-1}$. cm^{-1}), range assigned to the ligand field and C.T., respectively (Griffith et al., 2011). The third peak detected in the visible region at 610 nm (16666 cm^{-1}) (ϵ_{max}=1235 $molar^{-1}$. cm^{-1}), range attributed to the electronic transition ($^3T_1 \rightarrow {}^3T_{1P}$) (Dhanaraj and Nair, 2014).

Thus, the magnetic moment value is 3.7 B. M (Uppadin et al., 2001, and Al-Jeboori et al., 2010), which demonstrates that the Ni^n complex is paramagnetic and has high spin tetrahedral geometry Table III.

E. Molar Conductance

The prepared complex found to be solids. It is soluble in some organic solvents such as dimethylformamide and dimethyl sulfoxide. The lower value observed of molar conductivities in DMSO in the range of 19 indicates the non-electrolyte behavior of the Ni^n metal ion complex (Kai et al., 2009 and Kettle, 1975).

F. Elemental Analysis (C.H.N) and Metal Determination

Elemental analysis (C.H.N) and metal determination were in good agreement with the general formula given for the Ni^n metal ion complex. Table I gives, in details, the physical properties of the complexes.

T.L.C. measurement for the derivative ligands [N_4O_4] and its Ni^n complexare shown in Fig. 2. The appearance of new spots with different Rf. compared with the Rf. of the ligand Table IV for Ni^n indicated the formation of the complex. Since the spots positions belong to Ni^n ion complex, they differ from the position of the ligands spot.

http://dx.doi.org/10.14500/aro.10460

The biological activity of the $[N_4O_4]$ ligand and its Ni^{II} complex was tested on two types of pathogenic bacteria using inhibition method (Anacona, 2006, Tauber and Nau, 2008, Petra et al., 2005, and Sultana and Arayne, 2007). The two types of bacteria were Gram-positive *Staphylococcus aureus* and *Bacillus subtilis*. The ligand $[N_4O_4]$ was not affected by any of the two types of bacteria, whereas its $[Ni_2(L)]$ complex showed inhibition diameter against the two types of bacterial after 24 h, and this inhibition diameter was increased after 48 h Fig. 3.

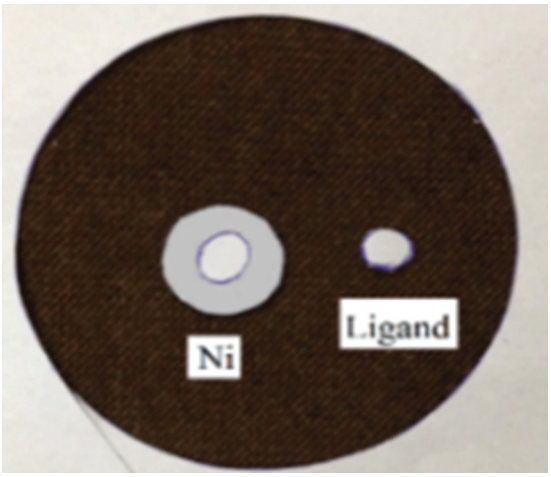

Fig. 3. The biological activity of the $[N_4O_4]$ ligand and its $[Ni_2(L)]$ metal ion complex after 48 h.

The mass spectrum shows the base peak at 654.72 related to the molecular weight of the ligand. Moreover, all the other fragmentations are compatible with the value of the fragments of the ligand as shown in Fig. 4.

The X-RD pattern of $[Ni_2(L)]$ complex shows well-defined crystalline peaks indicating that the sample is 53% crystalline in nature (Dokken et al., 2009 and Khalaj and Das, 2014). An X-RD powder diffraction pattern of $[Ni_2(L)]$ metal ion complex has been given in Fig. 5. The sample has been dried and then scanned in the 2θ range of 10–80°, confirming tetrahedral geometry around $[Ni_2(L)]$ ion complex (Kavitha and Lakshm, 2017 and Zheng et al., 2017).

The ^{1}H-NMR spectrum for $[N_4O_4]$ ligand in DMSO-d6 solvent Fig. 6 showed a single signal peak which appears at 2.1 ppm –CH(3H) attributed to a methyl group. Table V summarized the details of the other chemical shifts.

V. Conclusion

The reaction of 3-(ethoxymethylene) with DAB gives the required $[N_4O_4]$ ligand. The reaction of this ligand with metal (II) acetates resulted in the formation of the required

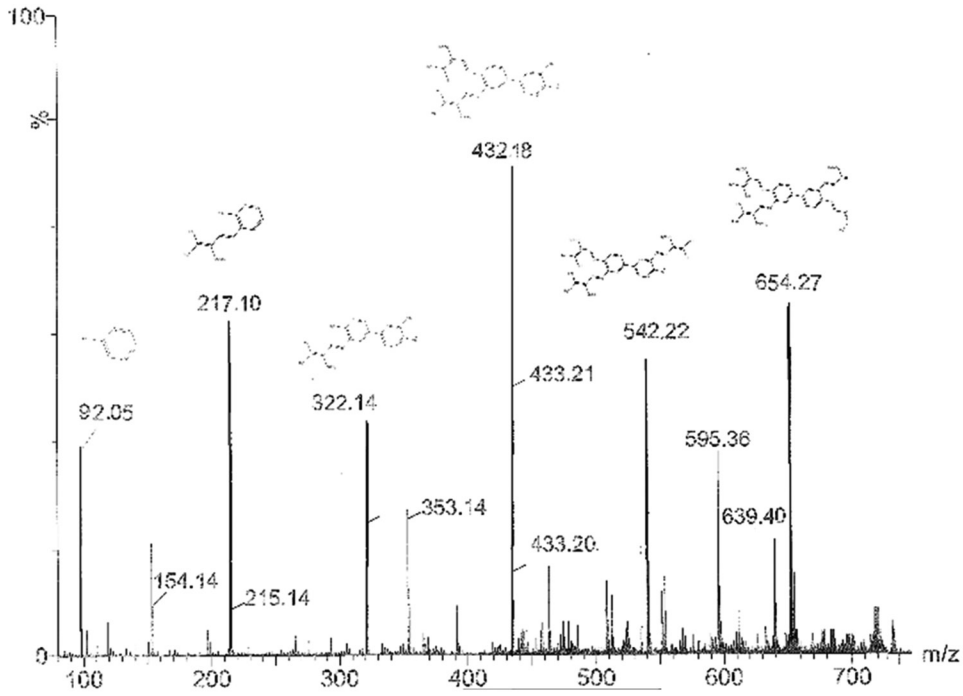

Fig. 4. The mass spectrum for the $[N_4O_4]$ ligand.

TABLE III
The Electronic Spectral Data for the Ligand and its $[Ni_2(L)]$ Metal Ion Complex

Compound	Band position λ_{nm}	Wave number (cm^{-1})	ε_{max} ($dm^3\ mol^{-1}\ cm^{-1}$)	Assignment	Magnetic moment (B.M)	Suggested configuration
$[N_4O_4]$ $C_{36}H_{38}N_4O_8$	210	47619	1421	$\pi \rightarrow \pi^*$	-	-
$C_{36}H_{35}N_4Ni_2O_8$	285	35087	1560	$\pi \rightarrow \pi^*$	3.4	Tetrahedral
	300	33333	90	Ch.T	paramagnetic	
	610	16666	1235	$^3T_1$–$^3T_{1P}$		

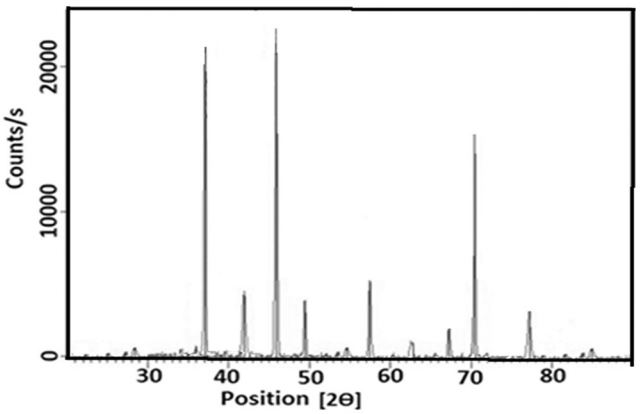

Fig. 5. The X-ray powder diffraction powder diffraction pattern for $[Ni_2(L)]$ complex.

TABLE IV
THE T.L.C. MEASUREMENTS FOR $[N_4O_4]$ LIGAND AND ITS $[Ni_2(L)]$ METAL ION COMPLEX

Compound	Range of R_f (mm)
$[N_4O_4]$ $C_{36}H_{38}N_4O_8$	4.1
$C_{36}H_{35}N_4Ni_2O_8$	1.2

T.L.C.: Thin-layer chromatography

TABLE V
THE CHEMICAL SHIFTS IN ^{1}H-NMR SPECTRA OF $[N_4O_4]$ LIGAND

Proton environment	H	Δ (ppm)
CH_3 methyl	8(C-H)	2.1
C-H benzene	6(C-H)	7.7
H ethylene	4(C-H)	7.7
C-H aldimine	4(C-H)	7.9
DMSO solvent	-	3.4

^{1}H-NMR: ^{1}H-nuclear magnetic resonance, DMSO: Dimethyl sulfoxide

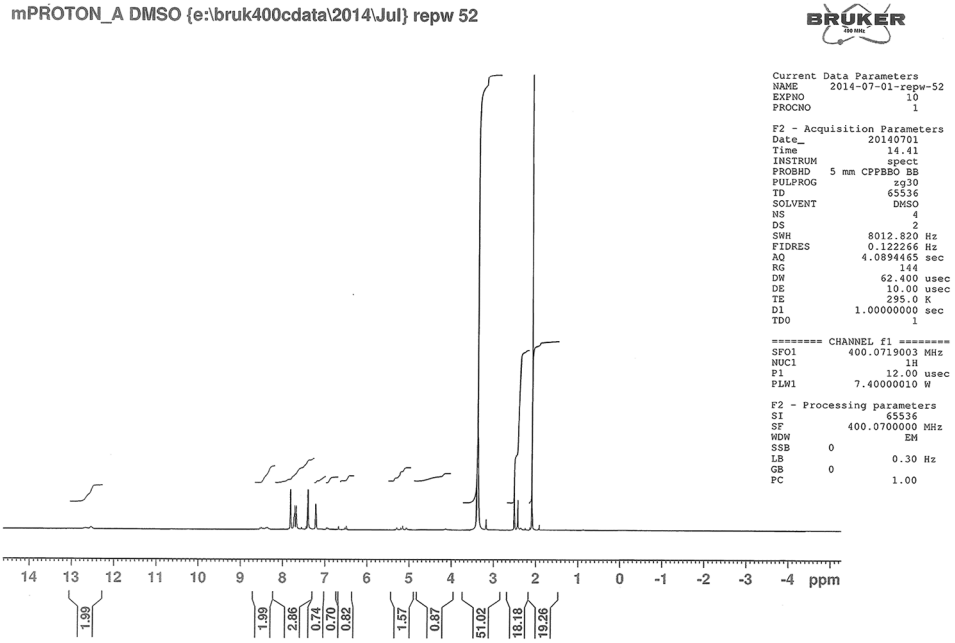

Fig. 6. The ^{1}H-nuclear magnetic resonance spectrum for the $[N_4O_4]$ ligand.

complex with tetrahedral geometry around $[Ni_2(L)]$ ion complex. Physical, chemical, and spectroscopic methods were used to investigate the mode of bonding and overall structure of the Ni^n complex of $[N_4O_4]$ ligand which has been synthesized and characterized by elemental analyses and spectroscopic techniques. The X-RD of the Ni^n ion complex revealed that the complexes are 53% crystalline. The F.T-I.R. measurements, U.V-Vis., and mass spectrum for the ligand and its complexes reveal the exact peak for each of the compounds functional groups. Moreover, the aims of this study are as follows:

1. The formation of a new complex by the reaction between DAB and 3-(ethoxymethylene) with Ni^n metal ion.
2. Determine some of the best metal complexes for activating the multiple bonds in M-N and M-O.
3. Syntheses of the new ligand with 3-(ethoxymethylene)
4. Studying the characteristic properties of the (3Z,3'Z,3''Z)-3,3',3''-((1E,1'E,1''E)-(4'-((E)-((E)-2-acetyl-3-hydroxybut-2-enylidene)amino)biphenyl-3,3',4-triyl)tris(azan-1-yl-1-ylidene)tris(methan-1-yl-1-ylidene))tris(4-hydroxypent-3-en-2-one) type $[N_4O_4]$ ligand.

REFERENCES

*A*bu-Dief Ahmed, A.M., and Mohamed, I.M.A., 2015. A review on versatile applications of transition metal complexes incorporating Schiff bases. *Beni-Suef University Journal of Basic and Applied Sciences*, 4, pp.119-133.

Ali, M.A., Mirza, A.H., and Butcher R.J., 2001. Synthesis and characterization of copper(II) complexes of the methylpyruvate Schiff base of S-methyldithiocarbazate (Hmpsme) and the X-crystal structures of Hmpsme and [Cu(mpsme)Cl]. *Polyhedron*, 20(9-10), pp.1037-1043.

Al-Jeboori, M.J., Al-Tawel, H.H., and Mahmood, R., 2010. New metal complexes of N2S2 tetradentate ligands: Synthesis and spectral studies. Inorganica Chimica Acta, 363, pp.1301-1305.

Anacona, J.R., 2006. Synthesis and antibacterial activity of some metal complexes of β-Lactams antibiotics. *Journal of Coordination Chemistry*, 54, pp.355-365.

Anne-Louise, H., Jack, T., Howard, S., Abdelwahid, M., Veronique, D., Georges, L., and Ian, B., 2005. Rate coefficients for the reactions of OH radicals with the keto/enol tautomers of 2,4-pentanedione and 3-methyl-2,4-pentanedione, allyl alcohol and methyl vinyl ketone using the enols and methyl nitrite as photolytic sources of OH. J*ournal of Photochemistry and Photobiology A: Chemistry*, 176(1-3), pp.183-190.

Anto, P.L., Anto, R.J., Varghese, H.T., Panicker, C.Y., Philipe, D. and Brolof, A.G., 2009. FT-IR, FT-Raman and SERS spectra of anilinium sulphate. *Journal of Raman Spectroscopy*, 40, pp.1810-1815.

Anuradha, K., and Rajarel, R., 2011. Synthesis, spectral characterization and biological activity of new symmetrical macrocyclic binuclear Schiff base complexes. Internatiol *Journal of Pharmacy and Technology*, 2, p.2217.

Asadi, M., Sepehrpour, H., and Mohammadi, K.H., 2011. Tetradentate schiff base ligands of 3,4-diaminobenzophenone: Synthesis, characterization and thermodynamics of complex formation with Ni(II), Cu(II) and Zn(II) metal ions. *Journal of the Serbian Chemical Society*, 76, pp.63-74.

Baran, E.J., Viera, I., and Torre, M.H., 2007. Vibrational spectra of the Cu(II) complexes of L-asparagine and L-glutamine. *Spectrochimica Acta, Part A: Molecular and Biomolecular Spectroscopy*, 66A, p.114.

Chamayou, A.C., Lüdeke, S., Brecht, V., Freedman, T.B., Nafie, L.A., and Janiak, C., 2011. Chirality and diastereoselection of the configured tetrahedral zinc complexes through enantiopure Schiff base complexes: Combined vibrational circular dichroism, density functional theory, 1H NMR, and X-ray structural studies. *Inorganic Chemistry*, 50, pp.11363-11374.

Da Silva Cleiton, M., da Silva Daniel, L., Modolo, L.V., Alves, R.B., de Resende, M.A., Martins, C.V.B., and Ângelode, F., 2011. Schiff bases: A short review of their antimicrobial activities. *Journal of Advanced Research*, 2, pp.1-8.

Dhanaraj, C.J., and Nair, M.S., 2014. Synthesis and characterization of cobalt (II) and zinc (II) complexes of poly(3-nitrobenzyli dene-1-naphthylamine-co-succinic anhydride). *Journal of Saudi Chemical Society*, 18(5), pp.479-485.

Dokken, K.M., Parsons, J.G., McClure, J., and Gardea-Torresdey, J.L., 2009. Synthesis and structural analysis of copper (II) cysteine complexes. *Inorganica Chimica Acta*, 362, pp.395-401.

Devi, G.K.D., and Mohamed, M.I.F., 2012. A facile synthesis of phenyl phenacyl ethers. *Der Chemica Sinica*, 3(1), pp.71-75.

Griffith, D.M., Szocs, B., Keogh, T., Suponitsky, K.Y., Farkas, E., Buglyó, P., and Marmion, C.J., 2011. Suberoylanilide hydroxamic acid, a potent histone deacetylase inhibitor; Its X-ray crystal structure and solid state and solution studies of its Zn(II), Ni(II), Cu(II) and Fe(III) complexes. *Journal of Inorganic Biochemistry*, 105, pp.763-769.

Hans, S., and Dieter, M., 2005. Benzidine and benzidine derivatives. In: *Ullmann's Encyclopedia of Industrial Chemistry*. Wiley-VCH, Weinheim.

Qian, H.F., and Huang, W., 2010. Biphenyl-3,3',4,4'-tetraamine. *Acta Crystallographica Section E, E66(5)*, p.1060.

Kai, Y., Gu, Z., Ji, R., and Lou, L.S., 2009. Heterogeneous chiral Mn(111) salen catalysts for the epoxidation of unfunvtionalized olefins immobilized on mesoporous materials with different pore sizes. *Tetrahedron*, 65, pp.305-311.

Kavitha, N., and Lakshm, P.V.A., 2017. Synthesis, characterization and thermogravimetric analysis of Co(II), Ni(II), Cu(II) and Zn(II) complexes supported by ONNO tetradentdate Schiff base ligand derived from hydrazine benzoxazine. *Journal of Saudi Chemical Society*, 21(Supplement 1), pp.S457-S466.

Kettle, S.F.A., 1975. *Coordination Compounds*. Thomas Nelson and Sons, London, p.165.

Khalaj, A.D., and Das, D., 2014. Synthesis and characterization of NiO nanoparticles via solid-state thermal decomposition of Nickal(II) Schiff base complexes. *International Nano Letters*, 4, p.117.

Monfared, H.H., Vahedpour, M., Yeganeh, M.M., Ghorbanloo, M., Mayer, P., and Janiak, C., 2011. Concentration dependent tautomerism in green [Cu(HL1)(L2)] and brown [Cu(L1)(HL2)] with H2L1=(E)-N′-(2-hydroxy- 3-methoxybenzylidene) benzoylhydrazone and HL2=pyridine-4-carboxylic (isonicotinic) acid. *Dalton Transactions*, 40, pp.1286-1294.

Petra, D., Tatjano, Z., and Boriset, P., 2005. Mixed-valence Cu(II)/Cu(I) complex of quinolone ciprofloxacin isolated by a hydrothermal reaction in the presence of l-histidine: Comparison of biological activities of various copper-ciprofloxacin compounds. J*ournal of Inorganic Biochemistry*, 2, pp.432-442.

Roeges, N.P.G., 1994. *A Guide to the Complete Interpretation of Infrared Spectra of Organic Structures*. Wiley, New York.

Shayma, A.S., Khaledi, H., Cheah, S.C., and Ali, H.M., 2016. New Mn(II), Ni(II), Cd(II), Pb(II) complexes with 2-methylbenzimidazole and other ligands. Synthesis, spectroscopic characterization, crystal structure, magnetic susceptibility and biological activity studies. *Arabian Journal of Chemistry,* 9(Supplement 2), pp.S1943-S1950.

Sultana, N., and Arayne, M.S., 2007. In vitro activity of cefadroxil, cephalexin, cefatrizine and cefpirome in presence of essential and trace elements. Pakistan *Journal of Pharmaceutical Sciences*, 20, pp.305-310.

Tauber, S.C., and Nau, R., 2008. Immunomodulatory properties of antibiotics. *Current Molecular Pharmacology*, 1, p.68.

Uppadin, L.H., Weeks, J.M., and Beer, P.D., 2001. Metal-directed self-assembly of terphenyl based dithiocarbamate ligands. *Journal of the Chemical Society Dalton Transactions*, 22, pp.3367-3372.

Varghese, H.T., Panicker, C.Y., Anto, P.L., and Philip, D., 2006. Potential□ dependent SERS profile of orthanilic acid on silver electrode. *Journal of Raman Spectroscopy*, 37, pp.1265-1271.

Yang, W., Yuanjun, S., Lei, Z., Nahla, R., Bo, J., and Yudong, H., 2016. An investigation of the high performance of a novel type of benzobisoxazole fiber based on 3,3-diaminobenzidine. *Polymers*, 8, p.420.

Zheng, Z., Junwei, X., Sisi, Y., Yangli, C., Yan, W., Zhuo, C., and Chunlin, N., 2017. Two organic cation salts containing tetra(isothiocyanate)cobaltate(II): Synthesis, crystal structures, spectroscopic, optical and magnetic properties. *Crystals*, 7(3), p.92.

The Study of Optical Energy Gap, Refractive Index, and Dielectric Constant of Pure and Doped Polyaniline with HCl and H_2SO_4 Acids

Amera G. Baker

Department of Physics, Faculty of Science and Health, Koya University,
Koya KOY45, Kurdistan Region - F.R. Iraq

***Abstract*—Polyaniline (PANI) salt in its pure and doped forms find extensive applications in making devices such as polymer light emitting diodes, photovoltaic, sensors, batteries, and super capacitors. PANI salt has been synthesized successfully through chemically oxidative polymerization of aniline in the presence of hydrochloric acid (HCl) and sulfuric acid (H_2SO_4) using ammonium peroxydisulfate as an oxidizing agent. The absorption spectra of pure PANI salt and its doped state, in HCl and H_2SO_4 media, have been studied in the wavelength range from 200 to 1100 nm using ultraviolet and visible near infrared spectrophotometer. Tauc's formula, Lambert-Beer's relation, and Fresnel's formula were employed in the MATLAB program to calculate the optical energy gap, refractive index, and dielectric constant. Results showed that doping with HCl and H_2SO_4 acidic mediums caused a reduction in the direct energy gap of the pure PANI from 2.69eV to 2.42 eV and 2.54 eV, respectively. The reduction in optical energy gap is associated with the increase in refractive index. The refractive index (2.92) has a higher value of PANI doped with HCl. Higher refractive index values are for better-structured films.**

***Index Terms*—Hydrochloric acid, Optical constants, Polyaniline, Sulfuric acid, Ultraviolet and visible spectroscopy.**

I. Introduction

Conducting polymers, especially polyaniline (PANI) is well-known as an environmentally stable and highly tunable conducting polymer, which can be produced as a bulk powder, cast films, or fibers. This is in conjunction with the feasibility of low-cost, large-scale production makes it an ideal candidate for devices such as supercapacitors (Liao et al., 2018; Du et al., 2017), polymer light emitting diodes (Xu et al., 2016), sensors (Dai et al., 2016), photovoltaic (Gizzie et al., 2015), and batteries (Ma, and Kan, 2013). The ability of PANI to exist in various forms through acid/base treatment and oxidation/reduction, either chemically or electrochemically has made PANI the most tunable member of the conducting polymer (Chaqmaqchee, and Baker, 2015; Lu et al., 2011). PANI has a rigid backbone originating from an extended conjugated double bond. The rigid structure of PANI restricts its common usage and results in the insolubility, infusibility, and incompatibility of this material with common polymers (Kenry and Liu, 2018; Bharti et al., 2018). To improve its processability various methods have been tried, and two significant attempts to overcome these drawbacks are chemical modification such as doped PANI and substituted derivatives of PANI, respectively (Liao et al., 2019). The chemically modified PANI not only shows improved processability but also exhibit better conductivity property and anti-corrosion property than pure PANI (Olinga et al., 2000). In the last few years, number of researchers have focused on producing high-quality of PANI by modification of PANI by doping through protonic organic and inorganic acids (Al-Daghman et al., 2016). The solubility and conductivity of PANI can be greatly enhanced by doping through protonic organic acids. Three reasons can possibly explain this phenomenon. First, the protonic organic acids doped into the molecular chain of PANI act as a surfactant, which can improve its solubility. Second, functional groups of the protonic organic acids further improve its solubility. Third, when the protonic organic acids are doped into the PANI molecular chain, it is beneficial to the ionization of charge and meanwhile increases its conductivity (Liao, and Xu, 2019). These protonic organic acids commonly contain long alkyl side chains such as camphorsulfonic acid, dodecylbenzene sulfonic acid, p-toluenesulfonic acid, phytic acid, carboxylic acid, acetic acid, and oxalic acid. Since, the size of protonic organic acids is slightly large, causing their diffusion rate slows down. Therefore, more and more researchers turn their attention to protonic inorganic acids due to its size is relatively small, which facilitate its diffusion. Heteropoly acid, as a high-intensity proton acid, can afford protons in the preparation process of PANI, and can also be taken as a solid-state acid in solid-state synthesis reaction (Ladera et al., 2014). (Hassan et al., 2012) studied the a.c

ARO-The Scientific Journal of Koya University
Volume VII, No.1(2019), Article ID: ARO.10483, 6 pages
DOI: 10.14500/aro.10483
Received 09 January 2019; Accepted 11 May 2019
Regular research paper: Published 30 May 2019
Corresponding author's e-mail: amera.baker@koyauniversity.org

http://dx.doi.org/10.14500/aro.10483

conductivity of PANI pure and doped with inorganic acids (such as HCl, and H_2SO_4) at room temperature. They found that the sample doped with HCl has higher conductivity from the other samples. Furthermore, they found that PANI doped with H_2SO_4 has improved the enhanced solubility which dissolvent partially in water. Kulkarni et al., 2004, studied the nanostructures of PANI doped with HCl, H_2SO_4, $HClO_4$, HNO_3, and H_3PO_4. The $HClO_4$ doped PANI showed the folded lamellar structure derived from the fibers. Moreover, a greater fraction of the conducting emeraldine salt phase was formed in $HClO_4$ as a protonic acid media. Zhang et al., 2002, studied the nanostructures of PANI doped with inorganic acids such as HCl, H_2SO_4, HBF_4, and H_3PO_4. They found that the morphology, size (150–340 nm), and conductivity (0.1–10 S/cm) of the obtained PANI nanostructures mainly relied on the dopant structures and the reaction conditions. Interestingly, the thermal stability of H_3PO_4 doped PANI was found to be improved compared to other acids doped PANI. Gong et al., 2002, described a novel solid-state synthesis method to prepare $H_4SiW_{12}O_{40}$ doped PANI. The conductivity property and fluorescence property of the $H_4SiW_{12}O_{40}$ doped PANI were found to be excellent. In this work, PANI salt has been synthesized through chemically oxidative polymerization of aniline in the presence of hydrochloric acid (HCl), and sulfuric acid (H_2SO_4) using ammonium peroxydisulfate (APS) as an oxidizing agent at room temperature. The synthesis of pure PANI and in its doped state, in HCl (PANI-HCl) and H_2SO_4 (PANI-H_2SO_4) media were studied and characterized in terms of absorption properties, optical energy gap, refractive index, and dielectric constant. The purpose of this work is to synthesis the easiest and cheapest method with a high quality of PANI for electronics device applications.

II. Materials and Methods

A. Materials

The chemicals used in the preparation of PANI are aniline hydrochloric ($C6H_5$ NH_2 HCl), ammonium persulfate $(NH_4)_2S_2O_8$, HCl, H_2SO_4, acetone, and dimethylformamide (DMF) are of high purity (>99%), which their supplier companies are Hopkin and Williams (UK) and BDH (Middle East LLC) were obtained from the Chemistry Department, College of Science, University of Baghdad.

B. Synthesis of Pure and Doped PANI

PANI salt has been synthesized through chemically oxidative polymerization of aniline in the presence of HCl and H_2SO_4 using APS as an oxidizing agent (Ninh et al., 2016; Hassan et al., 2012). The aniline hydrochloride and APS solutions were prepared by mixing (0.2 M) aniline hydrochloride with (0.25 M) APS in an aqueous medium. The pure sample was prepared in distilled water and the doped samples with (2) molarities of HCl and H_2SO_4 in aqueous solution. Three- necked round-bottomed flask equipped with a thermometer. Electromagnetic stirrer and condenser were used to polymerize PANI. To prepared sample doped with (2 M), aniline hydrochloride in (1 M) aqueous solution in a volumetric flask to (50 ml) of solution, ammonium pexroydisulfate is similarly dissolved in (1 M) HCl also to 50 ml of solution, both solutions are mixed at room temperature in a rounder, and gentle stirring to polymerize the mixture, and left the rest to the next day. The (PANI) precipitate is collected on a filter and washed with 3 times (100 ml) of 0.2 M HCl, and 150 M of acetone. PANI (emeraldine salt) hydrochloride powder was dried in air for 1 h than in the vacuum oven at 80°C for 6 h; the powder was thoroughly grounded in a mortar to obtain very fine particles. In a similar way, PANI has been doped with H_2SO_4 acid; Figs. 1 and 2 (Al-Daghman et al., 2016; Stejskal, and Polyaniline, 2002). The standard solution cast technique was used to prepare the pure and doped PANI films. The PANI solution was prepared by weighted 0.1 g of PANI salt and dissolved in 10 ml of DMF and stirring for 3 h. The solutions were then cast into different clean and dry dishes and allowed to evaporate at room temperature until solvent-free films were obtained.

C. Ultraviolet and visible (UV-Vis) Spectroscopy

UV-Vis spectrophotometer model UV/1601 manufactured by Shimadzu Co. (Japan) was carried out in the Chemistry Department, College of Science, University of Baghdad (Manual, 1994; Robert et al., 2005). UV-Vis spectroscopy is a reliable and accurate analytical laboratory assessment procedure that allows for both qualitative and quantitative analysis of a substance. Specifically, UV-Vis spectroscopy probes the electronic transitions of molecules as they absorb light in the UV and visible regions of the electromagnetic

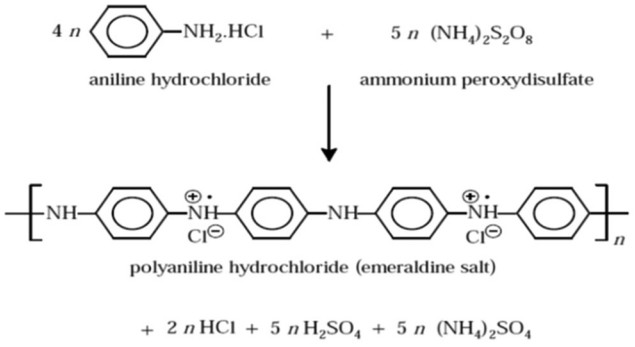

Fig. 1. Oxidation of aniline hydrochloride with ammonium peroxydisulfate yields polyaniline hydrochloride.

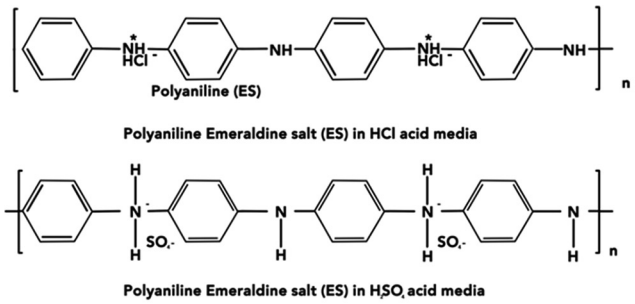

Fig. 2. Protonic acid media doping of polyaniline (PANI) (PANI-emeraldine salt).

radiation (Schymanski et al., 2014). The absorption spectra of the synthesized pure and doped PANI were recorded over a wavelength range of 200–1100 nm. The MATLAB program was used, and Tauc's formula, Beer-Lambert's relation, and Fresnel's formula were employed in the program to calculate the absorption coefficient and the optical constants.

III. Results and Discussions

A. Absorbance Spectra of Pure and Doped Samples

Fig. 3 shows the UV-visible absorption spectra at the range 200–1100 nm of pure and doped PANI with HCl and H_2SO_4. The absorption peaks occur at 200 and 553nm of pure PANI assigned to π→π* electronic transitions related to the benzenoid form of PANI and polaron→π* electronic transitions related to the quinoid rings of PANI, respectively (Melad, and Jarur, 2016). The absorption spectra of doped PANI with HCl showed two peaks around 200 nm and 870 nm assigned to π→π* electronic transitions and π→ polaron electronic transitions, respectively. The absorption spectra of doped PANI with H_2SO_4 showed three peaks around 200 nm, 271 nm, and 885 nm assigned to π→π* electronic transitions, polaron→π* electronic transitions, and π→ polaron electronic transitions, respectively (Hassan, 2013; Yin, and Ruckenstein, 2000). This confirms the polaron band formation in the band gap of the polymer on of protonic acid doping (Al-Daghman et al., 2016; Varma et al., 2012). In general, PANI-HCl exhibited the best optical absorbance in the UV, visible and Near Infrared regions among the other samples.

B. Optical Band Gap

Optical absorption spectra constitute one of the most important means to determine the optical energy gap (E_g) of organic and inorganic semiconductors (Muhammad et al., 2010). Energy gap is called band gap which is of fundamental importance because the energy gap determines the electrical conductivity and optical absorption character of the PANI. The absorption coefficient (α), at the corresponding wavelengths, is calculated using the Beer-Lambert's relation: α = 2.303A/l where l is the path length and A is the absorbance (Hassan, 2013). Fig. 4 shows the absorption coefficient as a function of the wavelength of pure and doped PANI. The photon absorption in many amorphous materials is found to obey the Tauc relation (Abdulla, and Abbo, 2012; Muhammad et al., 2011), which is of the form:

$$Ahv = B\,(hv - E_g)^m \quad (1)$$

Where hv is the energy of the incident photon, E_g is the optical energy band gap, B is a constant known as the disorder parameter which is nearly independent of photon energy parameter, and m is the power coefficient with the value that is determined by the type of possible electronic transitions. For the direct and indirect allowed transition = 1/2 or 2, respectively (Gupta et al., 2010). For high absorption coefficient $\alpha > 10^3$ cm^{-1} that refers to the direct transition (Zeadan et al., 2009; Ali et al., 2008). The index n = 1/2 represents the directly allowed transition energy gap. To determine the value of the energy gap, graphs of $(\alpha hv)^2$ against hv were plotted, as shown in Fig. 5. Extrapolation of this plot for $(\alpha hv)^2 = 0$ gives the value of E_g (Muhammad et al., 2017). The value of the optical direct transition energies

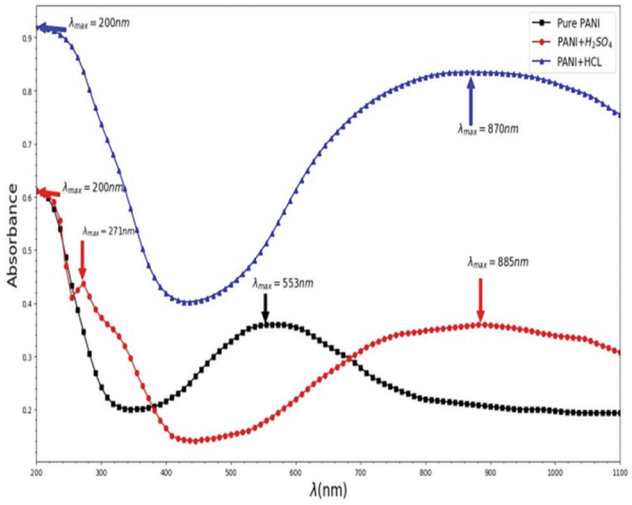

Fig. 3. Ultraviolet-visible absorbance spectra of pure and polyaniline doped with hydrochloric acid and sulfuric acid.

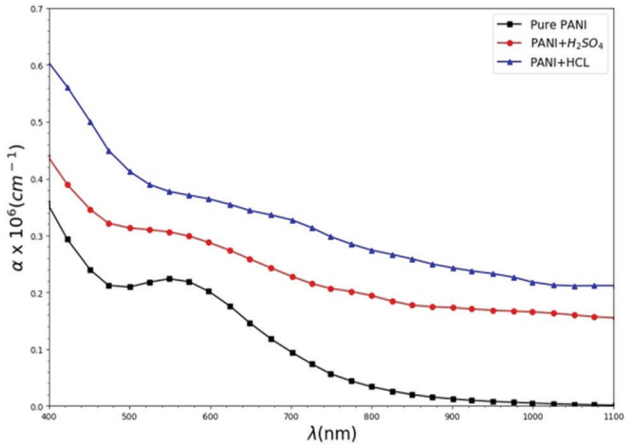

Fig. 4. Absorption coefficient as a function of the wavelength of pure and doped polyaniline with hydrochloric acid and sulfuric acid.

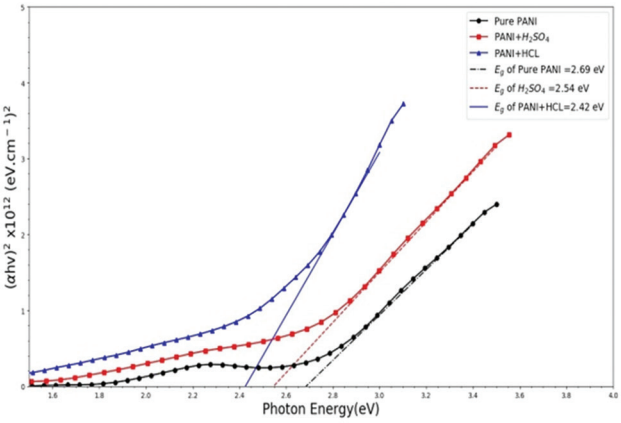

Fig. 5. Direct allowed transition energy of pure polyaniline (PANI) and doped PANI with hydrochloric acid and sulfuric acid.

http://dx.doi.org/10.14500/aro.10483

obtained from Fig. 5 is 2.69 eV, 2.42 eV, and 2.54 eV of pure and doped PANI with HCl, and H_2So_4, respectively. The reduction in the optical band gap is probably due to the modification of the polymer structure (Mathai et al., 2002). The energy gap determines the electrical conductivity and optical absorption character of the PANI. The reduction in the optical band gap to 2.42 eV due to the dimensions of resulting ions, which play an important role in the process of diffusion, it is known that acids are compounds that dissociate in water, only to give positive hydrogen ions and negative ions of the acid residue. In doping PANI with HCl, dissociation to cations and anions takes place: $HCl \quad H^{+}+Cl^{-}$ while in doping with H_2SO_4, the dissociation is:

$$H_2SO_4 \rightarrow 2H^{+} + SO_4^{-2} \tag{2}$$

In both cases, positive hydrogen cations are formed. The difference is in the negative anions that are in the first case the anions of non-metal (Cl^{-1}), and in the second case the anions (SO_4^{-2}) are composed as molecules, but the particle is negatively charged (Gazdic et al., 2016).

C. Refractive Index and Optical Dielectric Constant

The refractive index (n) is a fundamental optical property of polymers that are directly related to other optical, electrical, and magnetic properties, and also of interest to those studying the physical, chemical, and molecular properties of polymers by optical techniques. The optical properties of the samples can be characterized by the complex refractive index. The complex refractive index is expressed as $n = n(\omega) + ik(\omega)$ where $n(\omega)$ is the real part and $k(\omega)$ is the imaginary part of refractive index. The refractive index, n, can be estimated, using the Fresnel formulae as follows (Muhammad et al., 2017; Aziz et al., 2017; Hassan, 2013):

$$n = \left[\frac{4R}{(R-1)^2} - k^2\right]^{1/2} - \frac{(R+1)}{(R-1)} \tag{3}$$

Where R is the reflectivity and $k = \alpha\lambda/4\pi$ is the extinction coefficient. The extinction coefficient k describes the properties of the material with respect to light of a given wavelength and indicates the absorption changes when the electromagnetic wave propagates through the material (Al-Tememee et al., 2012). The values of reflective index n as a function of the wavelength of pure and doped PANI with HCl, and H_2SO_4 is shown in Fig. 6. It is observed that the refractive index decreases with the increase of the wavelength. The value of the refractive index at the wavelength 800 nm is 1.14, 2.92, and 1.82 of pure and doped PANI with HCL, and H_2So_4, respectively. The increase in the reflective index may be attributed to higher packing density and change in crystalline structure also by increasing the C–H bonds (Nahida, and Marwa, 2011). Higher refractive index values are for better-structured films (Al-Tememee et al., 2012). The dielectric constant (ε) consists of a real part (ε_r) and an imaginary part (ε_i), which depend on the frequency of the electromagnetic wave. ε_r is the real part associated with the term that shows how much it will slow down the speed of light in the material. ε_i is the imaginary part of the dielectric constant, which shows how a dielectric absorbs energy from an electric field due to dipole motion. The imaginary part of the dielectric constant was determined by the following relations (Ahmed et al., 2009; Aqili et al., 2000):

$$\varepsilon_r = n^2 - k^2 \tag{4}$$

$$\varepsilon_I = 2nk \tag{5}$$

The real part of dielectric constant is related to the dispersion, and the imaginary part represents the dissipative rate of electromagnetic wave propagation in the medium. The real and imaginary parts of the dielectric constant as a function of wavelength are shown in Figs. 7 and 8 of pure and doped PANI with HCl and H_2SO_4. The variation of ε_r depends on the values of n^2 as a result of small values of k^2 in comparison with n^2 ($\varepsilon_r = n^2$), whereas ε_i mainly depends on the k values which are related to the variation of absorption coefficient (Faramarzpour et al., 2008). From Fig. 7, the value of ε_r at the wavelength 800 nm is 1.33, 8.70, and 3.29 of pure and doped PANI with HCL, and H_2SO_4, respectively. The values of the optical properties of pure and doped PANI with HCL and H_2So_4 are presented in Table I. The reduction in optical band gap is associated with the increase in refractive index. The decrease in the optical band gap (Table I) can be related to an increase in optical dielectric constant. An increase in an optical dielectric constant means

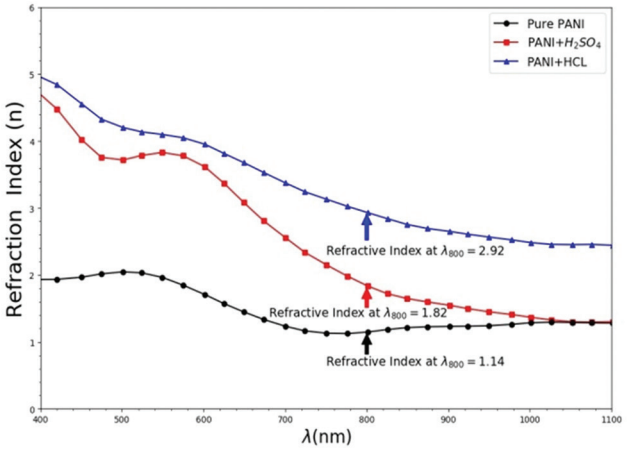

Fig. 6. Index of refraction as a function of the wavelength of pure polyaniline and doped with hydrochloric acid and sulfuric acid.

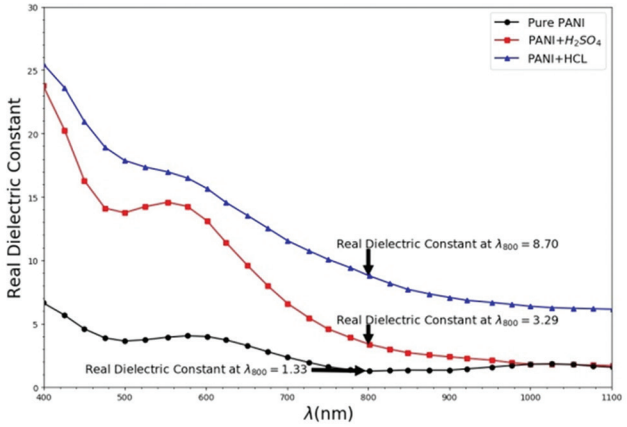

Fig. 7. Real dielectric constant *versus* wavelength of pure polyaniline and doped with hydrochloric acid and sulfuric acid.

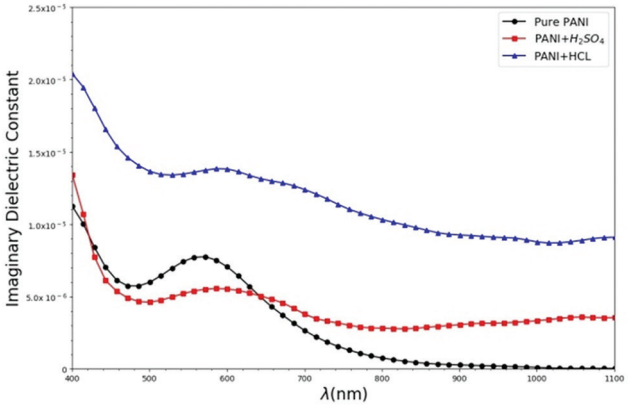

Fig. 8. Imaginary dielectric constant *versus* of wavelength of pure and doped polyaniline with hydrochloric acid and sulfuric acid.

TABLE I
THE OPTICAL PROPERTIES OF PURE AND PANI DOPED WITH HCL AND H_2SO_4

Sample	*Absorbance*	λ	ε_g	n from Fig.6 at 800 nm	ε_r from Fig.7 at 800 nm	$\varepsilon_r=n^2$
Pure PANI	0.61	200	2.699	1.14	1.33	1.29
	0.36	553				
-HCl	0.92	200	2.42	2.92	8.70	8.52
	0.83	870				
PANI- H_2SO_4	0.61	200	2.54	1.82	3.29	3.31
	0.44	271				
	0.36	885				

PANI: Polyaniline, HCl: Hydrochloric acid, H_2SO_4: Sulfuric acid.

the introduction of more charge carriers to the host material and thus an increase in the density of states.

IV. Conclusion

PANI salt has been synthesized via chemically oxidative polymerization of aniline in the presence of HCl and H_2SO_4 using APS as an oxidizing agent at room temperature. PANI salts were characterized using UV-Vis spectroscopy to investigate the variations in the optical properties. Doping with HCl and H_2SO_4 reduced the direct band gap of the pure PANI from 2.69eV to 2.42eV and 2.54eV. The reduction in optical band gap is associated with the increase in refractive index. The refractive index has a higher value of PANI doped with HCl (2.92). Higher refractive index values are for better-structured films.

References

Abdulla, H.S., and Abbo, A.I., 2012. Optical and electrical properties of thin films of polyaniline and polypyrrole. *International. Journal of Electrochemical Science*, 7, pp.10666-10678.

Ahmed, N.M., Sauli, Z., Hashim, U., and Al-Douri, Y., 2009. Investigation of the absorption coefficient, refractive index, energy band gap and film thickness for Al0. 11Ga0. 89N, Al0. 03Ga0. *International Journal of Nanoelectronics and Materials*, 2, pp.189-195.

Al-Daghman, A.N.J., Ibrahim, K., Ahmed, N.M., and Al-Messiere, M.A., 2016. Effect of doping by stronger ions salt on the microstructure of conductive polyaniline-ES: Structure and properties. *Journal of Optoelectronics and Biomedical Materials*, 8(4), pp.175-183.

Ali, Z.R., Zeadan, A.M., and Ziadan, K.M., 2008. The optical properties of polyaniline blend with poly-methal-methacrylate as conducting polymers alloys (PAni/PMMA). *Basrah Journal of Science*, 26(1), pp.12-17.

Al-Tememee, N.A., Saeed, N.M., Al-Dujayli, S.M., and Chiad, B.T., 2012. The effect of zn concentration on the optical properties of Cd10–xZnxS films for solar cells applications. *Advances in Materials Physics and Chemistry*, 2(2), p.69.

Aqili, A.K., Ali, Z., and Maqsood, A., 2000. Optical and structural properties of two-sourced evaporated ZnTe thin films. *Applied Surface Science*, 167(1-2), pp.1-11.

Aziz, S.B., Rasheed, M.A., and Ahmed, H.M., 2017. Synthesis of polymer nanocomposites based on [Methyl cellulose](1−x): (CuS) x (0.02 M≤ x≤ 0.08 M) with desired optical band gaps. *Polymers*, 9(6), p.194.

Bharti, M., Singh, A., Samanta, S., and Aswal, D.K., 2018. Conductive polymers for thermoelectric power generation. *Progress in Materials Science*, 93, pp.270-310.

Chaqmaqchee, F.A.I., and Baker, A.G., 2015. Study and characterization of polyaniline at various doping of LiCl wt.% using electrical measurements and XRF analysis. *Journal of Research Updates in Polymer Science*, 4(4), p.188.

Dai, H., Wang, N., Wang, D., Ma, H., and Lin, M., 2016. An electrochemical sensor based on phytic acid functionalized polypyrrole/graphene oxide nanocomposites for simultaneous determination of Cd (II) and Pb (II). *Chemical Engineering Journal*, 299, pp.150-155.

Du, X., Zhang, Z., Liu, W., and Deng, Y., 2017. Nanocellulose-based conductive materials and their emerging applications in energy devices a review. *Nano Energy*, 35, pp.299-320.

Faramarzpour, N., Deen, M.J., Shirani, S. and Fang, Q., 2008. Fully integrated single photon avalanche diode detector in standard CMOS 0.18-$\mu $ m Technology. *IEEE Transactions on Electron Devices*, 55(3), pp.760-767.

Gazdic, I., Modric-Šahbazovic, A., and Sulejmanovic, S., 2016. Analysis of specific electric conductivity of thin films of polyaniline doped with sulfuric and hydrochloric acid. *TEM Journal*, 5(1), p.38.

Gizzie, E.A., Niezgoda, J.S., Robinson, M.T., Harris, A.G., Jennings, G.K., Rosenthal, S.J., and Cliffel, D.E., 2015. Photosystem I-polyaniline/TiO 2 solid-state solar cells: Simple devices for biohybrid solar energy conversion. *Energy and Environmental Science*, 8(12), pp.3572-3576.

Gong, J., Cui, X.J., Xie, Z.W., Wang, S.G., and Qu, L.Y., 2002. The solid-state synthesis of polyaniline/$H4SiW_{12}O_{40}$ materials. *Synthetic Metals*, 129(2), pp.187-192.

Gupta, K., Jana, P.C., and Meikap, A.K., 2010. Optical and electrical transport properties of polyaniline silver nanocomposite. *Synthetic Metals*, 160(13-14), pp.1566-1573.

Hassan, S., Ghareeb, B.A., and Jafaar, H.I., 2012. AC electrical condutivity for polyaniline prepared in different acidic medium. *International Journal of Basic and Applied Science*, 1, pp.352-362.

Hassan, S.M., 2013. Optical properties of prepared polyaniline and polymethylmethacrylate blends. *International Journal of Application or Innovation in Engineering and Management*, 2(9), pp.232-235.

Kenry and Liu, B., 2018. Recent advances in biodegradable conducting polymers and their biomedical applications. *Biomacromolecules*, 19(6), pp.1783-1803.

Kulkarni, M.V., Viswanath, A.K., Marimuthu, R., and Seth, T., 2004. Synthesis and characterization of polyaniline doped with organic acids. *Journal of Polymer Science Part A: Polymer Chemistry*, 42(8), pp.2043-2049.

Ladera, R.M., Fierro, J.L.G., Ojeda, M., and Rojas, S., 2014. TiO2-supported heteropoly acids for low-temperature synthesis of dimethyl ether from methanol. *Journal of Catalysis*, 312, pp.195-203.

Liao, G., Li, Q., and Xu, Z., 2019. The chemical modification of polyaniline with enhanced properties: A review. *Progress in Organic Coatings*, 126, pp.35-43.

Liao, G., Li, Q., Zhao, W., Pang, Q., Gao, H., and Xu, Z., 2018. *In situ* construction of novel silver nanoparticle decorated polymeric spheres as highly active and stable catalysts for reduction of methylene blue dye. *Applied Catalysis A: General*, 549, pp.102-111.

Lu, X., Zhang, W., Wang, C., Wen, T.C., and Wei, Y., 2011. One-dimensional conducting polymer nanocomposites: Synthesis, properties and applications. *Progress in Polymer Science*, 36(5), pp.671-712.

Ma, Z., and Kan, J., 2013. Study of cylindrical Zn/PANI secondary batteries with the electrolyte containing alkylimidazolium ionic liquid. *Synthetic Metals*, 174, pp.58-62.

Manual, I., 1994. *Shimadzu Corporation*. Analytical Instrument Plant, Kyoto, Japan.

Mathai, C.J., Saravanan, S., Anantharaman, M.R., Venkitachalam, S., and Jayalekshmi, S., 2002. Effect of iodine doping on the bandgap of plasma polymerized aniline thin films. *Journal of Physics D: Applied Physics*, 35(17), p.2206.

Melad, O., and Jarur, M., 2016. Studies on the effect of doping agent on the structure of polyaniline. *Chemistry and Chemical Technology*, 10(1), pp.41-44.

Muhammad, F.F., and Sulaiman, K., 2011. Utilizing a simple and reliable method to investigate the optical functions of small molecular organic films Alq3 and Gaq3 as examples. *Measurement*, 44(8), pp.1468-1474.

Muhammad, F.F., Hapip, A.I.A., and Sulaiman, K., 2010. Study of optoelectronic energy bands and molecular energy levels of tris (8-hydroxyquinolinate) gallium and aluminum organometallic materials from their spectroscopic and electrochemical analysis. *Journal of Organometallic Chemistry*, 695(23), pp.2526-2531.

Muhammad, F.F., Yahya, M.Y., Aziz, F., Rasheed, M.A., and Sulaiman, K., 2017. Tuning the extinction coefficient, refractive index, dielectric constant and optical conductivity of Gaq3 films for the application of OLED displays technology. *Journal of Materials Science: Materials in Electronics*, 28(19), pp.14777-14786.

Ninh, D.H., Thao, T.T., Long, P.D. and Dinh, N.N., 2016. Characterization of electrochromic properties of polyaniline thin films electropolymerized in H_2SO_4 Solution. *Open Journal of Organic Polymer Materials*, 6(01), pp.30.

Nahida, J.H., and Marwa, R.F., 2011. Study of the optical constants of the PMMA/PC blends. *AIP Conference Proceedings*, 1400(1), pp.585-595.

Olinga, T.E., Fraysse, J., Travers, J.P., Dufresne, A., and Pron, A., 2000. Highly conducting and solution-processable polyaniline obtained via protonation with a new sulfonic acid containing plasticizing functional groups. *Macromolecules*, 33(6), pp.2107-2113.

Robert, M.S., Francis, X.W., and David, J.K., 2005. *Spectrometric Identification of Organic Compounds*. 7th ed. John Wiley and Sons, Inc., Hoboken, p.106.

Schymanski, E.L., Jeon, J., Gulde, R., Fenner, K., Ruff, M., Singer, H.P., and Hollender, J., 2014. Identifying small molecules via high resolution mass spectrometry: Communicating confidence. *Environmental Science and Technology*, 48(4), pp.2097-2098.

Stejskal, J., and Polyaniline, G.R.G., 2002. Preparation of a conducting polymer (IUPAC technical report). *Pure and Applied Chemistry*, 74(5), pp.857-867.

Varma, S.J., Xavier, F., Varghese, S., and Jayalekshmi, S., 2012. Synthesis and studies of exceptionally crystalline polyaniline thin films. *Polymer International*, 61(5), pp.743-748.

Xu, R.P., Li, Y.Q., and Tang, J.X., 2016. Recent advances in flexible organic light-emitting diodes. *Journal of Materials Chemistry C*, 4(39), pp.9116-9142.

Yin, W., and Ruckenstein, E., 2000. Soluble polyaniline co-doped with dodecyl benzene sulfonic acid and hydrochloric acid. *Synthetic Metals*, 108(1), pp.39-46.

Zeadan, K.M., Talab, R.A., and Satar, J., 2009. The optical properties of polyaniline (PAni) prepared by chemical method. *Journal of Kufa Physics*, 1(2), pp.1-11.

Zhang, Z., Wei, Z., and Wan, M., 2002. Nanostructures of polyaniline doped with inorganic acids. *Macromolecules*, 35(15), pp.5937-5942.

Changes in the Levels of Some Biochemical Parameters in the Serum of Children in Response to the Giardiasis Infection

Sarmad N. Mageed

Department of Medical Microbiology, Faculty of Science and Health, Koya University, Daniel Mitterrand Boulevard, Koya KOY45, Kurdistan Region – F.R. Iraq

***Abstract*–*Giardiasis* is one of the most common intestinal protozoan infections worldwide. The study aimed to determine the levels of a number of biochemical parameters in the sera of children with giardiasis without receiving any medication for the treatment of giardiasis or intestinal helminthic infections in the previous 7 days. The study conducted 34 (19 females and 15 males) children and 34 (18 females and 16 males) healthy children as a control group. The mean ages of infected children and control groups were 8 ± 2 and 7 ± 2 years, respectively. Serum levels of aspartate aminotransferase (AST), alanine aminotransferase (ALT), creatinine, urea, sodium, potassium, uric acid, and albumin were determined. AST level in males was significantly higher than healthy children control (14.20 ± 1.896 and 10.06 ± 0.699), respectively ($P < 0.05$), and no significant difference in females was noticed whereas the significant increases in ALT level were found when compared to control (12.43 ± 0.806 and 8.666 ± 0.449), for female, respectively, whereas no significant change in males was observed. Creatinine levels showed significant decrease in females when compared to control (57.72 ± 1.170 and 73.37 ± 1.635) ($P \leq 0.001$), respectively.**

***Index Terms*–Biochemical parameters, Children, Giardiasis, Males and females.**

I. Introduction

Giardia intestinalis (*G. intestinalis*) is a worldwide cause of gastrointestinal infection known as giardiasis, which infects the small intestine of human at different ages, particularly children (Magdieva et al., 1984; Mel'nik, 1985) (Khudair, 2010). It is a flagellated enteric protozoon that infects humans and other mammals and is a major cause of morbidity and mortality in tropical and subtropical countries (Bansal et al., 2005). Infants and young children have more susceptibility to giardiasis due to behavioral and immunological factors (Sotto and Gra, 1986). The infection is transmitted easily by direct fecal-oral contact, by contaminated drinking water (waterborne diseases) (Craun, 1984; Osterholm et al., 1981), food (Osterholm et al., 1981), or by abnormal sexual practices (Mildvan et al., 1977)(Miller and Hendrie 2000).

It exists in trophozoite and cyst forms, and the infective form is the cyst. Trophozoites of *G. intestinalis* are found in the upper part of the small intestine, where they live closely attached to the mucosa. They are found at times in the gallbladder and in biliary drainage. *G. intestinalis* infection causes severe intestinal disorder, most commonly, diarrhea and related symptoms due to malabsorption of fat; fat-soluble vitamins, and disaccharides (Bogitsh et al., 2013; Burke, 1975).

During infection, *Giardia* trophozoites colonize the proximal small intestine and adhere to the apical surface of the enterocyte. This close association between the parasite and the small intestinal epithelium initiates a succession of pathophysiological processes, leading to a diffuse shortening of the epithelial microvilli. The reduction of small intestinal absorptive surface area causes disaccharides deficiencies and malabsorption of nutrients, water, and electrolytes (Rosenberg et al., 1977).

There is a close relationship between intestinal parasitic infections such as giardiasis in particular, and malnutrition in children, especially those at school age that has directs effect on their growth and educational outcome (Nematian et al., 2008). Giardiasis infection has the ability to impede child growth even when asymptomatic, which can be through malabsorption and block the absorption of many essential biochemical elements for the child's growth (Simsek et al., 2004). The deficiency of these elements can adverse effect on the production of many other essential elements for the biochemical pathways to be performed and main the homeostasis of the body (Al-Mekhlafi et al., 2005; Botero-Garcés et al., 2009; Nematian et al., 2008; Prado et al., 2005; Simsek et al., 2004). Giardiasis was also found to have a close relationship with the development of malnutrition in infants as a result of absorption obstruction that reflected in more severely diarrhea in those children with prolonged nutrition deficiency (Mondal et al., 2012). Giardia infection may results in severe acute diarrhea in children at the age of less than 5 years old. Relatively, chronic infection may

ARO-The Scientific Journal of Koya University
Volume VII, No.1(2019), Article ID: ARO.10518, 6 pages
DOI: 10.14500/aro.10518
Received 09 April 2019; Accepted 12 June 2019
Regular research paper: Published 15 June 2019
Corresponding author's e-mail: sarmad.mageed@koyauniversity.org

consequently lead to weight loss and retardation of growth (Teixeira et al., 2007) (Júlio et al., 2012).

Liver and kidney function tests are known as a group of blood tests, which also referred to as a hepatic and renal panel that reveal and provide information regarding the general status of a patient's liver and kidney in relation to a specific disorder or abnormal health condition (Lee, 2009). These tests are performed on serum samples taken from patients of different ages. These tests comprise an assessment of a number of biochemical parameters such as serum levels of aspartate aminotransferase (AST), alanine aminotransferase (ALT), creatinine, urea, uric acid, and albumin.

Clinically, the most significant alterations in the activities of liver enzyme are found in the form of elevated aminotransaminase activities in case of hepatocellular damage, and elevated alkaline phosphatase, 5′-nucleotidase, and γ-glutamyltransferase activities in case of cholestasis (Burtis and Bruns 2015). As an effective way to detect hepatic dysfunction or abnormality, liver function tests are very helpful and practical screening tool. No single test is sufficient to provide a complete estimate of liver function due to that the liver carries out a number of various functions at the same time. Physicians are often faced reports that do not consist or comply with the clinical state of the patient and they face difficulty in interpreting the results (Thapa and Walia, 2007).

Creatinine, urea, and uric acid are considered as nonprotein nitrogenous metabolites that are excreted by the kidney out of the body following glomerular filtration. Measuring the concentrations of these metabolites in the plasma or serum (Concentrations of creatine, urea, and uric acid in serum, and plasma are equivalent) are commonly used as indicators of normal or abnormal kidney function and other conditions (Burtis and Bruns, 2015).

Albumin is the most commonly measured serum protein and is synthesized exclusively by the liver. With liver disease, hypoalbuminemia is noted primarily in cirrhosis, autoimmune hepatitis, and alcoholic hepatitis (Burtis and Bruns, 2015).

In general, infected individuals are not showing any symptoms; however, clinical appearances may involve simple flatulence, acute, or chronic diarrheal infection accompanied by abdominal pain and nausea, to severe malnutrition (Jasinska and Granicki, 1982; Misra et al., 1995; Prado et al., 2005; Sotto et al., 1990; Telichko et al., 1973). In severe cases, the malnutrition as a consequence of malabsorption can lead to a noticeable weight loss. The rate of infection is determine the severity of the malabsorption (Kremery et al., 1989).

There is still lack of understanding of the mechanisms of pathogenicity and malabsorption in giardiasis (Kremery et al., 1989; Roxström-Lindquist et al., 2006). Some patients exhibit a reduction in length of their small intestinal villi (Heyworth, 1996; Koot et al., 2009) or even obstruct the microvilli of the small intestine (Kremery et al., 1989).

To date, no research has been published that investigate the changes in biochemical parameters that accompany giardiasis infection in male and female children. This study has been undertaken to elucidate the effect of giardiasis on the levels of some biochemical parameters in the serum of infected children comparing with their non-infected counterparts. The study aimed to highlight the malnutrition and homeostasis complication consequences under conditions of natural human infection as a result of changes in the level of a number of essential biochemical parameters in the serum of studied children.

II. Materials and Methods

In this study, blood samples were taken from 34 children (19 females and 15 males) with chronic giardiasis and 34 healthy children (18 females and 16 males) as a control group was included. The study was conducted over a period of 8 months from April 2017 to November 2017.

The children with chronic giardiasis consisted of cases that were referred to the Azadi Hospital in Kirkuk city for diarrheal symptoms. Children at the age 2–12 years with giardia infection, as demonstrated by the identification of trophozoites and/or cysts of *Giardia lamblia* in stool specimens were entered in this study.

Those suffering from acute febrile conditions, chronic diarrhea, and severe malnutrition or receiving long-term therapy were excluded from the study. None of the children entered in this study had received any medication for the treatment of giardia or intestinal helminthic infection in the previous 7 days. The control group consisted of children who were referred to the same hospital outpatient clinic for a routine checkup and had normal physical examination and laboratory results.

The serum is the liquid portion of blood that remains after coagulation has occurred; it is the specimen of choice for many analyses, including but not limited to aminotransferases enzymes, creatinine, urea, sodium, potassium, uric acid, and albumin. Samples were collected into test tubes without any additives or clot activators and allowed to complete the coagulation process before further processing. Aspartate AST (glutamic-oxaloacetic transaminase [GOT]), ALT (glutamate pyruvate transaminase [GPT]), urea, uric acid, sodium, and potassium levels were measured (by colorimetric method), creatinine level (by kinetic method) and albumin (Bromcresol Green method) by specific kits of BIOLABO Company (France) through using spectrophotometric technique according to the manufacturer procedure, whereas levels of sodium and potassium were measured (colorimetric method) by linear company kit using spectrophotometric technique according to the manufacturer procedure.

A. Parasitological Examination

Stool samples were examined for cysts and/or trophozoites of *G. intestinalis* by a wet mount of the fresh specimen by direct saline and Lugol preparation. Stools were concentrated for examination using the formalin-ethyl acetate sedimentation technique and were also stained by acid-fast staining for cryptosporidiosis and cyclosporiasis. Slides were prepared from fresh and concentrated specimens.

III. Results and Discussion

The mean ages of children of both genders with chronic giardiasis and the control group were 8 ± 2 and 7 ± 2 years, respectively.

Table I shows serum levels of AST, ALT, creatinine, urea, sodium, potassium, uric acid, and albumin. The results showed that AST level significantly increased in males as a consequence of the infection in comparison to those from the healthy children controls (14.20 ± 1.896 and 10.06 ± 0.699), respectively ($P < 0.05$), and no significant difference was noticed in females, Table I, whereas the significant increase was found in females' ALT levels when compared with healthy control (12.43 ± 0.806 and 8.666 ± 0.449) ($P \leq 0.001$), respectively, whereas no significant increase was observed in males (Table I). Creatinine levels showed significant decrease in females comparing to controls (57.72 ± 1.170 and 73.37 ± 1.635), respectively ($P \leq 0.001$), which is consistent with the data that have been published by Charalabopoulos et al., 2004; Rosa et al., 2007, (Miller, L. and Hendrie, N. 2000) (Nash et al., 1987) (Table I).

As related with other parameters, the results showed significant decreases in the levels of urea, sodium, potassium, uric acid, and albumin in both males and females as compared with control (Table I). Decreases level of serum albumin was previously reported in giardiasis patients (Abdumadjidova and Inoyatova, 1998; Cusack et al., 2001), and with a history of infectious enterocolitis determined by *Escherichia coli* enteropathogenic (Melit et al., 2017). Diet with adequate calories but low protein intake has been known to lead to malnutrition due to protein deficiency, with decreased serum albumin (Burtis and Bruns, 2015).

The activity variation of liver enzymes (AST and ALT) in serum is commonly considered as an indicator of a number of pathological changes of tissue and liver. Improper regulation of ALT synthesis would have great effect on the liver's ability to metabolize amino acids for energy production within the cell (Ragbetli et al., 2014).

Table II revealed more interesting results when the comparison made between infected males and females with chronic giardiasis. Creatinine and urea levels were significantly increased in males comparing to females 73.73 ± 1.911 and 57.72 ± 1.170 and 4.013 ± 0.197 and 3.949 ± 0.114 ($P < 0.05$), respectively, providing further support to the previous results when compared between infected and healthy controls, whereas no significant changes were observed in the level of the remaining parameters ($P > 0.05$) as a comparison between the infected males and females.

Sandstead et al., 1965, have confirmed marked intermittent increases in serum liver transaminases aspartate transaminase (AST or serum GOT) and alanine transaminase (ALT or serum GPT) in children.

The results were inconsistent with previous studies by that have shown higher rates of infection among males (48%) than females (28%). Epidemiological studies have reported that giardiasis infection rates to be higher in males than in females. However, the reasons behind these observed differences still need to be explained. However, increased exposure to contaminated environments can illustrate the higher rates of infection in males, due to the nature of their normal daily tasks as being spend most of their times outdoors and mostly in low-level sanitation environments (Kasim and Elhelu, 1983). In contrast, females play and spend most of their time at or close to their homes in relatively more clean (In term of Giardia infections) environments (Cheesbrough, 1987).

Giardiasis as one of the parasitic diseases is characterized by undernutrition and deficiency of essential micronutrient, problems with digestion, reduction in nutrients absorption and chronic inflammation (Hesham et al., 2004).

In giardiasis patients, the levels of electrolytes are expected to decrease as a consequence of lack of absorption. Gastrointestinal parasitism can lead to similar electrolyte deficiency as it happens classically in hyperkalemia and hyponatremia (DiBartola et al., 1985; Willard et al., 1991).

For the purpose of acid-base balance as well as osmotic pressure, sodium (Na) and potassium (K) as electrolytes, play an important role in this regard. A decrease in the levels of these ions can result in severe complications and uncontrollable events in body functions. The lack of these

TABLE I
Serum Levels of Different Biochemical Parameters in Affected Male and Female Children with Giardiasis Comparing to Non-infected Controls

Parameters	Gender	Control	Patient	*P* value
AST (U/L)	Male	10.06±0.699	14.20±1.896	0.023
	Female	10.28±0.989	11.30±0.883	0.455
ALT (U/L)	Male	9.048±1.041	11.43±1.459	0.181
	Female	8.666±0.449	12.43±0.806	0.001
Creatinine (mg/dl)	Male	73.04±1.645	73.73±1.911	0.790
	Female	73.37±1.635	57.72±1.170	0.0001
Urea (mg/dl)	Male	5.077±0.208	4.013±0.197	0.032
	Female	5.027±0.126	3.949±0.114	0.0001
Sodium (mmol/L)	Male	140.2±0.713	138.0±0.317	0.01
	Female	141.2±0.772	138.7±0.387	0.002
Potassium (mmol/L)	Male	4.273±0.116	3.677±0.080	0.001
	Female	4.270±0.091	3.758±0.050	0.0001
Uric acid (mg/dl)	Male	300.9±9.620	264.0±11.90	0.020
	Female	294.6±6.369	275.6±6.837	0.04
Albumin (g/L)	Male	53.64±1.768	46.53±0.999	0.001
	Female	50.29±2.098	44.13±0.810	0.002

Table II
Comparison of Serum Levels of Biochemical Parameters between Infected Males and Females with Chronic Giardiasis

Parameters	Male	Female	*P* value
AST (U/L)	14.20±1.896	11.30±0.883	0.125
ALT (U/L)	11.43±1.459	12.43±0.806	0.518
Creatinine mg/dl)	73.73±1.911	57.72±1.170	0.0001
Urea (mg/dl)	4.013±0.197	3.949±0.114	0.007
Sodium (mmol/L)	138.0±0.317	138.7±0.387	0.971
Potassium (mmol/L)	3.677±0.080	3.758±0.050	0.397
Uric acid (mg/dl)	264.0±11.90	275.6±6.837	0.373
Albumin (g/L)	46.53±0.999	44.13±0.810	0.082

macro elements can consequently lead to clinical disorder, weight loss and may end in death, especially with an increased load of parasites if untreated (Krajničáková et al., 2003; Kulcu and Yur, 2003; Tanyuksel et al., 1995).

Hypokalemia was noticed more than hyponatremia, and significant decrease in the level of serum urea and creatinine was also observed in patients as a consequence of the infection. Therefore, electrolytes deficiency should be closely monitored in patients with acute gastroenteritis (Baghaei, 2015; Korman et al., 1990; Özçay et al., 2013).

In immunocompetent and immunocompromised patients, giardiasis has been reported to induce many cases of myopathy following hypokalemia (Cervello et al., 1993; Geovese et al., 1996). This leads to conclude that *Giardia* can work out of the control of the host's immune status by showing the ability to trigger muscular manifestations independently. Relatively, potassium loss during giardia infection is directly affected by the number of bouts of diarrhea per day (Geovese et al., 1996).

Severe and transient myopathy can be triggered by hypokalemia due to loss of potassium (Geovese et al., 1996). Evidently, muscular manifestation can improve dramatically alongside with recovery from diarrhea and increased levels of potassium (Cervello et al., 1993). Although it is very uncommon that hypokalemia results in myopathy due to diarrhea by *Giardia,* it looks like that the symptoms' period is critical for hypokalemic myopathy development (Geovese et al., 1996).

For the diagnosis purposes and to find the organism as a confirmation of the infection, stool samples or duodenal secretions were required, before taking blood samples. Giardia parasite can be readily found in the stool in acute infections, whereas repeated stool samples were essential in chronic cases, as excretion is irregular (Goka et al., 1990).

Studies of intestinal mucosa through using light microscope revealed that *G. intestinalis* attach to epithelial layer and mucosal filaments that are located at the intervillous space, where the active absorption occurs. This attachment results in a mechanical block and mucosal layer inflammation, which is consequently cause malabsorption and loss of many nutrients, such as proteins (Farthing et al., 1986).

Although that up to recent date, only few scientific researchers have revealed extra-intestinal manifestations due to giardiasis. However, approximately third of infected patients with giardia parasite have been estimated to exhibit long-term extra-intestinal complications according to a recent study, proposing that this phenomenon is less surprising and is not unexpected as considered in the past (Cantey et al., 2011).

The facts that have been revealed by recent studies in which *Giardia* may results in chronic post-infectious gastrointestinal complications have highlighted the topic as a very interesting for intense research. Post-infectious clinical aspects caused by *Giardia*, although that complete elimination of the parasite has been confirmed remains a mystery (Halliez and Buret, 2013).

IV. Conclusion

The study was able to demonstrate, by examining the blood serum of infected children, that there are significant changes in the level of a number of biochemical parameters among infected children with giardiasis that may be specifically recognized as a consequence of malabsorption during infection and may lead to transient or chronic malnutrition status.

Therefore, these transmitted infections among young generations, through contaminated water and food sources, require close attention, in term of prevention and control before treatment. The prevention strategies will avoid, to a great extent the consequence outcomes of having such long-term children patients with chronic malabsorption. Further studies on a large scale of cases are needed to investigate and confirm the health impact and consequences on infected individuals as a result of this infection.

V. Acknowledgment

The author would like to thank Professor Dr. Esmail Salih Ibrahim, Koya University/Faculty of Science and Health, Biology Department for his support in organizing the data, and M. Mushir Esmail Salih, Koya University/Faculty of Science and Health/Chemistry Department for helping in the statistical analysis of the data.

References

Abdumadjidova, S.U., and Inoyatova, F.I., 1998. Effects of *Giardia lamblia* infestation on the clinical course of chronic hepatitis B. *The Turkish Journal of Gastroenterology*, 1, pp.24-27.

Al-Mekhlafi, M.H., Azlin, M., Aini, U.N., Shaik, A., Sa'iah, A., Fatmah, M., and Rozlida, A., 2005. Giardiasis as a predictor of childhood malnutrition in Orang Asli children in Malaysia. *Transactions of the Royal Society of Tropical Medicine and Hygiene*, 99(9), pp.686-691.

Baghaei, M., 2015. Hypoproteinaemia and Edema Due to Giardiasis. *Iranian Journal of Medical Sciences*, 28(2), pp.98-99.

Bansal, D., Bhatti, H., and Sehgal, R., 2005. Altered lipid parameters in patients infected with Entamoeba histolytica, Entamoeba dispar and *Giardia lamblia*. *British Journal of Biomedical Science*, 62(2), pp.63-65.

Bogitsh, B.J., Carter, C.E., and Oeltmann, T.N., 2013. *Human Parasitology*. Academic Press, Amsterdam.

Botero-Garcés, J.H., García-Montoya, G.M., Grisales-Patiño, D., Aguirre-Acevedo, D.C., and Álvarez-Uribe, M.C., 2009. *Giardia intestinalis* and nutritional status in children participating in the complementary nutrition program, Antioquia, Colombia, May to October 2006. *Revista do Instituto de Medicina Tropical de São Paulo*, 51(3), pp.155-162.

Burke, J.A., 1975. Giardiasis in childhood. *American Journal of Diseases of Children*, 129(11), pp.1304-1310.

Burtis, C.A., and Bruns, D.E., 2015. *Tietz Fundamentals of Clinical Chemistry and Molecular Diagnostics (Fundamentals of Clinical Chemistry (Tietz)*. 7th ed. Saunders, Elsevier Inc., United States of America, p.1103.

Cantey, P.T., Roy, S., Lee, B., Cronquist, A., Smith, K., Liang, J., and Beach, M.J. (2011), Study of nonoutbreak giardiasis: Novel findings and implications for research. *The American Journal of Medicine*, 124(12), pp.e1171-1175.

Cervello, A., Alfaro, A., and Chumillas, M.J., 1993. Hypokalemic myopathy induced

by *Giardia lamblia*. *New England Journal of Medicine*, 329(3), pp.210-211.

Charalabopoulos, K., Charalabopoulos, A., Papadopoulou, C., and Papalimneou, V., 2004. *Giardia intesinalis*: A new pathogen with possible link to Kikuchi Fujimoto disease. An additional element in the disease jigsaw. *International Journal of Clinical Practice*, 58(12), pp.1180-1183.

Cheesbrough, M., 1987. Medical Laboratory Manual for Tropical Countries. 2nd ed. Elsevier Science and Technology Books, Amsterdam.

Craun, G.F., 1984. Waterborne Outbreaks of Giardiasis *Giardia* and Giardiasis. Springer, Berlin, pp.243-261.

Cusack, M.A., O'Mahony, M.S., and Woodhouse, K., 2001. *Giardia* in older people. *Age and Ageing*, 30(5), pp.419-421.

DiBartola, S.P., Johnson, S.E., Davenport, D., Prueter, J., Chew, D., and Sherding, R., 1985. Clinicopathologic findings resembling hypoadrenocorticism in dogs with primary gastrointestinal disease. *Journal of the American Veterinary Medical Association*, 187(1), pp.60-63.

Farthing, M., Mata, L., Urrutia, J.J., and Kronmal, R.A., 1986. Natural history of *Giardia* infection of infants and children in rural Guatemala and its impact on physical growth. *The American Journal of Clinical Nutrition*, 43(3), pp.395-405.

Geovese, A., Spadaro, G., Santoro, L., Rippa, P.G., Onorati, A., and Marone, G., 1996. Giardiasis as a cause of hypokalemic myopathy in congenital immunodeficiency. *International Journal of Clinical and Laboratory Research*, 26(2), pp.132-135.

Goka, A., Rolston, D., Mathan, V., and Farthing, M., 1990. The relative merits of feacal and duodenal juice microscopy in the diagnosis of *Giardia*. *Transactions of the Royal Society of Tropical Medicine and Hygiene*, 84(1), pp.66-67.

Halliez, M., and Buret, A.G., 2013. Extra-intestinal and long term consequences of *Giardia duodenalis* infections. *World Journal of Gastroenterology*, 19(47), pp.8974-8985.

Hesham, M., Edariah, A., and Norhayati, M., 2004. Intestinal parasitic infections and micronutrient deficiency: A review. *The Medical Journal of Malaysia*, 59(2), pp.284-293.

Heyworth, M., 1996. Giardiasis. Weatherall, D.J., Ledingham, J.C.C., Warrell, D.A., editorss. *Oxford Textbook of Medicine*. 3rd ed., Vol. 1. Oxford University Press, Oxford, pp.870-880.

Jasinska, G., and Granicki, O., 1982. Biliary-hepatic giardiasis and viral hepatitis. *Pediatria Polska*, 57(12), pp.1083-1085.

Júlio, C., Vilares, A., Oleastro, M., Ferreira, I., Gomes, S., Monteiro, L., Nunes, B., Tenreiro, R., and Ângelo, H., 2012. Prevalence and risk factors for *Giardia duodenalis* infection among children: A case study in Portugal. *Parasites and Vectors*, 5(1), p.22.

Kasim, A.A., and Elhelu, M.A., 1983. Giardiasis in Saudi Arabia. *Acta Tropica*, 40(2), pp.155-158.

Khudair, H.T., 2010. Prevalence and related risk factors for *Giardia lamblia* infection among children with acute diarrhea in thi-qar, southern Iraq. *Thi-Qar Medical Journal*, 4(4), pp.68-74.

Koot, B.G., ten Kate, F.J., Juffrie, M., Rosalina, I., Taminiau, J.J., and Benninga, M.A., 2009. Does *Giardia lamblia* cause villous atrophy in children? A retrospective cohort study of the histological abnormalities in giardiasis. *Journal of Pediatric Gastroenterology and Nutrition*, 49(3), pp.304-308.

Korman, S.H., Bar-Oz, B., Mandelberg, A., and Matoth, I., 1990. Giardiasis with protein-losing enteropathy: Diagnosis by fecal [alpha] 1-antitrypsin determination. *Journal of Pediatric Gastroenterology and Nutrition*, 10(2), pp.249-252.

Krajničáková, M., Kováč, G., Kostecký, M., Valocký, I., Maračeк, I., Šutiaková, I., and Lenhardt, Ľ., 2003. Selected clinico-biochemical parameters in the puerperal period of goats. *Bulletin of the Veterinary Institute in Pulawy*, 47, pp.177-182.

Kremery, V., Brix, M., and Gocar, E., 1989. Elevated indicators of liver metabolism in patients with giardiasis. *Vnitřní lékařství*, 35(5), pp.479-482.

Kulcu, R., and Yur, F., 2003. A study of some serum mineral levels before and during pregnancy and during lactation period of sheep and cattle. *Biological Trace Element Research*, 92(3), pp.275-279.

Lee, M., 2009. *Basic Skills in Interpreting Laboratory Data*. American Society of Health-System Pharmacists, Bethesda, MD.

Magdieva, S., Asletdinova, N., and Ziganshina, N., 1984. Effect of hymenolepiasis and enterobiasis on the course of viral (infectious) hepatitis in children. *Meditsinskaia Parazitologiia i Parazitarnye Bolezni*, 5, pp.31-35.

Mel'nik, G., 1985. Viral hepatitis and lambliasis. *Klinicheskaia Meditsina*, 63(5), pp.99-102.

Melit, L.E., Marginean, C.O., Dinca, A., Damian, R., and Marginean, C.D., 2017. Protein-losing enteropathy after infectious enterocolitis in child-a case report and a review of the literature. *Romanian Journal of Infectious Diseases*, 20(1), pp.26-30.

Mildvan, D., Gelb, A.M., and William, D., 1977. Venereal transmission of enteric pathogens in male homosexuals: Two case reports. *JAMA*, 238(13), pp.1387-1389.

Miller, L.C., and Hendrie, N.W., 2000. Health of children adopted from China. *Pediatrics*, 105(6), p.e76.

Misra, P., Kumar, A., Agarwal, V., and Jagota, S., 1995. A comparative clinical trial of albendazole versus metronidazole in giardiasis. *Indian Pediatrics*, 32, pp.291-291.

Mondal, D., Minak, J., Alam, M., Liu, Y., Dai, J., Korpe, P., and Petri, W.A., 2012. Contribution of enteric infection, altered intestinal barrier function, and maternal malnutrition to infant malnutrition in Bangladesh. *Clinical Infectious Diseases*, 54(2), pp.185-192.

Nash, T.E., Herrington, D.A., Losonsky, G.A., and Levine, M.M., 1987. Experimental human infections with Giardia lamblia. *Journal of Infectious Diseases*, 156(6), pp.974-984.

Nematian, J., Gholamrezanezhad, A., and Nematian, E., 2008. Giardiasis and other intestinal parasitic infections in relation to anthropometric indicators of malnutrition: A large, population-based survey of schoolchildren in Tehran. *Annals of Tropical Medicine and Parasitology*, 102(3), pp.209-214.

Osterholm, M.T., Forfang, J.C., Ristinen, T.L., Dean, A.G., Washburn, J.W., Godes, J.R., and McCullough, J.G., 1981. An outbreak of foodborne giardiasis. *New England Journal of Medicine*, 304(1), pp.24-28.

Özçay, F., Harmanci, K., and Özbek, N., 2013. Giardiasis as the cause of oedema and hypoproteinaemia in a child. *Annals of Tropical Paediatrics: International Child Health*, 22(1), pp.63-65.

Prado, M., Cairncross, S., Strina, A., Barreto, M.L., Oliveira-Assis, A., and Rego, S., 2005. Asymptomatic giardiasis and growth in young children; a longitudinal study in Salvador, Brazil. *Parasitology*, 131(1), pp.51-56.

Ragbetli, C., Tanritanir, P., Yilmaz, H., Yoruk, I., and Ozdemir, H., 2014. Effect on biochemical parameters in naturally infected calves with giardiasis after treatment with albendazole in Van Province, Turkey. *Indian Journal of Animal Research*, 48(1), pp.38-44.

Rosa, L., Gomes, M., Mundim, A., Mundim, M., Pozzer, E., Faria, E., and Cury, M., 2007. Infection of dogs by experimental inoculation with human isolates of *Giardia duodenalis*: Clinical and laboratory manifestations. *Veterinary Parasitology*, 145(1), pp.37-44.

Rosenberg, I., Solomons, N., and Schneider, R., 1977. Malabsorption associated with diarrhea and intestinal infections. *The American Journal of Clinical Nutrition*, 30(8), pp.1248-1253.

Roxström-Lindquist, K., Palm, D., Reiner, D., Ringqvist, E., and Svärd, S.G., 2006. *Giardia* immunity an update. *Trends in Parasitology*, 22(1), pp.26-31.

Sandstead, H.H., Shukry, A.S., Prasad, A.S., Gabr, M.K., EL Hifney, A., Mokhtar, N., and Darby, W.J., 1965. Kwashiorkor in Egypt: I. Clinical and

biochemical studies, with special reference to plasma zinc and serum lactic dehydrogenase. *The American Journal of Clinical Nutrition*, 17(1), pp.15-26.

Simsek, Z., Zeyrek, F.Y., and Kurcer, M., 2004. Effect of *Giardia* infection on growth and psychomotor development of children aged 0-5 years. Journal of *Tropical Pediatrics*, 50(2), pp.90-93.

Sotto, A., Alvarez, J., and Garcia, B., 1990. Acute hepatic lesion caused by *Giardia lamblia. Revista Española de Enfermedades Digestivas*, 77(1), pp.24-28.

Sotto, E.A., and Gra, O.B., 1986. *Giardia lamblia* and chronic hepatitis. *Revista Española de Enfermedades Digestivas*, 69(6), pp.583-586.

Tanyuksel, M., Sayal, A., and Aydin, A., 1995. Trace element levels in some parasitic disease. *Acta Parasitol Turcica*, 19, pp.315-321.

Teixeira, J.C., Heller, L., and Barreto, M.L., 2007. *Giardia duodenalis* infection: Risk factors for children living in sub-standard settlements in Brazil. *Cadernos de Saúde Pública*, 23(6), pp.1489-1493.

Telichko, A., Mirzoian, M., and Nersesova, A., 1973. Course of infectious hepatitis in patients with biliary tract lambliasis. *Voen Med Zh*, 2, pp.56-57.

Thapa, B.R., and Walia, A., 2007. Liver function tests and their interpretation. *The Indian Journal of Pediatrics*, 74(7), pp.663-671.

Willard, M., Fossum, T., Torrance, A., and Lippert, A., 1991. Hyponatremia and hyperkalemia associated with idiopathic or experimentally induced chylothorax in four dogs. *Journal of the American Veterinary Medical Association*, 199(3), pp.353-358.

Optimization of Wastewater Treatment Plant Design using Process Dynamic Simulation: A Case Study from Kurdistan, Iraq

Hayder M. Issa

Department of Geography, College of Human Science, University of Garmian, Sulaimaniyah Province 46021, Kurdistan Region - F.R. Iraq

***Abstract*—Satisfactory effluent characteristics are indispensable to evaluate the performance of any wastewater treatment plant (WWTP) design. Dynamic simulation software has a great role in pursuing this objective, in which an efficient and cost-effective design is constantly performed. In this study, a dynamic simulator sewage treatment operation analysis over time (STOAT) has been used under certain influent conditions to optimize design possibilities for modifying an existing primary WWTP College of Engineering Wastewater Treatment Plant (COEWWTP) at Erbil, Kurdistan, Iraq. The optimization was established on the basis of total suspended solids (TSS) and biochemical oxygen demand (BOD) characteristics in the effluent. Two alternative design schemes were proposed; trickling biofilter and aeration basin. In the dynamic simulation for the investigated design schemes, the predicted effluent profile showed that each of the existing and trickling biofilter processes has failed to correspond to the valid effluent limitation, whereas predicted results of the aeration basin exhibited an effluent profile that meets TSS and BOD allowable limits. Different simulation models have been implemented by STOAT to simulate treatment processes in studied design approaches: ASAL 1 model; BOD model; BOD semi-dynamic model; and SSED 1 model. This study offers an additional understanding of WWTP design and facilitates the application of dynamic simulators as tools for wastewater treatment development in Kurdistan.**

***Index Terms*—Wastewater dynamic simulation, Sewage treatment operation analysis over time, Trickling biofilter, Activated sludge, Aeration tank.**

I. Introduction

The performance of units and processes in wastewater treatment plants (WWTPs) is regularly organized according to effluent profile parameters (Drinan and Spellman, 2015) and operation condition (Issa, 2016). Effluent limits have been built and sustained in respecting valid environmental regulations and legislation (Spellman, 2008). Respecting these regulations are obligatory for WWTPs to maintain the continuity of effluent discharge into diverse natural water bodies such as rivers, lakes, and seas (Davis, 2010). WWPTs have always structured programs for controlling the process units to eliminate any possible failure and to improve their performances (Matsuo et al., 2001; Williams, 2013).

Permanently, WWTPs are facing an important challenge when they try to reach optimal design and operation due to the stringent regulatory standards (Hreiz et al., 2015). Various design and assessment methods have been followed to perform a treatment process analysis and optimization of WWPTs units (Spiller et al., 2015). The uncertainty analysis by Monte Carlo simulations and multi-criteria assessment in wastewater treatment process development is often (Martin and Vanrolleghem, 2014; Spiller et al., 2015). Other techniques have also been implemented toward this objective, like artificial neural networks (Oliveira and Franca, 1998). Most of the established models in wastewater and sludge treatments are belonging to biological or physical treatments (Hakanen et al., 2013). Besides, the many conventional WWTPs proposed models (Kabouris, 1999), various predictive models have been also established for particular influent wastewater (Fung et al., 2012; Varank et al., 2014; Wang et al., 2014). The nature of mathematical models used in WWTP optimization is not the same, there are steady-state and dynamic based models (Rivas et al., 2008). Furthermore, the approach to reach the optimum design of WWTPs is different, some of the studies focus on particular parameters to be enhanced such as total suspended solids (TSS) (Verma et al., 2013), or solids retention time STM (Smith et al., 2014), whereas many other studies proposed a wider view of treatment evaluation by involving various controlling parameters for a single process such as the activated sludge process (Francisco et al., 2015) or the whole wastewater treatment process (Garrido-Baserba et al., 2012; Gillot et al., 1999; Guerrero et al., 2011; Khiewwijit et al., 2015; Revollar et al., 2017).

To achieve an accurate and adequate design of efficient WWTPs operating at optimum conditions, commercial simulation software has been developed in depending on previously proposed models (Gernaey et al., 2004). Software such as EnviroPro or SuperPro Designer built by Intelligen Inc., BioWin built by EnviroSim Associates Ltd., and sewage

ARO-The Scientific Journal of Koya University
Volume VII, No.1 (2019), Article ID: ARO.10488, 6 pages
DOI: 10.14500/aro.10488
Received 11 January 2019; Accepted 11 June 2019
Regular research paper: Published 22 June 2019
Corresponding author's e-mail: hayder.mohammed@garmian.edu.krd

 http://dx.doi.org/10.14500/aro.10488

treatment operation analysis over time (STOAT) software built by WRc Plc. is useful for simulation purposes. The developed WWTP process simulator of EnviroPro emphasize mainly on the environmental requirement to control the heavy metals and volatile organic compounds (Petrides et al., 1998). SuperPro Designer simulator is suitable for the purpose of environmental applications: Economic and pollution parameters determination (Kotoupas et al., 2007). Whereas the dynamic simulator STOAT has been applied mainly to develop the biological and physical process of secondary treatment in WWTPs, focusing on treating high nutrient using various models like activated sludge models ASMs (Sarkar et al., 2010). BioWin wastewater simulator aids to configure the various activated sludge reactor dimensions (Oleszkiewicz et al., 2004).

This work shows the results of plant design and optimization for an abandoned WWTP COEWWTP in its current condition (without modification) scheme and in proposed condition (with modification) scheme, by means of dynamic simulation performed using STOAT software simulations. In the development of COEWWTP, particular importance has been paid on the requirement to maintain effluents within the integrated local wastewater environmental regulations in the Kurdistan region of Iraq.

II. Methodology

A. Description of Erbil Wastewater Characteristics and the Studied WWTP COEWWTP Processes

Erbil is a big city of one million inhabitants, located in the North of Iraq. Nearly, all the neighborhoods of Erbil city are covered by sewage networks of dozens of kilometers long. There is no main WWTP in Erbil city; there are only a few small WWTPs serve in a few residential districts. Without treatment for the greater part of the wastewater effluents, this main part of wastewater discharge is directed to a nearby channel southwest of the city. Shekha et al., 2016, have determined the mean values of Erbil wastewater characteristics at the site Southwest of Erbil. They found that the dissolved oxygen (DO), biochemical oxygen demand (BOD) 5 nitrates NO_3, and phosphates PO_4 are 1.2 mg/l, 75 mg/l, 650 (μg NO_3-N/l), and 720 (μg PO_4-P/l), respectively, at a mean temperature of 19.7°C, whereas Al-Barzingy et al., 2010, have found that the mean TSS of Erbil wastewater at the same previous site is 80.15 mg/l.

The WWTP in the University of Salahaddin, College of Engineering Compound COEWWTP is the first plant established at Erbil. It was designed and constructed by a Japanese company in 1979, and it then was operated by the staff of the college of engineering. The plant released the effluents to the main discharge channel. After 14–15 working years, nearly in 1994, COEWWTP was stopped working due to economic conditions. In the years 2001, the plant was maintained by the staff of college of engineering and started working for another 7 years and stopped again. COEWWTP has been constructed with a capacity of about 2000 M^3/d, involving only primary treatment of sedimentation basin, as shown in Fig. 1.

B. Design and Dynamic Simulation of COEWWTP Units and Processes

STOAT (standard for STOAT) is a software that uses modeling to simulate dynamically of WWTP performances (Dudley and Dickson, 1992). It has been developed by WRc plc, England. The software can be used to simulate individual treatment processes or the whole treatment plant. The simulator adopted models that enable optimization the response of WWTPs in the influent loads and operating conditions. It addressed various models for all common wastewater treatment processes and established standard methods for performing these evaluations. The bio-kinetic models include the common IWA models of ASMs of biological nitrification and denitrification processes (Siegrist and Tschui, 1992).

In this work, the design was carried out using STOAT for three different scenarios: The first is redesign and simulate the existing processes units of COEWWTP without any modification; the second and third are design and simulate a modified WWTP by adding two different secondary treatment units to the plant.

The complete design for the WWTP COEWWTP2 has been achieved for the secondary biological treatment proposing two approaches: A trickling biofilter with a secondary sedimentation basin (COEWWTP2) (Fig. 2) or an activated sludge aeration basin with secondary settling tank (COEWWTP3) (Fig. 3).

Verification of the design and simulation of COEWWTP, COEWWTP2, and COEWWTP3 processes by applying STOAT simulation software is preferable. The fact that the verification could be privileged makes no change since the obstacle of privilege is excluded as there is no main WWTP operating nowadays at Erbil city and the main objective of this work is to explore the upgrading and renovation possibilities for the abandoned COEWWTP.

A comparison between the existing COEWWTP with two proposed alternatives of COEWWTP2 and COEWWTP3 has been made in terms of effluent quality. The returns of simulation analysis gave a valuable inside view of design criteria and opportunities to establish an extensive understanding of the prospected operating performance of the COEWWTP processes with and without modifications. The quality of effluent was employed to determine differences among the three WWTP processes.

Using STOAT for optimizing with dynamic simulating has been based on the soluble BOD and TSS profile in intended influents for the current COEWWTP and the proposing

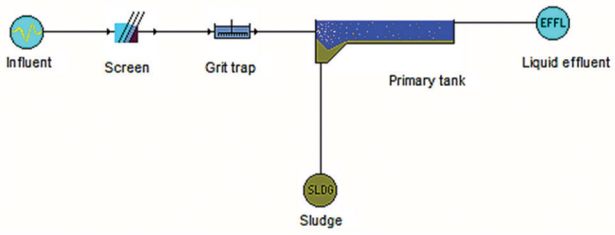

Fig. 1. Process flow diagram of COEWWTP using sewage treatment operation analysis over time simulator.

alternative schemes of COEWWTP2 and COEWWTP3. The ratios of nutrients were considerably low in the influent, and hence they were not taken into account in decision-making. The dimensions and some parameters for certain units were kept constant and default in all the scenarios to reach a reasonable cost similarity. Influent values used in the simulation were adopted from previous works on Erbil wastewater, as stated in Table I.

The influent and treated effluent volumetric flow rates are kept the same to match the efficiency of the tested schemes. Details on dimensions and streams of utilized units are presented in Table I. In COEWWTP3 scenario, the volumetric flow rate of recycle stream of the aeration tanks has been kept constant, and its ratio equals one, as shown in Table II.

In the STOAT dynamic simulation, the run in all wastewater treatment scenarios and the initial level of influent parameters are kept the same, where the processes runs were in a cold state with no previous operation. The initial influent is illustrated in Fig. 4, where some parameters were taken as default values in executed runs for a duration of 48 h and a profile of sinusoidal pattern. The initial data for the inlet stream to the primary treatment tank in the three examined simulation scenarios are displayed in Table III.

The performed dynamic simulation is depending on previously established models that are implied in STOAT for various units. Four models have been used in this work; BOD model in the primary and secondary treatment tanks; BOD semi-dynamic model in the trickling biofilter; ASAL1 model in the activated sludge aeration tank; and SSED1

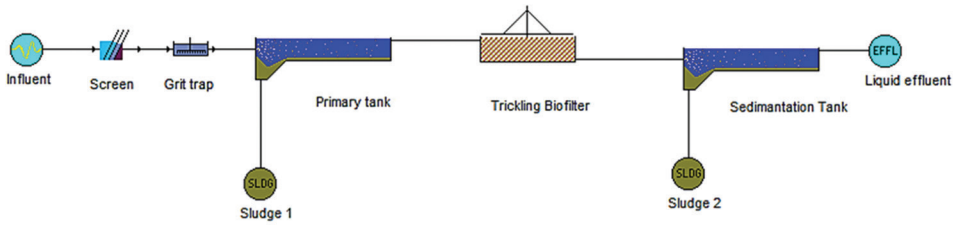

Fig. 2. Process flow diagram of COEWWTP2 using sewage treatment operation analysis over time simulator.

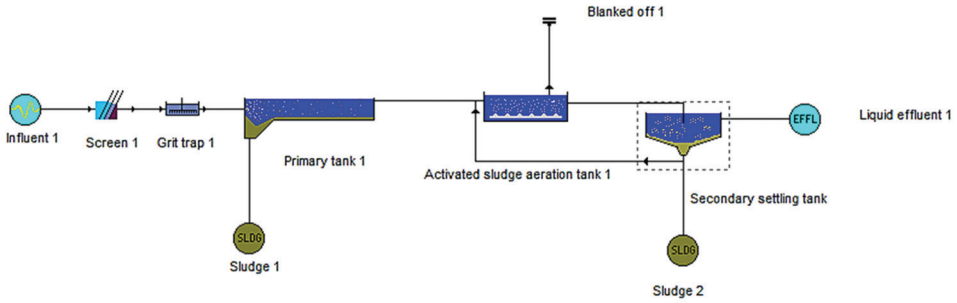

Fig.3. Process flow diagram of proposed COEWWTP3 with an activated sludge aeration basin with secondary sedimentation basin using sewage treatment operation analysis over time simulator.

TABLE I
DIMENSIONS AND VOLUMETRIC FLOW RATES OF PROPOSED THREE SCENARIOS FOR WASTEWATER TREATMENT

Parameters	Scenario 1 (COEWWTP)	Scenario 2 (COEWWTP2)	Scenario 3 (COEWWTP3)
Wastewater temperature (°C)	19.7	19.7	19.7
Screen bar spacing (m)	0.3	0.3	0.3
Grit trap volume (m^3)	30	30	30
Primary treatment tank volume (m^3)	600	600	600
Primary treatment tank surface area (m^2)	200	200	200
Primary treatment tank stages	1	1	1
Trickling biofilter surface area (m^2)	-	500	-
Trickling biofilter depth (m)	-	1.5	-
Secondary treatment tank volume (m^3)	-	600	-
Secondary treatment tank surface area (m^2)	-	200	-
Secondary sedimentation tank stages	-	1	-
Activated sludge aeration tank volume (m^3)	-	-	300
Stages of activated sludge aeration tank	-	-	1
Secondary sedimentation tank surface area (m^2)	-	-	250
Secondary settling tank stages	-	-	1
Secondary settling tank depth (m)	-	-	3
Secondary settling tank feed depth (m)	-	-	2

 http://dx.doi.org/10.14500/aro.10488

model in secondary settling tank. BOD based model handles the biomass in the influents.

TABLE II
Operational Data of the Secondary Settling Tank in the Scheme of Coewwtp 3

Parameters	Value
Change at time (h)	0.0
RAS flow (m^3/h)	112.0
RAS ratio	1.0
Sludge wastage flow (m^3/h)	5.0
Wastage pump run time (h)	24.0
Wastage cycle time (h)	24.0
MLSS set-point (mg/l)	0.0

MLSS: Mixed liquor suspended solids, RAS: Return activated sludge

TABLE III
The Initial Condition of the Primary Treatment Tank in all Executed Dynamic Simulation Runs Using STOAT for All Wastewater Treatment Scenarios

Parameters	Value
Soluble BOD (mg/l)	75.00
Soluble inert COD (mg/l)	0.00
Ammonia (mg/l)	0.01
Nitrate (mg/l)	0.65
Soluble organic nitrogen (mg/l)	1.00
Soluble phosphate (mg/l)	0.72
Dissolved oxygen (mg/l)	1.20
BOD of volatile fatty acids (mg/l)	0.00
Settable particulate BOD (mg/l)	35.00
Non-settable particulate BOD (mg/l)	15.00
Settable particulate inert COD (mg/l)	0.00
Non-settable particulate inert COD (mg/l)	0.00
Settable volatile solids (mg/l)	45.00
Non-settable volatile solids (mg/l)	15.00
Settable non-volatile solids (mg/l)	14.00
Non-settable non-volatile solids (mg/l)	6.00
Settable particulate organic N (mg/l)	0.00
Temperature (°C)	19.7

STOAT: Sewage treatment operation analysis over time, BOD: Biochemical oxygen demand, COD: Chemical oxygen demand

The ratio of phosphates, nitrates, and ammonia are very low in influent wastewater according to Iraqi environmental limitations of sewage discharges (Ministry of Environment, 2010). The key factors that were considered in the study to design and optimize the studied COEWWTP are the TSS and BOD. Therefore, the ASAL 1 model has been implemented to simulate the operation of activated sludge aeration tank in COEWWTP3 scenario. This model handles mainly the BOD removal in the influents, whereas the other processes such as nitrification or denitrification are not clearly embedded in it (Stokes et al., 2000). To facilitate the simulation in this work, ASAL 1 dynamic model has been used as it does not distinguish viable or nonviable biomass (Stokes et al., 2000).

The existing condition of COEWWTP contains only a primary treatment stage, which is currently out of work. Therefore, this work examines any intended essay to recommence or renovate this plant that must indubitably take into account the treatment efficiency. This step may require redesigning the current WWTP that can be separated into various scenarios. A dynamic simulation software STOAT has been used to perform and optimize the design scenarios. The optimization of design using the implemented models for investigated scenarios is established depending on the BOD and TSS outcome in the predicted effluent. The simulation for each design scenario has been conducted with implementing several models that mainly determine BOD behavior as an indicator of biomass strength like ASAL 1. The reason for exploring COEWWTP case study scenarios is to predict an optimum design regarding TSS and BOD removal capacities.

III. Results and Discussion

A. Dynamic Simulation of the Existing COEWWTP (Scenario 1)

Considering the characteristics presented in Fig. 4 as a proposed influent comes from Erbil city sewage, the dynamic simulation using STOAT of the existing COEWWTP's processes (Fig. 1) generated an effluent profile shown

	Elapsed time (h)	Flow (m^3/h)	Temperature (deg. C)	Soluble BOD (mg/l)	Particulate BOD (mg/l)	Volatile solids (mg/l)	Non-volatile solids (mg/l)	Ammonia (mg/l)	Nitrates (mg/l)
1	0.000000	75.000000	19.700000	75.000000	50.000000	60.000000	20.000000	0.012700	1.000000
2	1.000000	84.718810	19.700000	84.718810	56.479210	67.775050	22.591680	0.014346	1.129584
3	2.000000	93.773480	19.700000	93.773480	62.515660	75.018780	25.006260	0.015879	1.250313
4	3.000000	101.545200	19.700000	101.545200	67.696840	81.236210	27.078730	0.017195	1.353937
5	4.000000	107.503000	19.700000	107.503000	71.668690	86.002430	28.667480	0.018204	1.433374
6	5.000000	111.239700	19.700000	111.239700	74.159810	88.991770	29.663920	0.018837	1.483196
7	6.000000	112.499900	19.700000	112.499900	74.999940	89.999930	29.999980	0.019050	1.499999
8	7.000000	111.197500	19.700000	111.197500	74.131690	88.958030	29.652680	0.018829	1.482634
9	8.000000	107.421600	19.700000	107.421600	71.614390	85.937260	28.645750	0.018190	1.432288
10	9.000000	101.430100	19.700000	101.430100	67.620050	81.144060	27.048020	0.017175	1.352401
11	10.000000	93.632450	19.700000	93.632450	62.421630	74.905950	24.968650	0.015855	1.248433
12	11.000000	84.561560	19.700000	84.561560	56.374370	67.649250	22.549750	0.014319	1.127487
13	12.000000	74.837280	19.700000	74.837280	49.891520	59.869820	19.956610	0.012672	0.997830
14	13.000000	65.124120	19.700000	65.124120	43.416080	52.099300	17.366430	0.011028	0.868322
15	14.000000	56.085830	19.700000	56.085830	37.390560	44.868670	14.956220	0.009497	0.747811
16	15.000000	48.340060	19.700000	48.340060	32.226710	38.672050	12.890680	0.008186	0.644534
17	16.000000	42.416110	19.700000	42.416110	28.277410	33.932890	11.310960	0.007182	0.565548
18	17.000000	38.718800	19.700000	38.718800	25.812540	30.975040	10.325010	0.006556	0.516251
19	18.000000	37.500790	19.700000	37.500790	25.000530	30.000640	10.000210	0.006350	0.500011
20	19.000000	38.845320	19.700000	38.845320	25.896880	31.076250	10.358750	0.006578	0.517938
21	20.000000	42.660500	19.700000	42.660500	28.440330	34.128400	11.376130	0.007224	0.568807
22	21.000000	48.685610	19.700000	48.685610	32.457080	38.948490	12.982830	0.008244	0.649142
23	22.000000	56.508940	19.700000	56.508940	37.672630	45.207150	15.069050	0.009569	0.753453
24	23.000000	65.595870	19.700000	65.595870	43.730580	52.476700	17.492230	0.011108	0.874612
25	24.000000	75.325430	19.700000	75.325430	50.216960	60.260350	20.086780	0.012755	1.004339
26	25.000000	85.032760	19.700000	85.032760	56.688510	68.026210	22.675400	0.014399	1.133770

Close Save Reset Help

Fig. 4. The hourly influent profile in all executed dynamic simulation runs using sewage treatment operation analysis over time.

in Fig. 5. This effluent profile of seven parameters with simulation run time elapsed (48 h) is displayed by way of graphs, as shown in Fig. 5. Table III presents that the mean values of effluent parameters are generated from the existing COEWWTP scheme employing the STOAT dynamic simulation. The investigated effluent parameters are flow rate, TSS, soluble BOD, particulate BOD, volatile suspended solids (VSS), non-VSS, and DO. After a run time of 48 h, the dynamic simulation shows that the wastewater plant operation reached an agreeable steady state, as shown in Fig. 5. The fluctuation of effluent's flow rate and parameters values that appear in Fig. 5 is due to the divergence between daytime and nighttime loads corresponding to the sinusoidal simulation profile.

Both Table IV and Fig. 5 show that the concentrations of TSS and BODs in the COEWWTP effluent are much higher than the Iraqi and the WHO environmental allowable limits.

From Table IV, it can be seen that performance of COEWWTP scheme (scenario 1) is not satisfactory as stated by valid legislation and standards regarding the wastewater effluent disposal, and hence this scenario is out of consideration. It can be said that these results are expected as the COEWWTP involves only a primary treatment which is simply convenient for physical treatment to remove heavy solids. No remarkable influence of this treatment was found on the soluble and particulate biological matter. Even though there is no lower limit of DO of WWTP's effluent, DO of COEWWTP's effluent is quite low which may disturb the DO level of any receiving water body.

The single changing that has been made through this scenario is the TSS and VSS mean values was slightly lowered, where about 13% has been removed for both. It can be said that this scenario is useful only for an influent with low BOD and biomass levels. It is interesting to see that the solute BOD level was increased instead of to be decreased after the primary sedimentation. This increase might happen because more biological activities took place in the primary tank. From these results of primary sedimentation, it can be understood that the biomass is in a soluble state and with a small size in which a primary sedimentation tank makes no significant improvement in the wastewater situation.

B. Dynamic Simulation of the Proposed COEWWTP2 (Scenario 2)

Fig. 6 and Table V present the effluent profile produced by the suggested treatment scenario of COEWWTP2. In this option, a biofilter and secondary sedimentation tank were added to the primary sedimentation tank, as shown in Fig. 2. In Fig. 6, it is clear that biological treatment has been accomplished successfully. As an indicator of this achievement, the DO has been elevated substantially to reach a maximum level that can be made according to water solubility limit to DO. This means no extensive demand for oxygen exists in the effluent any more. Moreover, so the BOD mean value was declined accordingly to 30.29 mg/l. All these signs imply that the created biofilm on filter bed is performing the treatment positively.

On the other hand, as presented in Table V, the TSS is still high. In this proposed scheme, a secondary sedimentation tank was recommended to remove the suspended solids created in the trickling biofilter. However, according to the dynamic simulation results generated by STOAT, it can be seen that high levels of various kinds of solids still occur in the effluent. The cause of these high levels is most probably due to the shape, size, and state of the solids, which makes it difficult for the sedimentation tank to trap and remove them.

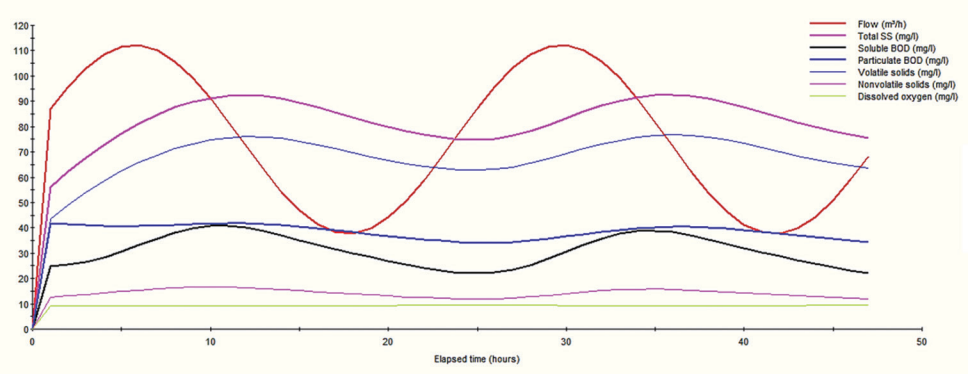

Fig. 5. Effluent profile from COEWWTP scheme (Scenario 1) as simulated by sewage treatment operation analysis over time along 48 h run time.

TABLE IV
CHARACTERISTICS OF THE EFFLUENT GENERATED FROM CEEWWTP SCHEME

Parameters	Flow (m≥/h)	TSS (mg/l)	BOD (mg/l)	VSS (mg/l)	Non VSS (mg/l)	DO (mg/l)
Mean±Standard deviation	73.36±28.71	69.83±16.01	82.0±15.77	52.34±11.99	17.49±4.01	0.15±0.24
Total mass (kg)	-	261.95	301.22	196.34	65.61	0.65
Peak load (g/s)	-	2.71	2.95	2.03	0.68	0.024
Iraqi sewage disposal limits	-	60	40	-	-	-
WHO disposal guidelines*	-	30	20	-	-	-

*WHO guidelines limits as presented by (Chipofya and Avramenko, 2010). TSS: Total suspended solids, BOD: Biochemical oxygen demand, VSS: Volatile suspended solids, DO: Dissolved oxygen

From another point of view, the simulation results displayed in Fig. 6 show that the trickling biofilter is working perfectly on the soluble BOD, in which BOD mean value has been lowered by 60%. Whereas the performance of trickling biofilter on particulate BOD is not in the same way, as the VSS in the effluent was increased instead to be decreased. A part of this increase might come from the waste generated from the biological treatment in the trickling biofilter itself. However, for this scenario, the TSS is too high and cannot be accepted according to Iraqi limits or the WHO guidelines; therefore, this scheme was ignored.

C. Dynamic Simulation of the Proposed COEWWTP3 (Scenario 3)

To optimize the design of COEWWT to obtain an effluent that agrees with the permissible limits for both BOD and TSS, an alternative design scheme of COEWWTP3 (scenario 3) was proposed. The flow diagram of this scheme is illustrated in Fig. 3. In this scheme, an activated sludge aeration tank has been used to achieve the biological treatment and followed by a secondary settling tank to remove the suspended solids with a recycle stream. The operation parameters of the secondary settling tank are demonstrated in Table II.

The effluent profile as shown in Fig. 7 reveals that significant biological treatment has been accomplished for both soluble and particulate biomass along the time of simulation run of 48 h. It is shown in Fig. 7 that low levels of volatile and non-volatile solids have been reached even at early hours of the simulation which means a successful removal was attained by the secondary settling tank of produced flocks in the aeration tank. Only BOD took more time to be lowered in this proposed scheme; this looks to be reasonable as the activated sludge biomaterials need a specific period to reach an efficient activity in treating the included soluble and suspended organic mass in the influent. As shown in Fig. 7, the BOD starts to drop after passing 24 h, this gives an idea of the time required by the activated sludge in the aeration take to reach a suitable treatment level. DO profile in the generated effluent shows that it has reached a steady state according to the ongoing treatment occurring in the activated sludge aeration tank. This process prevents the DO to increase because the working activated sludge biomaterials originate a high demand on the existed oxygen to accomplish their work. Off course, the oxygen transfer in the tank is affected by many factors such as flow pattern and tank configuration (Issa, 2017).

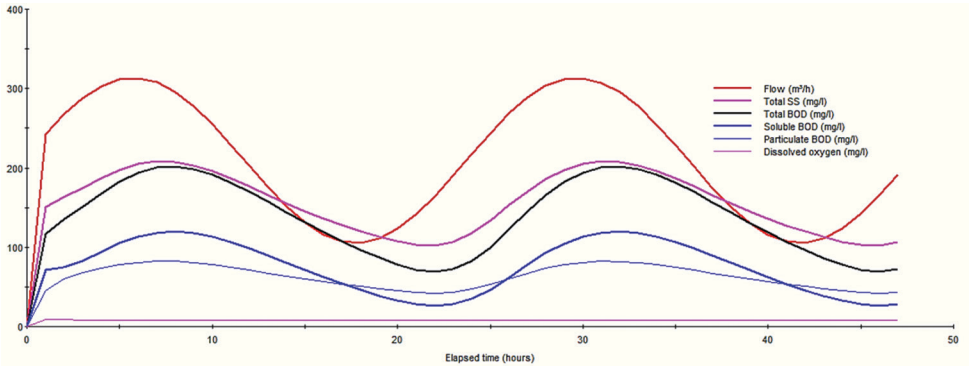

Fig. 6. Effluent profile from COEWWTP2 scheme (Scenario 2) as simulated by sewage treatment operation analysis over time along 48 h run time.

TABLE V
CHARACTERISTICS OF THE EFFLUENT GENERATED FROM CEEWWTP2 SCHEME (SCENARIO 2)

Parameters	Flow (m≥/h)	TSS (mg/l)	BOD (mg/l)	VSS (mg/l)	Non VSS (mg/l)	DO (mg/l)
Mean±Standard deviation	73.36±28.71	80.87±14.44	30.29±7.45	66.96±12.16	13.89±2.52	9.10±1.34
Total mass (kg)	-	288.69	109.61	238.43	50.26	32.70
Peak load (g/s)	-	2.63	1.21	2.18	0.49	0.29
Iraqi sewage disposal limits	-	60	40	-	-	-
WHO disposal guidelines	-	30	20	-	-	-

TSS: Total suspended solids, BOD: Biochemical oxygen demand, VSS: Volatile suspended solids, DO: Dissolved oxygen

TABLE VI
CHARACTERISTICS OF THE EFFLUENT GENERATED FROM CEOWWTP3 SCHEME (SCENARIO 3)

Parameters	Flow (m≥/h)	TSS (mg/l)	BOD (mg/l)	VSS (mg/l)	Non VSS (mg/l)	DO (mg/l)
Mean	68.46	5.47	24.30	1.18	4.29	1.89
Standard deviation	28.45	3.16	18.92	0.60	2.61	0.38
Total mass (kg)	-	20.15	80.65	4.20	15.92	6.25
Peak load (g/s)	-	0.40	1.43	0.09	0.32	0.06
Iraqi sewage disposal limits	-	60	40	-	-	-
WHO disposal guidelines	-	30	20	-	-	-

TSS: Total suspended solids, BOD: Biochemical oxygen demand, VSS: Volatile suspended solids, DO: Dissolved oxygen

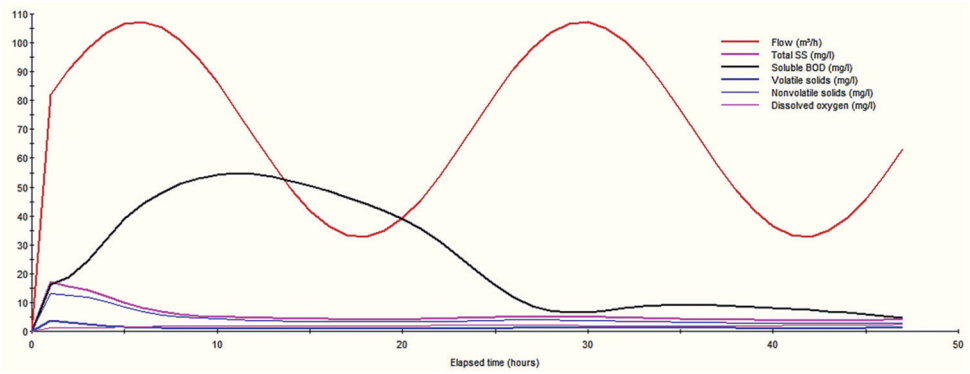

Fig. 7. Effluent profile from COEWWTP 3 scheme (Scenario 3) as simulated by sewage treatment operation analysis over time along 48 h run time.

The results presented in Table VI show that the treatment efficiency made by the scheme COEWWT3 is satisfactory for both TSS and BOD mean values. The removal percentage of TSS and BOD was 93.2 and 68%, respectively. Comparing with the previous schemes, these results lead to only consider the last scenario of COEWWTP3 for further modification and renovation for the existed and abandoned WWTP of COEWWTP.

IV. Conclusion

In this work, a dynamic simulator like STOAT that has been widely validated in many previous studies was chosen to optimize the design possibilities of modification and renovation of an abandoned WWTP COEWWTP located at Erbil, Iraq. First, the existing scheme COEWWTP was simulated using STOAT software. Simulated effluent data were obtained with this scheme disclose that the current plant configuration has failed to assure accepted effluent levels regarding the TSS and BOD allowable limits according to Iraqi and the WHO guidelines. Two alternative design schemes have been then proposed by applying STOAT simulation software to improve effluent quality: COEWWTP2 and COEWWTP3. The design of COEWWTP2 scheme involves a trickling filter with a secondary sedimentation basin showed that this approach is unsuitable due to high TSS level in the effluent. However, the second design approach COEWWTP3, in which the activated sludge aeration basin conjugated with the secondary sedimentation basin, is more convenient and achieved reasonable results. The final scheme looks to be a technically feasible scheme with respect to TSS and BOD profile in the plant effluent. This scheme might be able to give considerable treatment efficiency compared to that in the existing COEWWTP or the proposed COEWWTP2. This study thus leads to taking into consideration the dynamic simulators potentials in optimizing and development of the WWTP design approaches, especially in the Kurdistan region of Iraq.

References

Al-Barzingy, Y.O.M., Haydar, N.H., and Shekha, Y.A., 2010. The effect of wastewater disposal on the water quality and phytoplankton in Erbil wastewater channel. *Baghdad Science Journal*, 7(2), pp.984-993.

Chipofya, V., and Avramenko, Y., 2010. Comparison of pollutant levels in effluent from wastewater treatment plants in Blantyre, Malawi. *International Journal of Water Resources and Environmental Engineering*, 4(2), pp.79-86.

Davis, M.L., 2010. *Water and Wastewater Engineering.* 1st ed., McGraw-Hill Education, New York.

Drinan, J.E., and Spellman, F., 2015. *Water and Wastewater Treatment. A Guide for the Nonengineering Professional*. 1st, 2nd ed., CRC Press, Boca Ratón, Florida.

Dudley, J., and Dickson, C., 1992. Dynamic Sewage Treatment Works Modelling. WRC, Report No. UM, 1352.

Francisco, M., Skogestad, S., and Vega, P., 2015. Model predictive control for the self-optimized operation in wastewater treatment plants: Analysis of dynamic issues. *Computers and Chemical Engineering*, 82, pp.259-272.

Fung, K.Y., Lee, C.M., Ng, K.M., Wibowo, C., Deng, Z., and Wei, C., 2012. Process development of treatment plants for dyeing wastewater. *AIChE Journal*, 58(9), pp.2726-2742.

Garrido-Baserba, M., Reif, R., Hernández, F., and Poch, M., 2012. Implementation of a knowledge-based methodology in a decision support system for the design of suitable wastewater treatment process flow diagrams. *Journal of Environmental Management*, 112, pp.384-391.

Gernaey, K.V., van Loosdrecht, M.C.M., Henze, M., Lind, M., and Jørgensen, S.B., 2004. Activated sludge wastewater treatment plant modelling and simulation: State of the art. *Environmental Modelling and Software*, 19(9), pp.763-783.

Gillot, S., De Clercq, B., Defour, D., Simoens, F., Gernaey, K., and Vanrolleghem, P. 1999. Optimisation of Wastewater Treatment Plant Design and Operation Using Simulation and Cost Analysis. Paper Presented at the Proceedings 72nd Annual WEF Conference and Exposition. New Orleans, USA.

Guerrero, J., Guisasola, A., Vilanova, R., and Baeza, J.A., 2011. Improving the performance of a WWTP control system by model-based setpoint optimisation. *Environmental Modelling and Software*, 26(4), pp.492-497.

Hakanen, J., Sahlstedt, K., and Miettinen, K., 2013. Wastewater treatment plant design and operation under multiple conflicting objective functions. *Environmental Modelling and Software*, 46, pp.240-249.

Hreiz, R., Latifi, M.A., and Roche, N., 2015. Optimal design and operation of activated sludge processes: State-of-the-art. *Chemical Engineering Journal*, 281, pp.900-920.

Issa, H.M., 2016. Scale-up criterion of power consumption for a surface aerator used in wastewater treatment tank. *International Journal of Energy and Environment*, 7(5), pp.427-434.

Issa, H.M., 2017. Dependence of aeration efficiency in projected water spray on hydrodynamic profile in a water treatment tank. *ZANCO Journal of Pure and Applied Sciences*, 28(2), pp.9-16.

Kabouris, J.C., 1999. Modeling, instrumentation, automation, and optimization of wastewater treatment facilities. *Water Environment Research*, 71(5), pp.729-736.

Khiewwijit, R., Temmink, H., Rijnaarts, H., and Keesman, K.J., 2015. Energy and nutrient recovery for municipal wastewater treatment: How to design a feasible plant layout? *Environmental Modelling and Software*, 68, pp.156-165.

Kotoupas, A., Rigas, F., and Chalaris, M., 2007. Computer-aided process design, economic evaluation and environmental impact assessment for treatment of cheese whey wastewater. *Desalination*, 213(1), pp.238-252.

Martin, C., and Vanrolleghem, P.A., 2014. Analysing, completing, and generating influent data for WWTP modelling: A critical review. *Environmental Modelling and Software*, 60, pp.188-201.

Matsuo, T., Hanaki, K., Takizawa, S., and Satoh, H., 2001. *Advances in Water and Wastewater Treatment Technology: Molecular Technology, Nutrient Removal, Sludge Reduction, and Environmental Health*. 1st ed., Elsevier Science B. V, Amsterdam.

Ministry of Environment., 2010. Iraqi Environmental Limitations of Discharged Sewage. Unpublished Report, Baghdad, Iraq.

Oleszkiewicz, J.A., Kalinowska, E., Dold, P., Barnard, J.L., Bieniowski, M., Erenc, Z.F., and Udol, J.S., 2004. Feasibility studies and pre-design simulation of Warsaw's new wastewater treatment plant. *Environmental Technology*, 25(12), pp.1405-1411.

Oliveira, M.E.C., and Franca, A.S., 1998. Simulation of oxygen mass transfer in aeration systems. *International Communications in Heat and Mass Transfer*, 25(6), pp.853-862.

Petrides, D., Cruz, R., and Calandranis, J., 1998. Optimization of wastewater treatment facilities using process simulation. *Computers and Chemical Engineering*, 22(1), pp.S339-S346.

Revollar, S., Vega, P., Vilanova, R., and Francisco, M., 2017. Optimal control of wastewater treatment plants using economic-oriented model predictive dynamic strategies. *Applied Sciences*, 7(8), p.813.

Rivas, A., Irizar, I., and Ayesa, E., 2008. Model-based optimisation of wastewater treatment plants design. *Environmental Modelling and Software*, 23(4), pp.435-450.

Sarkar, U., Dasgupta, D., Bhattacharya, T., Pal, S., and Chakroborty, T., 2010. Dynamic simulation of activated sludge based wastewater treatment processes: Case studies with Titagarh sewage treatment plant, India. *Desalination*, 252(1), pp.120-126.

Shekha, Y.A., Toma, J.J., and Al-Barzingy, Y.O.M., 2016. Algal survey in wastewater channel of Erbil city, *Iraq. Diyala Journal for Pure Science*, 12, pp.39-57.

Siegrist, H., and Tschui, M., 1992. Interpretation of experimental data with regard to the activated sludge model no. 1 and calibration of the model for municipal wastewater treatment plants. *Water Science and Technology*, 25(6), pp.167-183.

Smith, R., Elger, S., and Mleziva, S., 2014. Wastewater: Solids retention time control in wastewater treatment. *Filtration and Separation*, 51(3), pp.12-17.

Spellman, F.R., 2008. *Handbook of Water and Wastewater Treatment Plant Operations*. 2nd ed., Taylor and Francis, Boca Raton.

Spiller, M., Vreeburg, J.H.G., Leusbrock, I., and Zeeman, G., 2015. Flexible design in water and wastewater engineering definitions, literature and decision guide. *Journal of Environmental Management*, 149, pp.271-281.

Stokes, A.J., Forster, C.F., West, J.R., and Davies, W.J., 2000. Stoat and the oxygen requirements of an activated Sludge Plant. *Environmental Technology*, 21(11), pp.1223-1231.

Stokes, A.J., West, J.R., Forster, C.F., and Davies, W.J., 2000. Understanding some of the differences between the COD and BOD-based models offered in STOAT. *Water Resources*, 34(4), pp.1296-1306.

Varank, G., Erkan, H., Yazýcý, S., Demir, A., and Engin, G., 2014. Electrocoagulation of tannery wastewater using monopolar electrodes: Process optimization by response surface methodology. *International Journal of Environmental Research*, 8(1), pp.165-180.

Verma, A., Wei, X., and Kusiak, A., 2013. Predicting the total suspended solids in wastewater: A data-mining approach. *Engineering Applications of Artificial Intelligence*, 26(4), pp.1366-1372.

Wang, Y., Li, W., Irini, A., and Su, C., 2014. Removal of organic pollutants in tannery wastewater from wet-blue fur processing by integrated anoxic/oxic (A/O) and fenton: Process optimization. *Chemical Engineering Journal*, 252, pp.22-29.

Williams, P.T., 2013. *Waste Treatment and Disposal.* 1st ed., Wiley, Chichester, UK.

General Information

ARO's Mission: ARO seeks to publish those papers that are most influential in their fields or across fields and that will significantly advance scientific understanding. Selected papers should present novel and broadly important data, syntheses, or concepts. They should merit the recognition by the scientific community and general public provided by publication in ARO, beyond that provided by specialty journals.

We welcome submissions from all fields of science and engineering, and from any source. We are committed to the prompt evaluation and publication of submitted papers. ARO is published biannually; selected papers are published online ahead of print.

Submission

Manuscripts should be submitted by the correspondent authors of the manuscript via the on-line submission page. Regardless of the source of the word-processing tool, only electronic Word (.doc, .docx, .rtf) files can be submitted on-line. There is no page limit. Only online submissions are accepted to facilitate rapid publication and minimize administrative costs. Submissions by any other one but the authors will not be accepted. The submitting author takes responsibility for the paper during submission and peer review. If for some technical reason submission through the email is not possible, the author can contact ARO.journal@koyauniversity.org for support. Before submitting please check ARO's guide to authors thoroughly to avoid any delay in the review and publication process.

Authors are explicitly responsible for the language of their texts. Paper should be submitted in a well written in understandable English. Authors should not expect the editor or editorial board to rewrite their paper. Prior to submission, authors should have their paper proofread by a possible academic native speaker of English.

- Submit the Article with contact Information
- File name should be your article tittle
- Don't submit your article in multiple journal, we are taking only minimum time for review process. please don't waste our time
- Once the paper is accepted, it can't be withdrawn
- Please follow publication ethics and regulation
- Avoid plagiarism and copied material
- Strictly Follow ARO's Template

Terms of Submission

Papers must be submitted on the understanding that they have not been published elsewhere and are not currently under consideration by another journal or any other publisher. ARO accepts original articles with novel impacts only. Post conference papers are not accepted "as is", however, regular papers on the same topic but with a different title can be submitted. The new paper should contain significant improvements in terms of extended content, analysis, comparisons with popular methods, results, figures, comments, etc. Please do not forget that the publication of the same or similar material in ARO constitutes the grounds for filing of an (auto) plagiarism case.

The submitting author is responsible for ensuring that the article’s publication has been approved by all the other co-authors. It is also the authors’ responsibility to ensure that the articles emanating from a particular institution are submitted with the approval of the necessary institution. Only an acknowledgement from the editorial office officially establishes the date of receipt. Further correspondence and proofs will be sent to the author(s) before publication unless otherwise indicated. It is a condition of submission of a paper that the authors permit editing of the

paper for readability. All enquiries concerning the publication of accepted papers should be addressed to aro.journal@koyauniversity.org.

Peer Review

All manuscripts are subject to peer review and are expected to meet standards of academic excellence. Submissions will be considered by an editor and "if not rejected right away" by peer-reviewers, whose identities will remain anonymous to the authors.

Guide to Author

We welcome submissions from all fields of science and engineering, and from any source. We are committed to the prompt evaluation and publication of submitted papers. Selected papers are published online ahead of print. Authors are encouraged to read the instructions below before submitting their manuscripts. This section arranged into an overview speedy guidelines below and more detailed at the bottom section of this page

Manuscript Preparation

Submitting your manuscript will be in two stages namely before final acceptance and after.

Stage one:

At the first stage manuscript needs to be prepared electronically and submitted online via the online submission page in a Word (.doc, .docx, .rtf) format of one column double-spaced page, Times New Roman font type, and 12 p font size. A pdf version of the submitted manuscript should be submitted too. All authors' names, affiliations, e-mail addresses, and mobile phone numbers should be typed on a cover page, indicating the correspondent author.

Stage two:

- File type: MS-Word version 2003 or later.
- Format: The preferred format of the manuscript two-column template with figures and captions included in the text. This template can be downloaded via the following link. Please follow instructions given in the template; http://aro.koyauniversity.org/about/submissions#onlineSubmissions
- Text: All text is in Times New Roman font. The main text is 10-point, abstract is 9-point font and tables, references and captions are 8-point font.
- Figures: Figures should be easily viewed on a computer screen.

Units of Measurement

Units of measurement should be presented simply and concisely using System International (SI) units.

Title and Authorship Information

The following information should be included;

- Paper title.
- Full author names.
- Affiliation.
- Email addresses.

Abstract

The manuscript should contain an abstract. The abstract should be self-contained and citation-free and should not exceed 200 words.

Introduction

This section should be succinct, with no subheadings.

Materials and Methods

This part should contain sufficient detail so that all procedures can be repeated. It can be divided into subsections if several methods are described.

Results and Discussion

This section may each be divided by subheadings or may be combined.

Conclusions

This should clearly explain the main conclusions of the work highlighting its importance and relevance.

Acknowledgements

All acknowledgements (if any) should be included at the very end of the paper before the references and may include supporting grants, presentations, and so forth.

References

References must be included in the manuscript and authors are responsible for the accuracy of references. Manuscripts without them will be returned. ARO is following Harvard System of Referencing. (Learn how to import and use Harvard Styling in your Microsoft Office by following this link:
http://bibword.codeplex.com/releases/view/15852)

Preparation of Figures

Upon submission of an article, authors are supposed to include all figures and tables in the PDF file of the manuscript. Figures and tables should be embedded in the manuscript. Figures should be supplied in either vector art formats (Illustrator, EPS, WMF, FreeHand, CorelDraw, PowerPoint, Excel, etc.) or bitmap formats (Photoshop, TIFF, GIF, JPEG, etc.). Bitmap images should be of 300 dpi resolution at least unless the resolution is intentionally set to a lower level for scientific reasons. If a bitmap image has labels, the image and labels should be embedded in separate layers.

Preparation of Tables

Tables should be cited consecutively in the text. Every table must have a descriptive title and if numerical measurements are given, the units should be included in the column heading. Vertical rules should not be used.

ARO Reviewer/Associate Editor Application Form

ARO is a scientific journal of Koya University (p-ISSN: 2410-9355, e-ISSN: 2307-549X) which aims to offer a novel contribution to the study of science. The purpose of ARO is twofold: first, it will aim to become an ongoing forum for debate and discussion across the science and engineering. We hope to advance our problem solving capacity and deepen our knowledge regarding a comprehensive range of collective actions. Second, ARO accepts the challenges brought about by multidisciplinary scientific areas and aspires to expand the community of academics who are able to learn from and help to produce advances in a variety of different disciplines.

The Journal is seeking reviewers who can provide constructive analysis of papers thus enhancing overall reputation of the Journal. If any expert is interested in participating of the review process, we highly encourage you to sign up as a reviewer for our Journal and help us improve our presence in domain of your expertise. Appropriate selection of reviewers who have expertise and interest in the domain relevant to each manuscript are essential elements that ensure a timely, productive peer review process. We require proficiency in English.

How to apply

To apply for becoming a reviewer of ARO, please submit the application form by following the link:
http://aro.koyauniversity.org/user/register
To apply for becoming a member of the Editorial Board of ARO, please submit the application form by following the link: http://aro.koyauniversity.org/pages/view/AEB

Both Associate Editor and Reviewers should specify their areas of research and expertise. Applicants must have a doctorate (or an equivalent degree), and if Master degree they need to have significant publishing experience. Please note that;

- You will need to write your full official name.
- Please provide an email which reflects your official name, such as nameOne.NameTwo@... , or your institute's official email.
- All data need to be written in English.

Note: For more information, kindly visit the following websites:

1. aro.koyauniversity.org.
2. http://libweb.anglia.ac.uk/referencing/harvard.htm.
3. http://bibword.codeplex.com/releases/view/15852.

INDEXING


THOMSON REUTERS
Emerging Sources Citation Index
WEB OF SCIENCE™


Crossref


PKP
PUBLIC
KNOWLEDGE
PROJECT


PRESERVED IN
LOCKSS


INDEXED IN
DOAJ


DOAJ
SEAL


SHERPA
RoMEO


ROAD
DIRECTORY
OF OPEN ACCESS
SCHOLARLY
RESOURCES


BASE


OCLC
WorldCat


Google
Scholar


ResearchGATE
scientific network

Koya University (KOU) is a young University established in 2003 and it is located in the city of Koya (Koysinjaq), short distance to the East of the regional capital city of Erbil (Arbil, Hewlêr) in Kurdistan Region of Iraq. It is on the foothills of beautiful High Mountain. Its campus has been carefully laid out to embrace the beautiful mountainous nature. The Koya University has a Faculty system which enhances the interactions between similar academic fields. Today, Koya University has four Faculties: Engineering, Science and Health, Humanities and Social Sciences and Education in addition to the School of Medicine, which all consist of twenty-five scientific departments in different fields, such as Petroleum Engineering, Geotechnical Engineering, Software Engineering, Physics, Chemistry, Clinical Psychology, Social Science, Medical Microbiology and Sport Education.

ARO-The Scientific Journal of Koya University is a biannual journal of original research articles, review articles, and letters to editor in the areas of Science and Engineering. ARO is a Peer-reviewed Open Access journal with CC BY-NC-SA 4.0 license. It provides immediate, worldwide and barrier-free access to the full text of research articles without requiring a subscription to the journal, and has no article processing charge (APC). ARO Journal seeks to publish those papers that are most influential in their fields or across fields and that will significantly advance scientific understanding. ARO Journal is a member of ROAD and Crossref agencies and has got ESCI, DOAJ seal, SHERPA/RoMEO deposit policy, and LOCKSS archiving policy.

Aro the Scientific Journal Office

Koya University (KOU)
University Park
Danielle Mitterrand Boulevard
Koya KOY45, Kurdistan Region - Iraq

aro.koyauniversity.org

ISSN: 2410-9355 (printed version) ISSN: 2307-549X (electronic version)
ARO - DOI: 10.14500/2307-549X